



LUND UNIVERSITY

Learning control for flex-fuel CI engine and fuel cell

Li, Xiufei

2022

Document Version:

Publisher's PDF, also known as Version of record

[Link to publication](#)

Citation for published version (APA):

Li, X. (2022). *Learning control for flex-fuel CI engine and fuel cell*. Department of Energy Sciences, Lund University.

Total number of authors:

1

General rights

Unless other specific re-use rights are stated the following general rights apply:

Copyright and moral rights for the publications made accessible in the public portal are retained by the authors and/or other copyright owners and it is a condition of accessing publications that users recognise and abide by the legal requirements associated with these rights.

- Users may download and print one copy of any publication from the public portal for the purpose of private study or research.
- You may not further distribute the material or use it for any profit-making activity or commercial gain
- You may freely distribute the URL identifying the publication in the public portal

Read more about Creative commons licenses: <https://creativecommons.org/licenses/>

Take down policy

If you believe that this document breaches copyright please contact us providing details, and we will remove access to the work immediately and investigate your claim.

LUND UNIVERSITY

PO Box 117
221 00 Lund
+46 46-222 00 00

Learning control for flex-fuel CI engine and fuel cell

XIUFEI LI

DEPARTMENT OF ENERGY SCIENCES | FACULTY OF ENGINEERING | LUND UNIVERSITY



Learning control for flex-fuel CI engine and fuel cell

Learning control for flex-fuel CI engine and fuel cell

Xiufei Li



LUND
UNIVERSITY

Thesis for the degree of Doctor of Philosophy
Thesis advisors: Prof. Per Tunestål, Prof. Rolf Johansson
Faculty opponent: Prof. Gregory Shaver

To be presented, with the permission of the Faculty of Engineering of Lund University, for
public criticism in the KC:C lecture hall at Kemicentrum on Friday, the 29th of April 2022
at 10:15

Organization LUND UNIVERSITY Department of Energy Sciences Box 188 SE-221 00 LUND Sweden		Document name DOCTORAL DISSERTATION	
		Date of disputation 2022-04-29	
		Sponsoring organization	
Author(s) Xiufei Li			
Title and subtitle Learning control for flex-fuel CI engine and fuel cell			
Abstract <p>This thesis investigated the modeling and control problems in the context of the flex-fuel compression-ignition (CI) engine and fuel cell.</p> <p>The modeling parts included the flex-fuel engine combustion process and intake system, and the system scale fuel cell model. The flex-fuel engine gas system models describing the intake pressure, temperature, oxygen concentration dynamics were established and validated with experimental data. The ignition delay was modeled with a physical model and data-based models. A fuel cell physical model was built to illuminate the electrochemical behavior, and Gaussian process (GP) models were used to predict the voltage and hydrogen pressure.</p> <p>Model predictive control (MPC) approaches based on physical models were applied to the flex-fuel CI engine and the fuel cell. An adaptive MPC method was proposed to control the combustion process of the flex-fuel CI engine. The control targets were combustion phasing and ignition delay. The adaptivity was accomplished by estimating the physical ignition delay model parameters by Kalman filter. The proposed adaptive MPC approach showed the successful application in the fuel transition scenario. An MPC with control constraints was developed to keep the fuel cell voltage at a reference value under current disturbance while satisfying the hydrogen pressure safety requirements. The proposed MPC controller fulfilled the control task and was compared with a PI controller.</p> <p>One learning-based MPC (LBMPC) method that decoupled the robustness and performance by maintaining two system models was proposed and applied to the control of combustion phasing when running with diesel. The comparison of LBMPC and MPC showed the improvement of performance by LBMPC. A GP MPC was developed to solve the fuel cell voltage control task with current disturbance and hydrogen pressure limit. Two GP predicting voltage and hydrogen pressure were integrated into the state-space model. The GP MPC showed comparable performance with MPC based on a detailed system physical model while requires less system information during operation.</p>			
Key words Flex-fuel CI Engine, Fuel Cell, Model Predictive Control, Learning Control, Adaptive Control, Gas System Model, Ignition Delay Model, Data-based Modeling, Gaussian process			
Classification system and/or index terms (if any)			
Supplementary bibliographical information		Language English	
ISSN 0282-1990		ISBN 9789180391818 (print) 9789180391825 (pdf)	
Recipient's notes		Number of pages 253	Price
		Security classification	

I, the undersigned, being the copyright owner of the abstract of the above-mentioned dissertation, hereby grant to all reference sources the permission to publish and disseminate the abstract of the above-mentioned dissertation.

Signature Xiufei Li

Date 2021-02-07

Learning control for flex-fuel CI engine and fuel cell

Xiufei Li



LUND
UNIVERSITY

Funding information: The thesis work was financially supported by the Swedish Energy Agency (grant number 22485-4), the KCFP Engine Research Center, and the Chinese Scholarship Council.

© Xiufei Li 2022

Faculty of Engineering, Department of Energy Sciences

ISBN: 9789180391818 (print)

ISBN: 9789180391825 (pdf)


ISSN: 0282-1990

ISRN: LUTMDN/TMHP-22/1167-SE

Printed in Sweden by Media-Tryck, Lund University, Lund 2022



Media-Tryck is a Nordic Swan Ecolabel certified provider of printed material. Read more about our environmental work at www.mediatryck.lu.se

MADE IN SWEDEN 

Dedicated to the present and future

Contents

List of publications	iv
Acknowledgements	vii
Abstract	ix
Popular science	xi
Nomenclature	xiii
1 Introduction	1
1.1 Background	1
1.2 Flex-fuel CI engine	3
1.3 Fuel cell	6
1.4 The control problem	7
1.5 Motivations and contributions	11
1.6 Thesis outline	12
2 Modeling	15
2.1 Introduction	15
2.2 Data-based modeling	17
2.3 Flex-fuel engine model	20
2.3.1 In-cylinder model	20
2.3.2 Gas system models	24
2.3.3 Ignition delay model	31
2.4 Fuel cell model	35
2.4.1 Physical-based PEFC model	35
2.4.2 Gaussian process model	40
3 Control synthesis	45
3.1 Control methods	45
3.1.1 PI control	45
3.1.2 Model predictive control	46
3.2 Estimation method	47
4 Experimental set-up	49
4.1 Flex-fuel CI engine	49
4.1.1 Engine	49

4.1.2	Measurement system	50
4.1.3	Fuel	52
4.1.4	Control system	53
4.2	Fuel cell	53
5	Adaptive MPC	55
5.1	Introduction	55
5.2	Flex-fuel CI engine control	56
5.2.1	Introduction	56
5.2.2	System modeling	57
5.2.3	Adaptive MPC design	58
5.2.4	Experimental set-up	64
5.2.5	Experimental results	64
5.2.6	Discussion	69
5.2.7	Conclusion	71
5.3	Fuel cell control	72
5.3.1	Introduction	72
5.3.2	System modeling	74
5.3.3	Adaptive MPC design	75
5.3.4	Experimental set-up	78
5.3.5	Experimental results	79
5.3.6	Discussion	84
5.3.7	Conclusion	88
6	Learning-based MPC	89
6.1	Introduction	89
6.2	Compression-ignition engine control	90
6.2.1	Introduction	90
6.2.2	System modeling	92
6.2.3	Learning-based MPC design	93
6.2.4	Experimental results	96
6.2.5	Discussion	98
6.2.6	Conclusion	99
6.3	Fuel cell control	100
6.3.1	Introduction	100
6.3.2	System modeling	101
6.3.3	Gaussian process MPC design	101
6.3.4	Experimental set-up	106
6.3.5	Experimental results	106
6.3.6	Discussion	110
6.3.7	Conclusion	113

7 Conclusions and future research	115
Bibliography	119
Summary of papers	145

List of publications

Paper I

Learning Based Model Predictive Control of Combustion Timing in Multi-Cylinder Partially Premixed Combustion Engine

Xiufei Li, Lianhao Yin, Per Tunestål, Rolf Johansson

SAE Technical Paper 2019-24-0016, 2019

Paper II

Adaptive Model Predictive Control of Combustion in Flex-Fuel Heavy Duty Compression-Ignition Engine

Xiufei Li, Per Tunestål, Rolf Johansson

21st IFAC World Congress (virtual), July, 2020

Paper III

A Multi-Input and Single-Output Voltage Control for a Polymer Electrolyte Fuel Cell System using Model Predictive Control Method

Xiufei Li, Yuanxin Qi, Shian Li, Per Tunestål, Martin Andersson

International Journal of Energy Research, 2021

Paper IV

Voltage Control for a Polymer Electrolyte Fuel Cell System by Gaussian Process Model Predictive Control

Xiufei Li, Yuanxin Qi, Martin Andersson, Rolf Johansson, Per Tunestål

Submitted to International Journal of Hydrogen Energy, 2022

Paper V

Neural Network Based Model Predictive Control of Voltage for a Polymer Electrolyte Fuel Cell System with Constraints

Xiufei Li, Yuanxin Qi, Martin Andersson, Rolf Johansson, Per Tunestål

Submitted to eTransportation, 2022

Other publications:

Temperature Control Strategy for Polymer Electrolyte Fuel Cells

Yuanxin Qi, **Xiufei Li**, Shian Li, Tingshuai Li, Mayken Espinoza-Andaluz, Per Tunestål, Martin Andersson

International Journal of Energy Research, 44:4352–4365, 2020

Optimization and Evaluation of a Low Temperature Waste Heat Recovery System for a Heavy Duty Engine over a Transient Cycle

Vikram Singh, **Xiufei Li**, Jelmer Rijpkema, Karin Munch, Sven Andersson, Sebastian Verhelst

SAE Powertrains, Fuels and Lubricants conference, September, 2020

Acknowledgements

My Ph.D. study is a wonderful and amazing journey, opening the door to a new world and a lot of opportunities. I will be grateful for this experience forever.

First of all, I want to send my deepest gratitude to my supervisor Per Tunestål, my most solid backing. He was the starter of this journey and made everything possible. He has the greatest patience in helping me solving any problems both in work and life and guides me in a most concerned and personalized way.

I would like to express my sincere appreciation to Rolf Johansson, my co-supervisor from the Department of Automatic Control. He is so erudite that all my puzzles will get the clearest explanation instantly from him. He supervises me in all aspects. I will always have a lot more to learn from him.

I am very lucky that I have Per and Rolf as my supervisors. I have learned a lot from their precepts and deeds, from professional knowledge, way of thinking, to how to become a better person. I can not imagine that I could have two better mentors.

I want to thank all my colleagues. The time we spent together makes this journey rich and joyful. I also thank the lab manager and the technicians for helping me with the various experimental stuff. Special thanks to Yuanxin for the great cooperation with our research. Thank you Marcus for the organization and helps. Thank you Lianhao for guiding me as a senior student. Thank you Anders for the all engine and experiment stuff. Thank you Miao Zhang for helping in his power when I asked. Thanks to Carlos for the discussion and co-work in TC 8. Thanks to Changle for the thesis template. Thank you, Xinda, Erik, Cheng, Vikram, Nika, Miaoxin, Ted, Ola, Andre, Anupam, Maya, Menno for the fun time working together.

Thanks to all my friends in Sweden, the wonderful time we have fun together embellishes this journey. Thank you Senbin, Miao Yang, Shijie, Yan, Shenghui, Leilei, Li...all of you. I will miss those joyful moments. Thanks to my friends in China as well, for supporting me with sincerity. Thank you Wenxing and Xiaoxiao. Special thanks to Tia; you were the shining star on my way.

Finally, I want to thank my family. My dad and uncle, your selfless love and firm support let me explore the world willingly. Indescribable thanks to my

grandpa and grandma, who brought me up. You aren't even able to read but able to teach me the most essential qualities by your actions. The love you irrigated on me is so much, enough for my whole life to enjoy. I wish you all good health and longevity. I love you all.

Abstract

This thesis investigated the modeling and control problems in the context of the flex-fuel compression-ignition (CI) engine and fuel cell, which shows great potential in the transition from fossil fuel to renewable energy sources.

The modeling parts included the flex-fuel engine combustion process and intake system, and the system scale fuel cell model. The flex-fuel engine gas system models describing the intake pressure, temperature, oxygen concentration dynamics were established and validated with experimental data. The ignition delay was one key indicator of the combustion process and fuel properties and was modeled with a physical model and data-based models. A fuel cell physical model was built to illuminate the electrochemical behavior, and Gaussian process (GP) models were used to predict the voltage and hydrogen pressure with the collected data.

Model predictive control (MPC) approaches based on physical models were applied to the flex-fuel CI engine and the fuel cell. An adaptive MPC method was proposed to control the combustion process of the flex-fuel CI engine. The control targets were combustion phasing and ignition delay. The adaptivity was done by estimating the physical ignition delay model parameters with real-time data online by Kalman filter. The proposed adaptive MPC approach showed the successful application in the fuel transition scenario with diesel, gasoline/n-heptane mixture, and ethanol/n-heptane mixture. An MPC with control constraints was developed to keep the fuel cell voltage at a reference value under current disturbance while satisfying the hydrogen pressure safety requirements. The state-space model was built by the simplification and linearization of the detailed system model. The proposed MPC controller fulfilled the control task and was compared with a PI controller.

Learning-based MPC (LBMPC) integrated the learning models to the state-space model to improve the controller performance. One learning-based MPC method that decoupled the robustness and performance by maintaining two system models was proposed and applied to the control of combustion phasing when running with diesel. The comparison of LBMPC and MPC showed the improvement of performance by LBMPC. A GP MPC was developed to solve the fuel cell voltage control task with current disturbance and hydrogen pressure limit. Two GP predicting voltage and hydrogen pressure were integrated into the state-space model. The GP MPC showed comparable performance with MPC based on a detailed system physical model while requires less system information during operation.

Popular science

Transportation plays an important role in our modern society. The food inventory would be empty in the supermarkets if transportation failed for weeks or days. Meanwhile, the need for transportation, especially commercial transportation, is increasing with the development of population, living standards, and economic activity.

The transportation energy source relies heavily on traditional fossil fuel with the usage of the internal combustion engine (ICE). To reduce carbon emissions and protect the environment from harmful pollutants, a transition from a fossil energy-centered supply to more dependence on renewable energy sources is necessary. Meanwhile, the internal combustion engine is still the main propellant of modern society, especially for commercial transportation like long-haul trucks. The use of alternative fuels like bio-diesel, bio-alcohol for ICE as energy sources is an interesting idea to mitigate the environmental impact. But along with the alternative fuels, the fuel property diversity is a challenge. This situation makes the flex-fuel engines an attractive solution, which is able to run with different fuel species instead of one specific fuel. Besides, the flex-fuel engine could also run with traditional fossil fuels, which contributes to a smooth energy source transformation. For long-distance commercial transportation, the compression-ignition (CI) engine, one type of ICE, is the main power source. The flex-fuel CI engine is a promising concept in this context. The engine controller is a key pivot in realizing this concept. The complexity of the flex-fuel CI engine requires advanced control algorithms.

In the long run, the fuel cell together with hydrogen energy shows great potential. If hydrogen were produced from renewable energy, the operation of the fuel cell system would have low or zero carbon emission and environmental impact. The fuel cell also has higher efficiency as compared to other renewable energy conversion technology and the lack of moving parts reduces some requirements of maintenance. However, its commercialization is still limited by some technical issues, among which reliable operation poses a big challenge. Control algorithms play a significant role in fuel cell system reliability.

Both the flex-fuel CI engine and the fuel cell put high demands on the control algorithms. Model predictive control (MPC) stands out from other controllers because of its ability to handle the multi-input multi-output problem and the constraints explicitly. MPC utilizes models to predict the system behavior and calculate the inputs. The models adopted in this work includes physical

models and data-based models, like the Gaussian process (GP) and neural network (NN).

A physical model was developed to describe the ignition delay behavior. Based on the physical model, an adaptive MPC approach was proposed. The proposed adaptive MPC method showed successful application in the fuel transition scenario with diesel, gasoline/n-heptane mixture, and ethanol/n-heptane mixture. Besides, a learning-based MPC method was proposed and applied to the control of combustion phasing when running with diesel.

A system scale fuel cell physical model focusing on the macro behavior was built. Two Gaussian processes were trained to predict the fuel cell voltage and hydrogen pressure. The voltage was the control target and the hydrogen pressure should be under a certain constraint value to ensure safe operation. An MPC based on the physical models was developed. The Gaussian process model required less system information during operation than the physical model when used in MPC design. An MPC based on the Gaussian process was developed, and the Gaussian process MPC showed comparable performance with MPC based on the detailed system physical model.

Based on the traditional truck engine, the flex-fuel CI engine expands the fuel choice beyond fossil fuels. Its adaptivity to renewable fuels makes it a promising concept in the transition to a carbon-neutral society. Besides, the flexibility empowers the commercial vehicle's high tolerance to fuel differences in a wide transportation area. The proposed control method was applied in the flex-fuel engine concept to ensure the engine gives the desired performance. The fuel cell is a high-potential clean energy source to achieve zero-carbon emission transportation. The MPC method developed was used to ensure that the fuel cell operates as expected while satisfying the safety requirements. Overall, this thesis researched the advanced control method to regulate the flex-fuel CI engine and fuel cell under complicated dynamic scenarios with safety constraints. The control methods actuate the flex-fuel CI engine and fuel cell towards carbon-neutral transportation.

Nomenclature

Abbreviations

0D	Zero dimensional
AD	Automatic differentiation
ARD	Automatic relevance determination
ATDC	After top dead center
BDC	Bottom dead center
CAD	Crank angle degree
CFD	Computational fluid dynamics
CI	Compression ignition
CNN	Convolutional neural network
CO₂	Carbon dioxide
CPU	Central processing unit
DMC	Dynamic matrix control
EGR	Exhaust gas recirculation
EKF	Extended Kalman filter
EVO	Exhaust valve opening
FC	Fuel cell
FPGA	Field programmable gate arrays
GHG	Greenhouse gas
GP	Gaussian Process
HCCI	Homogeneous charge compression ignition
ICE	Internal combustion engine
IMEP	Indicated mean effective pressure
IPOPT	Interior-point optimizer
IVC	Intake valve closing
KF	Kalman filter
L-BFGS	limited-memory Broyden–Fletcher–Goldfarb–Shanno
LBMPC	Learning-based model predictive control
LHS	Latin hypercube sampling
LHV	Lower heating value
LTC	Low temperature combustion
MEA	Membrane electrode assembly
MISO	Multi-input single-output
MPC	Model predictive control
NI	National Instruments

NN	Neural network
PEFC	Polymer electrolyte fuel cell
PI	Proportional integral control
PID	Proportional integral derivative control
PPC	Partially premixed combustion
PXI	PCI eXtensions for Instrumentation
QP	Quadratic programming
RBF	Radial basis function
RCCI	Reactivity controlled compression ignition
ReLU	Rectified linear unit
RPM	Revolutions per minute
SCR	Selective catalytic reduction
SI	Spark ignition
SGD	Stochastic gradient descent
SOI	Start of injection
SVM	Support vector machine
TDC	Top dead center
UEGO	Universal exhaust gas oxygen
VGT	Variable-geometry turbocharge

Symbols

γ	Ratio of specific heat
γ_c	Effective compression ratio
γ_e	Exhaust gas heat capacity
η_g	Gross efficiency
η_m	Turbocharger mechanical efficiency
η_n	Net efficiency
θ_{CA10}	Crank angle where 10% total heat is released
θ_{CA50}	Crank angle where 50% total heat is released
θ_{CA90}	Crank angle where 90% total heat is released
θ_{cool}	Actual cool valve opening
θ_{EGR}	Actual EGR valve opening
θ_{hot}	Actual hot valve opening
θ_{SOI}	Crank angle degree at the start of injection
θ_{VGT}	Actual VGT valve opening
ρ_{H_2}	Hydrogen density
ρ_{N_2}	Nitrogen density

ρ_{O_2}	Oxygen density
ρ_m	Membrane resistivity
τ	Ignition delay
ϕ_c	Compressor volumetric flow coefficient
ϕ_{EGR}	EGR valve normalized pressure ratio
Φ_{EGR}	EGR volumetric flow coefficient
ϕ_{opt}	Optimal pressure ratio in EGR valve
ϕ_t	Turbocharger volumetric flow coefficient
A_{em}	Maximum nominal EGR flow area
A_{vm}	Maximum nominal VGT flow area
C_{O_2}	Oxygen concentration at the cathode catalytic interface
C_p	Constant pressure molar specific heat
c_{pe}	Exhaust gas heat capacity
C_v	Constant volume molar specific heat
d	Piston diameter
d_{inj}	Injection duration
dQ_c	Heat release rate from combustion
dQ_{ht}	Heat transfer rate
dU	The difference of internal energy
dW	The difference of work
E_a	Apparent activation energy
E_n	Reversible voltage
I	Fuel cell current
J_{max}	Maximum current density
J_t	Turbocharger rotating inertia
K_P	Proportional gain
K_I	Integral gain
l	Connecting rod length
m_f	Fuel amount injected into the cylinder
m_{H_2}	Hydrogen mass in the anode volume
M_{H_2}	Hydrogen molar mass
$m_{H_2,in}$	Inlet hydrogen mass flow
$m_{H_2,out}$	Outlet hydrogen mass flow
$m_{H_2,rea}$	Hydrogen reaction mass flow
m_{N_2}	Nitrogen mass in the cathode channel
$m_{N_2,in}$	Inlet nitrogen mass flow
$m_{N_2,out}$	Outlet nitrogen mass flow
m_{O_2}	Oxygen mass in the cathode volume
M_{O_2}	Oxygen molar mass

$m_{O_2,in}$	Inlet oxygen mass flow
$m_{O_2,out}$	Outlet oxygen mass flow
$m_{O_2,rea}$	Oxygen reaction mass flow
n_{cell}	Cell numbers
n_t	Turbocharger speed
$O_{2\ air}$	Oxygen percentage at atmosphere
$O_{2\ in}$	Measured intake oxygen concentration in percentage
$O_{2\ IVC}$	Measured intake oxygen concentration in percentage at intake valve closing
p	In-cylinder pressure
p_{amb}	Ambient pressure
P_{ca}	Cathode pressure
p_{EGR}	Pressure after EGR valve
p_{ex}	Exhaust manifold pressure
p_{H_2}	Hydrogen pressure
p_{IMEPg}	Gross indicated mean effective pressure
p_{IMEPn}	Net indicated mean effective pressure
p_{in}	Intake pressure
p_{IVC}	Cylinder pressure at intake valve closing
p_{N_2}	Nitrogen pressure
p_{O_2}	Oxygen pressure
p_t	Exhaust gas pressure after turbine
P_t	Turbocharger power
N_s	Engine speed
Q_{air}	Air volumetric flow rate
Q_c	Accumulated heat release
Q_{H_2}	Hydrogen volumetric flow rate
Q_{LHV}	Fuel lower heating value
R	Universal gas constant
R_a	Intake gas constant
R_c	Compressor blade radius
R_C	Electronic resistance
R_e	Exhaust gas constant
R_m	Membrane resistance
s	Crankshaft diameter
T	Cylinder temperature
T_{amb}	Ambient temperature
T_{cool}	Gas temperature after intercooler
T_{ex}	Exhaust manifold temperature
T_{hot}	Gas temperature after compressor

T_{in}	Intake temperature
T_{IVC}	Cylinder temperature at intake valve closing
T_s	Stack temperature
T_t	Exhaust gas temperature after turbine
u_{cool}	Normalized cool valve opening
u_{EGR}	Normalized EGR valve opening
u_{hot}	Normalized hot valve opening
u_{VGT}	Normalized VGT valve opening
V	Cylinder volume
V_a	Activation voltage drop
V_c	Mass transport voltage drop
V_{FC}	Output voltage of the fuel cell system
V_o	Ohmic voltage drop
V_{in}	Intake manifold volume
V_{IVC}	Cylinder volume at intake valve closing
V_c	Clearance volume
V_d	Displacement volume
w_{air}	Air mass flow
w_c	Compressor mass flow
w_{EGR}	EGR mass flow
w_t	Turbine mass flow

1.1 Background

Under the pressure of global warming, major countries have released long-term outlooks and published mandatory regulations for greenhouse gases (GHGs), of which the carbon dioxide (CO_2) accounts for three-quarters of the total amount [69]. Figure 1.1 shows the European Union's vision for reducing GHGs by 2050 [7], [16], [17]. The total reduction is 80% in 2050 compared to 1990 levels, of which the transportation sector has a reduction of 60%.

To reduce carbon emissions and protect the environment from harmful pollutants, a transition from fossil energy-centered supply to more dependence on renewable energy sources is necessary. Many countries and companies have invested in renewable and alternative energy sources to facilitate the transformation sustainably.

However, the internal combustion engine (ICE) is still the main propellant of modern society, especially for commercial transportation. As shown in Figs. 1.2 and 1.3, heavy-duty transportation keeps increasing due to the economic activity expansion, and the transportation energy source relies heavily on traditional fossil fuel [132]. In the short term, the elimination of ICE and fossil fuel is undesirable. In this case, the flex-fuel engine, which can operate with different fuels including traditional fossil fuels and renewable fuels like ethanol, is a promising choice for the smooth energy

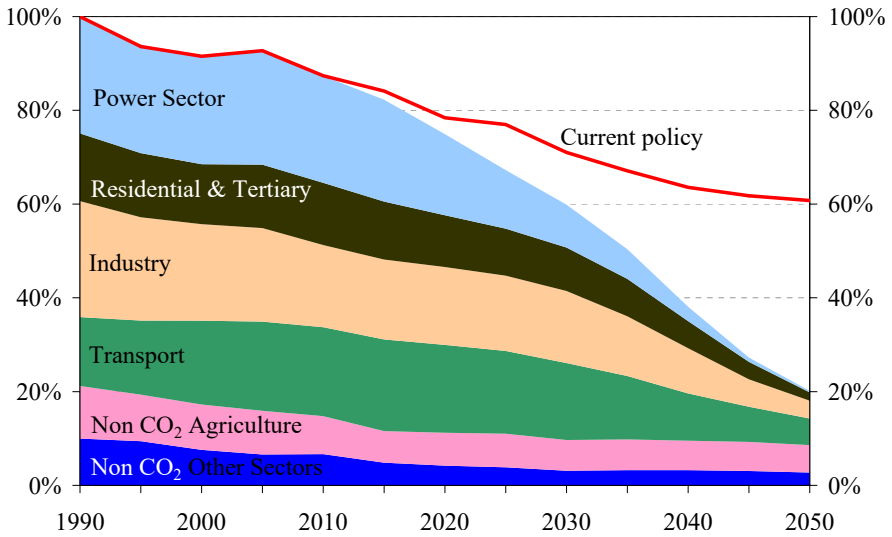


Figure 1.1: The European Union's vision for reducing GHGs (100%=1990) [7], [16], [17].

source transformation. The fuel flexibility can also provide the ICE adaptivity to local fuels in a vast area during long-distance transportation.

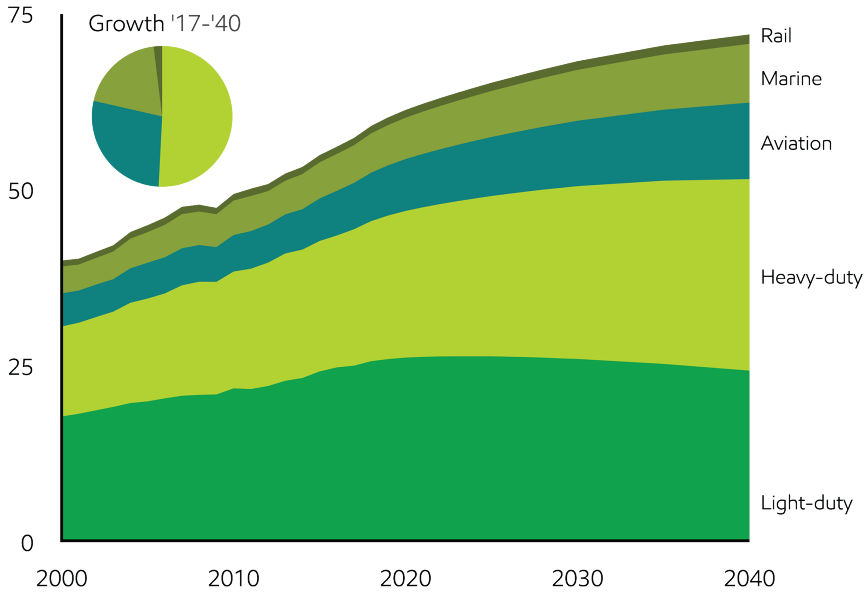


Figure 1.2: Transportation energy demand growth driven by commerce [132].

In the long run, the fuel cell together with hydrogen energy, which has

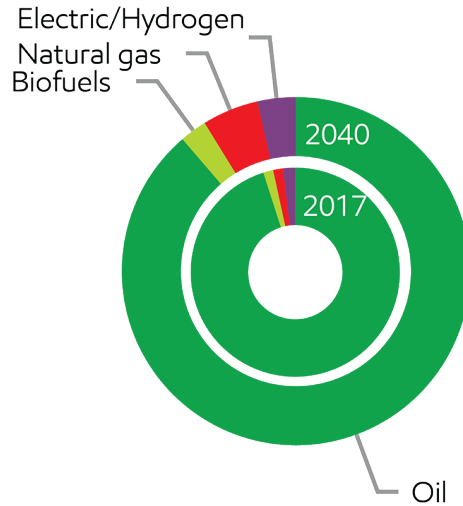


Figure 1.3: Commercial transportation energy demand by fuel [132].

low or zero carbon emission and environmental impact if the hydrogen is produced from renewable energy, shows great potential. Meanwhile, it is also possible to use carbon-based fuel such as methanol, gasoline, and natural gas as a hydrogen source, which contributes to a smooth transition. The fuel cell also has higher efficiency as compared to other renewable energy conversion technology and the lack of moving parts reduces some requirements of maintenance.

The main target of this work is to develop efficient and reliable control methods for the flex-fuel CI engine and fuel cell.

The following part of this chapter provides an introduction to flex-fuel CI engines, fuel cells, and modeling and control methods.

1.2 Flex-fuel CI engine

ICE basics

The internal combustion engine is used to produce mechanical power from the chemical energy contained in the fuel by burning or oxidizing the fuel inside the engine [78]. Traditionally, the main kinds of ICE are spark-ignition engines (also called Otto engines) and compression-ignition engines. The

spark-ignition engine generally operates with gasoline, where the combustion of the air-fuel mixture is ignited by a spark plug. Different from SI engines, the CI engine combustion process is ignited by the heat of compression and normally operating with diesel. These two kinds of engines have wide applications in transportation and power generation due to their simplicity, ruggedness, high power-to-weight ratio [78].

The reciprocating internal combustion engine adopts a cylinder-piston-crank arrangement. The structure of the arrangement is shown in Fig. 1.4. The four-stroke cycles of ICE start with airflow inducted through the intake valves due to the vacuum generated by piston downward motion. Then the air is compressed by upward moving piston to high-pressure and high-temperature conditions. The fuel is injected when the piston moves close to the top-dead center (TDC) position. For CI engines, the temperature and pressure are high enough shortly after injection, such that autoignition happens. Combustion increases the in-cylinder pressure, pushing the piston downward and the linear motion of the piston is converted to rotation of the crankshaft during expansion. Finally, the combustion products are expelled out of the cylinder after the exhaust valve opening. The full cycle process is shown in Fig. 1.5.

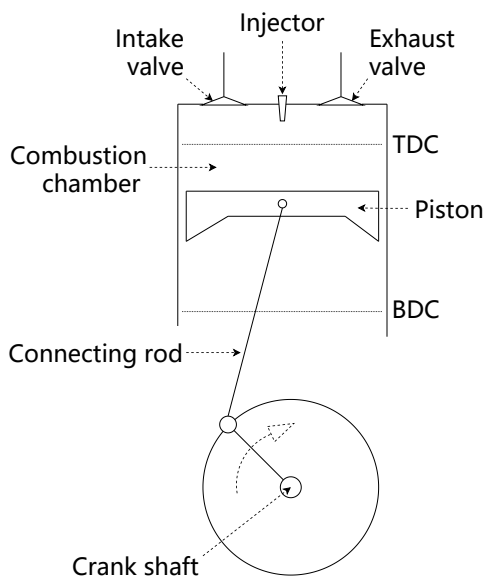


Figure 1.4: The mechanical arrangement of an engine cylinder.

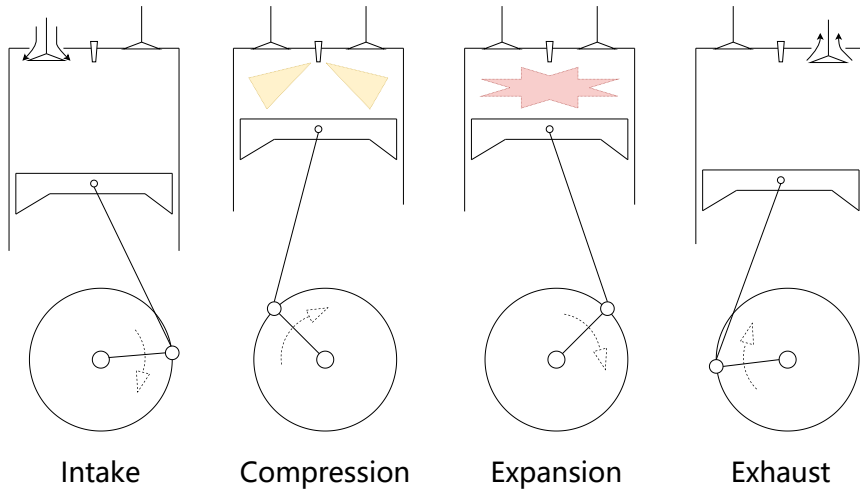


Figure 1.5: Four-stroke process of a CI engine.

Flex-fuel engine

Nowadays, the flex-fuel engine concept commonly refers to the spark-ignition (SI) engine. The flex-fuel SI engine operates on gasoline and ethanol up to 85% volumetric percentage. However, the compression-ignition engine is also promising to serve as a flex-fuel engine. It provides more flexible fuel choices and combustion modes. At the same time, it brings new control challenges comparing with single-fuel engines due to the unknown fuel species which demands advanced control methods.

The flex-fuel engine can operate on different fuels and their mixtures. Nowadays, flex-fuel engine mainly refers to spark-ignition engine operating on a blend of ethanol and gasoline in any volumetric concentration of up to 85% ethanol (93% in Brazil) [13]. The Brazilian market started to offer flex-fuel vehicles equipped with flex-fuel SI engines since 2003, and a total of 30.5 million flex-fuel vehicles were registered by March 2018 [39]. The applications of flex-fuel engines achieve fruitful results. However, the definition of flex-fuel engines can be broadened for wider applications. The CI engine, normally running with diesel, can also serve as flex-fuel engines.

CI engines can have more flexible fuel choices and combustion modes. Extensive studies have been carried out on the combustion mode of CI engine with gasoline. Well-known modes include homogeneous charge compression ignition (HCCI) [157], partially premixed combustion (PPC) [116], and reactivity controlled compression ignition (RCCI) [142]. Ethanol also has

been proven to be a possible fuel for the CI engine. Mack et al. showed the use of wet ethanol in HCCI mode [114]. The flex-fuel CI engine concept in this thesis is the first time being proposed to the author’s knowledge.

1.3 Fuel cell

The fuel cell is electrochemical equipment that converts chemical energy inside fuels like hydrogen to direct current electricity with oxygen in the air [47].

Normally, the fuel cell has higher efficiency and less operation noise than the thermal generator with the same power since there is no combustion in the process. The fuel cell is also clean in the way that its byproducts are only water and heat when using pure hydrogen, which makes the fuel cell an attractive way to reduce carbon emission.

Figure 1.6 gives an illustration of the fuel cell reaction [137].

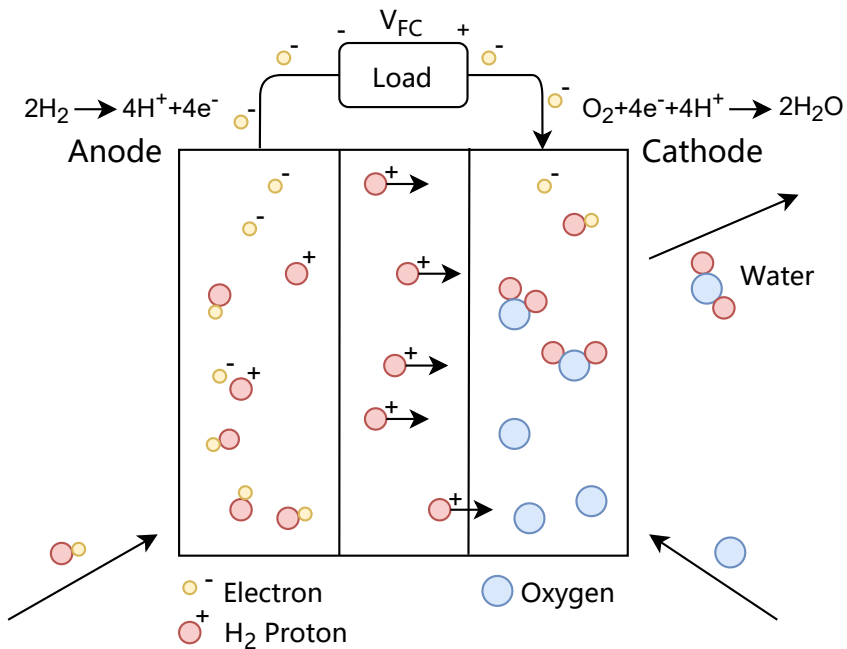


Figure 1.6: Fuel cell reaction.

The fuel cell type investigated in this work is the polymer electrolyte fuel cell (PEFC). The PEFC is one promising fuel cell technology because of its

high efficiency, fast start-up, low operating temperature, and environmental friendliness. It has been increasingly employed in portable stationary and transport units to replace traditional power sources [65], [102], [148], [186]. According to the E4tech Fuel Cell Industry Review [155], the fuel cell (FC) sector showed a remarkable increase in the supply chain of more than a gigawatt of shipments with PEFC dominating the shipments both in number and capacity.

The core part of the PEFC stack is the membrane electrode assembly (MEA). The MEA consists of proton exchange membranes sandwiched by electrodes, anode, and cathode on either side. The electric power is produced by the electrochemical redox reactions when hydrogen and air are supplied [47]. The membrane is an electrical insulator but allows hydrogen ions to move freely. The electrodes are normally made from highly conducting materials like porous graphite [137].

1.4 The control problem

Automatic control involves the automatic operation and regulation of systems. In most cases, the system states \mathbf{x} is influenced by system inputs \mathbf{u} . The control target \mathbf{x} can be obtained by the measured system outputs \mathbf{y} . The controller design process finds the suitable inputs \mathbf{u} to achieve the specific system performance demands.

Closed-loop control is more resilient to disturbances and variations in the system by incorporating measured system outputs. Figure 1.7 shows the diagram of the closed-loop control system. System dynamic instability and

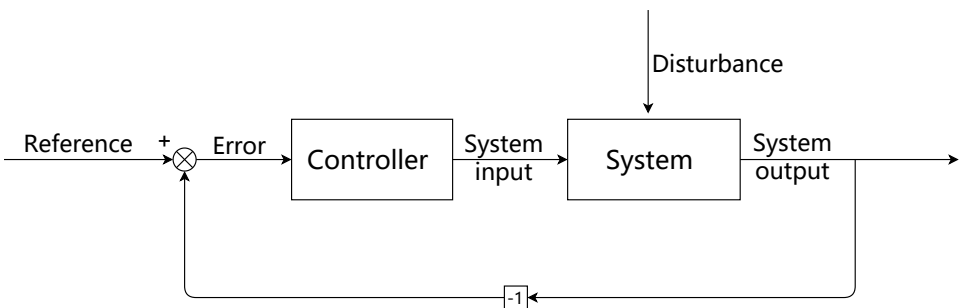


Figure 1.7: Negative feedback control system block diagram. The system input is determined by the deviation between reference and system output.

sensor noises are the possible drawbacks of closed-loop control. This gives the trade-off between reachable system performance and robustness in controller design [22].

The control framework employed in this thesis is optimal control, which represents the control target as a mathematical optimization objective subject to constraints, as shown in Eq. (1.1):

$$\begin{aligned} \min_{\mathbf{u}} \quad & J(\mathbf{u}, \mathbf{x}) \\ \text{subject to} \quad & g(\mathbf{u}, \mathbf{x}, \mathbf{y}) = 0 \\ & f(\mathbf{u}, \mathbf{x}) \leq 0 \end{aligned} \tag{1.1}$$

The cost function J is the mathematical formulation of control objectives like reference tracking. The equality represents the model of the system being controlled, expressing the relation between inputs \mathbf{u} , states \mathbf{x} , and outputs \mathbf{y} . The inequality constraint is the constraint that needs to be fulfilled by \mathbf{u} and \mathbf{x} . This formulation of the control problem is suitable for engine control where the common purposes are minimizing fuel consumption and reference deviation while satisfying the constraints imposed by actuator characteristics, noise, and emission limitations. Typically, the solution near the constraint boundary gives better performance.

The optimization problem of Eq. (1.1) is solved repeatedly cycle by cycle with respect to certain predictive and control horizon and measured outputs. This technique is known as model predictive control (MPC) when the optimization objective includes the prediction horizon and the equality constraints include the state-space equations. MPC has gained academic attention and shown successful applications in many areas including process control, automotive control, and advanced engine concept control. More details about the control approach can be found in Chapter 3.

Intuitively, an adaptive or learning controller is a controller that can adjust its behavior in response to changes in the dynamics of the process and the character of the disturbances [20].

Learning control concepts have gained attention from multiple research areas including control and computer science disciplines under different names. Reinforcement learning, a learning optimal control approach which originated from the control society, has been a vigorous topic nowadays in artificial intelligence research. Combining optimal control and statistical learning methods also shows successful applications in recent years [23], [64], [152].

Those methods normally require much higher computational resources than traditional control methods, however, the rapidly growing computing power gives space and possibility for them.

For the optimal control problem of Eq. (1.1), the adaptivity means the cost function J , the system model g , and the constraints f are changing according to varying system dynamics.

In this thesis, the main focus is the learning ability of the system model g , whose ability to describe the system is vital for the controller performance.

The modeling methods conventionally contain the white-box model, grey-box model, and black-box model. A white-box model is a purely theoretical and normally physical-based model which commonly lacks the learning ability. A grey-box model, which is partially theory-based and partially data-based, collects information from data to complete the theoretical structure and has the adaptivity to the environment changes. Furthermore, the pure data-based model, the black-box model, concerns the system inputs and outputs relations without consideration of its internal working mechanisms. Black-box models encapsulate the as of now hot machine learning methods, such as support vector machines (SVM), Gaussian processes (GP), and neural networks (NN). Statistical modeling is another way of black-box modeling. Black-box models usually have more parameters than grey-box models, requiring more data for parameter estimation and more careful regulation to ensure controller stability. A comparison of grey-box modeling and black-box modeling for the flex-fuel engine is detailed Sec. 2.3.3.

Flex-fuel engine control

For the engine control process, the system performance includes combustion efficiency, noise, and emission levels while satisfying certain system constraints.

Traditionally, CI engine control uses the open-loop form. The fuel injection amounts are decided by a calibrated map of engine speed, accelerator pedal position, and air-fuel ratio concerning the output work. The injection times are normally determined by predefined maps [66]. The open-loop control is simple and effective for diesel CI engines due to the stability of the conventional diesel combustion mode. When various fuels and combustion modes are used, the open-loop control fails to handle the various combustion situations and noises introduced to the system.

The work in this thesis concerns the decision of fuel injection timings and duration and gas system valve opening to control the engine combustion process using the measured in-cylinder pressure signal as the feedback. The solenoid injector connected to the common-rail fuel system is the actuator for injection. The injection timing is controlled by the solenoid injector opening timing and the fuel injection quantity is controlled by the injector nozzle opening duration and common-rail pressure. The solenoid injector is driven by current pulses. A detailed description can be found in [36]. The gas system includes the variable geometry turbocharger (VGT) system, low-pressure exhaust gas recirculation (EGR) system, and a thermal management system. The gas system actuators are the EGR valve, the VGT valve, and a hot and cool valve controlling the intake oxygen concentration, pressure, and temperature.

Flex-fuel engine CI operating with more than two different fuels and the fuel transition can happen any time during engine operation. The combustion process is sensitive to the inlet conditions and the cylinder mixture composition. This puts high demands on the engine controller design. In this case, the feedback in-cylinder pressure signal is necessary to collect information about current running fuel and to reduce the combustion sensitivity. The main goals of the controller are to maintain the combustion phases like ignition delay and combustion timing following set-points which should be properly controlled and shaped to achieve clean and efficient combustion.

When operating with a gasoline mixture in CI engines, the high pressure rise rate as a result of the high combustion rate is an identified issue. Introducing a pilot injection is a solution to this problem, which is adopted for all fuel cases.

The unknown fuel composition changes during flex-fuel CI engine operation bring up the main control challenge. When operating only on gasoline and ethanol, the flex-fuel SI engine primitive task is the detection of ethanol concentration in the fuel. This can be done by using an ethanol sensor, or by exploiting the difference in stoichiometric air-to-fuel ratio or the latent heat of vaporization between ethanol and gasoline [13]. Once the volumetric ethanol concentration is determined, the fuel properties can be assumed all known, and further control algorithms are applied. However, the flex-fuel CI engine is expected to operate on more than two specific fuels. Unlike the flex-fuel SI engine, the flex-fuel CI engine doesn't know the fuel species in advance. Consequently, the control method based on detecting specific fuel concentrations, and thus getting the exact fuel-property information will

not work. In this case, a predefined system model is insufficient to fulfill the control task under unknown dynamically changing circumstances. In the worst cases, it could cause a system failure or, at least, interruption of operation. Thus, the adaptivity of the controller is required to deal with the flex-fuel scenario.

Fuel cell control

The target of fuel cell control in this work is to ensure continuous operation at steady voltage under the workload disturbance by manipulating the hydrogen and air flow rate. This is an important demand in electrical equipment usage [95], [165]. The workload of the fuel cell is categorized by its current. Efficient and robust control strategies are considered as one of the key solutions to ensure the fuel cell system's high reliability [97].

1.5 Motivations and contributions

There were some unique challenges in the flex-fuel CI engine and fuel cell control. For the flex-fuel CI engine, this work was the first application of the flex-fuel concept on a CI engine. What modeling and control method should be used in this concept? The research of the flex-fuel SI engine and the PPC engine gave some knowledge [13], [81], [179], but fuel species choices of SI engine and CI engine were different. The flex-fuel SI engine only needed to know the ratio between ethanol and gasoline, while the fuel species is unknown for a flex-fuel CI engine. What modeling and control method should be adopted to deal with the variation and uncertainty in a flex-fuel CI engine? There was no other literature on this specific question yet. For the fuel cell control, what was the systematic way to integrate machine learning modeling methods and control approach under safety requirements? The black-box nature of the data-based modeling method brought a challenge to constraint handling. There was some work regarding the machine learning modeling methods for fuel cell [68], [120], [184], [188] and also some work regarding the control methods with data-based models [60], [149], [187], but the way to handle data-based models and constraints was not well studied.

The main motivation of this work was to develop the control framework for flex-fuel CI engines and fuel cells. This work mainly answered two categories of research questions: the modeling part and the control approach. For the modeling, how to model the variation in the combustion process caused by

variable fuel properties in a flex-fuel CI engine? This work used ignition delay to reflect the fuel properties, where the adaptivity to changing fuel properties was done by parameter estimation with Kalman filter. Which data-based modeling method is suitable for fuel cell control usage under safety requirements? This work investigated the Gaussian process, where the prediction variance was used for constraints handling under uncertainty. What were the advantages and disadvantages of the different modeling methods in the flex-fuel CI engine and fuel cell applications? The physical models had good interpretability while needing expert knowledge, and the data-based model gave a good performance with enough data but was a black-box. They can both be successfully adopted in an MPC framework. For the control approach, how did MPC behave in the flex-fuel CI engine and fuel cell control task, did it able to achieve the control performance while handling the constraints with different models? This work showed that MPC was a flexible framework that worked in both scenarios. It could incorporate both the physical models and data-based models. The constraint handling ability of MPC made it desirable when facing safety requirements. What modifications should be made in MPC to deal with the black-box nature of data-based modeling? For the Gaussian process model, the prediction variance was included in the constraints under a statistic MPC style. This helped give a comparative performance of MPC controller with the knowledge of underlying system dynamics.

The contribution of this work was that it made a step from the flex-fuel SI engine to the flex-fuel CI engine, and broaden the fuel choices. Besides, it provided an MPC framework to handle the fuel cell control problem with safety requirements, even with black-box data-based models. In this work, models describing the engine gas system dynamic, ignition delay, and fuel cell characteristics were designed and explored. Investigated models included physical models and data-based models. The MPC approach was proposed for the flex-fuel CI engine and fuel cell based on the models. This study was limited to CI engines and PEFC fuel cells. Only cycle-to-cycle engine control was studied. Only macro performances of fuel cells with the length scale being above centimeters were considered.

1.6 Thesis outline

The thesis outline is as follows. Chapter 2 describes the detailed models and their validation, including a flex-fuel engine in-cylinder model, gas system model, and ignition delay model, and fuel cell system scale model. Chapter 3

includes a review of the control and estimation methods. Chapter 4 shows the experimental setup in this work. Chapter 5 gives the MPC approaches for the flex-fuel engine and the fuel cell. An adaptive MPC approach for flex-fuel CI engine based on the physical ignition delay model was proposed and tested in fuel transitions including diesel, gasoline/n-heptane, and ethanol/n-heptane. An MPC approach with constraints control was developed to keep the fuel cell voltage at a reference value under current disturbances while satisfying the hydrogen pressure safety constraints. Chapter 6 presents learning-based MPC approaches. Learning-based MPC combining the physical-based model and the data-based learning model is shown and applied to CI engine combustion process control. A Gaussian-process MPC controller is detailed and used for fuel-cell voltage control. Chapter 7 contains the summary and conclusions.

2.1 Introduction

Efforts for modeling have been made in different levels of complexity and detail.

The modeling process for the engine includes multiple areas such as thermodynamics, fluid mechanics, and chemical kinetics. Of those models, computational fluid dynamics (CFD) provides the most detailed and complicated model. CFD solves partial differential equations by numerical computing methods to describe the dynamic engine working process in high temporal and spatial resolution with consideration of detailed chemical reactions. CFD has been applied to investigate advanced combustion concepts such as fuel spray and flame characteristics [8], [96], [141], [180]. CFD models are also applied to study fuel-cell characteristics. It is used to simulate the fluid flow, heat transfer, electrochemical reaction, and species transport in different PEFC settings [71], [112], [144]. It helps the understanding and explanation of physical phenomena due to the in-depth description. However, the CFD model simulation can take a lot of time ranging from hours to months even with the help of supercomputers, making it impractical for real-time control applications.

Zero-dimensional (0D) models utilize mean variables over space, such as mean temperature and pressure inside the cylinder, to represent the engine. This

approach has a much lower complexity as compared to CFD models, making it possible to be used in real-time control applications. Normally zero-dimensional models are obtained from first principles along with empirical parameters. Despite the low spatial resolution, zero-dimensional models may have a satisfactory temporal resolution in engine behavior prediction. The engine zero-dimensional models are widely used. Examples can be found in [29], [50], [51], [93], [127].

For gas system modeling, the dynamics are slower than the cycle-based combustion process. The characteristic is utilized by averaging over certain engine cycles, assuming faster processes to be static [52]. This method results in a low spatial resolution mean-value model, which is also called control-oriented models for its application in the control context. Although still complicated, the system scale model goes further towards the control-oriented model as compared to other more fine-grained models.

Instead of deriving physical-based models from first principles, data-based modeling exploits the observed input-output data to obtain the prediction model. It focuses on the model representation capability instead of the inner physical laws [77]. This approach has a wide branch of methods, from linear regression to statistical models, and artificial neural networks with hundreds or thousands of parameters. Although originated from system identification in the control area [109], it develops actively beyond the control discipline and has been vigorous in multiple areas under various new names. One advantage of data-based modeling is its universality [123]. Using the same methodology with minor modifications, one modeling method can be applied to different plants. For example, the Gaussian process is built for both engine and fuel cell in this work.

Some data-based models, characterized by large numbers of parameters, have a strong ability to represent nonlinearities. This kind of model has gained success in areas where the system nonlinearity is too complicated to be built as an explicit model by human experts. For example, a convolutional neural network (CNN) can achieve or exceed the human average level in the image recognition task [58]. Though normally more complicated than zero-dimensional models and requiring a longer time for training, the data-based model prediction time is relatively short and useful in real-time control with contemporary hardware. In the engine control area, the data-based model applications include emission system modeling, cylinder pressure information extraction, engine performance modeling and optimization, misfire detection, etc. [25], [74], [75], [156], [169]. For fuel-cell control, applications include neural networks and support vector machines for

polymer electrolyte membrane fuel cell modeling, diagnosis, and prediction [103], [111], [128].

In this work, the in-cylinder processes were modeled using a zero-dimensional model on a crank angle resolved base. The gas systems were modeled by mean value models with suitable simplification for control purposes. The ignition delay, one key indicator for variable fuel properties, was modeled by empirical chemical reaction expressions and data-based models. The fuel cell was modeled with detailed system scale physical models as well as data-based methods.

2.2 Data-based modeling

There exist many approaches designed for linear dynamic system identification [86]. However, for the non-linear system identification, such as the flex-fuel CI engine and fuel cell considered here, more sophisticated methods are needed. Standard choices include fuzzy models, neural networks, and some other machine learning models. The Gaussian process is also one frequently used method [135].

Gaussian process

The Gaussian process is a probabilistic black-box model. It searches the relationship between measured data instead of optimizing the parameters of the chosen functions to fit data. A Gaussian process is defined as a collection of random variables, any finite number of variables which have a joint Gaussian distribution [139]. A Gaussian process can be fully defined by a mean function $\bar{f}(\mathbf{x})$ and covariance function $k(\mathbf{x}, \mathbf{x}')$:

$$f(\mathbf{x}) \sim \mathcal{GP}(\bar{f}(\mathbf{x}), k(\mathbf{x}, \mathbf{x}')) \quad (2.1)$$

where \mathbf{x} is one data point with dimension d ; the same is true for \mathbf{x}' . The $k(\mathbf{x}, \mathbf{x}')$ is also called the kernel function. The mean function $\bar{f}(\mathbf{x})$ is assumed to be zero to simplify the analysis.

The observations y are represented by the variable:

$$y = f(\mathbf{x}) + e, \quad e \sim \mathcal{N}(0, \sigma_n^2) \quad (2.2)$$

where e is the additive independent identically distributed Gaussian noise with variance σ_n^2 .

Assuming there are n training points and n^* test points, when making inferences, the prior is:

$$\begin{bmatrix} \mathbf{y} \\ \mathbf{f}^* \end{bmatrix} \sim \mathcal{N} \left(\mathbf{0}, \begin{bmatrix} K(\mathbf{X}, \mathbf{X}) + \sigma_n^2 \mathbf{I} & K(\mathbf{X}, \mathbf{X}^*) \\ K(\mathbf{X}^*, \mathbf{X}) & K(\mathbf{X}^*, \mathbf{X}^*) \end{bmatrix} \right) \quad (2.3)$$

where (\mathbf{X}, \mathbf{y}) are the training data with dimension $n \times d$ and $n \times 1$, respectively; \mathbf{X}^* contains the test data points with dimension $n^* \times d$ on which the prediction is made; \mathbf{f}^* are the n^* dimension predicted value; $K(\mathbf{X}, \mathbf{X}^*)$ denotes the $n \times n^*$ matrix of the covariances evaluated at all pairs of training and test points, and similarly for $K(\mathbf{X}, \mathbf{X})$, $K(\mathbf{X}^*, \mathbf{X}^*)$ and $K(\mathbf{X}^*, \mathbf{X})$. Those matrices constitute the covariance matrix of size $(n + n^*) \times (n + n^*)$.

The posterior is:

$$\mathbf{f}^* | \mathbf{X}^*, \mathbf{X}, \mathbf{y} \sim \mathcal{N} (\mathbb{E}\{\mathbf{f}^*\}, \text{cov}\{\mathbf{f}^*\}) \quad (2.4)$$

where

$$\begin{aligned} \mathbb{E}\{\mathbf{f}^*\} &= K(\mathbf{X}^*, \mathbf{X}) [K(\mathbf{X}, \mathbf{X}) + \sigma_n^2 \mathbf{I}]^{-1} \mathbf{y} \\ \text{cov}\{\mathbf{f}^*\} &= K(\mathbf{X}^*, \mathbf{X}^*) - K(\mathbf{X}^*, \mathbf{X}) [K(\mathbf{X}, \mathbf{X}) + \sigma_n^2 \mathbf{I}]^{-1} K(\mathbf{X}, \mathbf{X}^*) \end{aligned} \quad (2.5)$$

General GP regression is equivalent to Bayesian linear regression with an infinite number of basis functions.

The kernel functions adopted in this work include the squared exponential kernel (Gaussian kernel) and the Matérn kernel [59]. The squared exponential kernel is defined as:

$$k_{SE}(\mathbf{x}, \mathbf{x}') = \sigma^2 \exp\left(-\frac{\|\mathbf{x} - \mathbf{x}'\|^2}{2l^2}\right) \quad (2.6)$$

where the l is the length scale and σ is the signal standard deviation; the $\|\mathbf{x} - \mathbf{x}'\|$ is the Euclidean norm of $\mathbf{x} - \mathbf{x}'$, and represents the distance between \mathbf{x} and \mathbf{x}' .

The Matérn kernel with a specification of 5/2 [10] is:

$$k_{5/2}(\mathbf{x}, \mathbf{x}') = \sigma^2 \left(1 + \frac{\sqrt{5} \|\mathbf{x} - \mathbf{x}'\|}{l} + \frac{5 \|\mathbf{x} - \mathbf{x}'\|^2}{3l^2} \right) \exp\left(-\frac{\sqrt{5} \|\mathbf{x} - \mathbf{x}'\|}{l}\right) \quad (2.7)$$

The length scale l can be interpreted as the reflection of how close the points \mathbf{x} and \mathbf{x}' have to be to influence each other significantly. When the length

scale l is a scalar, the kernel is isotropic. In contrast, when the length scale is different for each dimension of data points, the kernel is called an automatic relevance determination (ARD) kernel [139]. The ARD kernel allows the model to determine the separate relevance for every dimension, providing a feature selection ability. In this case, the length scale related expressions in Eq. (2.6) and Eq. (2.7) are changed to a summation form. The addition of kernels is also possible and extends the model flexibility.

The optimal parameters of the GP are found by maximizing the log marginal likelihood:

$$\log p(\mathbf{y}|\mathbf{X}, \boldsymbol{\theta}) = -\frac{1}{2}\mathbf{y}^T \mathbf{K}_y^{-1} \mathbf{y} - \frac{1}{2} \log \|\mathbf{K}_y\| - \frac{n}{2} \log 2\pi \quad (2.8)$$

where $\mathbf{K}_y = K(\mathbf{X}, \mathbf{X}) + \sigma_n^2 \mathbf{I}$ is the covariance matrix for the noisy targets \mathbf{y} ; n is the number of training points; $\boldsymbol{\theta}$ are the hyperparameters, including the length scale of each dimension and signal and noise variance.

For more details about Gaussian processes, see [139].

Neural network

A neural network is a connectionist system inspired by a biological neural network in the animal brain [15]. It makes great success in several topics and has been a hot research area in recent years due to the massive data available and cheap computational power. Normally, it is constituted by the input layer, hidden layers, and output layer. An illustration diagram of its structure can be found in Fig. 2.1. There can be more than one hidden layer in the network. A neural network with multiple hidden layers is also called a deep neural network. Each circle in Fig. 2.1 is a node, or a neuron, with an activation function defining the output with respect to the inputs after an affine transformation. Many kinds of activation functions are available. Each arrow shows a data flow.

For each hidden node, the output is:

$$\begin{aligned} \mathbf{h}(\mathbf{x}) &= g(\mathbf{w}^T \mathbf{x} + \mathbf{b}) \\ g(z) &= \max(0, z) \end{aligned} \quad (2.9)$$

where \mathbf{h} and \mathbf{x} are the unit outputs and inputs; \mathbf{w} and \mathbf{b} are the parameters to be optimized on; $g(z)$ is the activation function adopted in this work, which is called the rectified linear unit (ReLU).

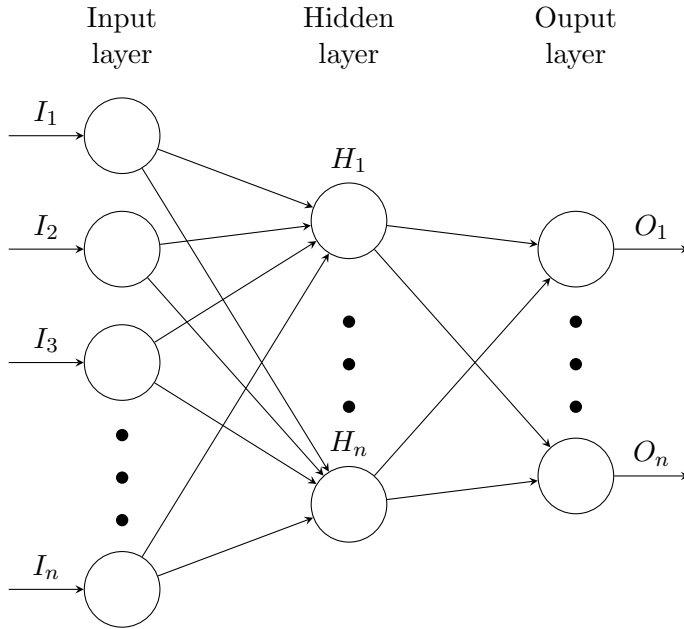


Figure 2.1: Neural network structure

2.3 Flex-fuel engine model

2.3.1 In-cylinder model

The objective of the in-cylinder model is to investigate the combustion process and obtain the feedback signals from the measured in-cylinder pressure data.

Heat release rate

The assumption for the model is that the in-cylinder gas is a closed thermodynamic system when in the closed part of the cycle whose boundary is the combustion chamber. An illustration of the thermodynamic system is shown in Fig. 2.2.

From the first law of thermodynamics, the system fulfills the following energy balance equation:

$$dU = dQ - dW \quad (2.10)$$

where the dU is the system internal energy change; dW is the work; dQ is

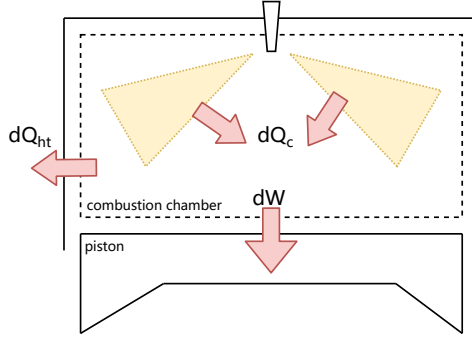


Figure 2.2: Closed thermodynamic system with the combustion chamber as the boundary. The combustion release heat dQ_c into the system; the cylinder gas performs work dW on the piston; dQ_{ht} is the heat transferred through cylinder walls.

the absorbed energy; dQ includes the dQ_c , the energy from combustion, and the dQ_{ht} , the heat transferred to outside.

For simplicity, the heat loss dQ_{ht} is assumed to be 0. Then the dQ equals the dQ_c , the heat released from combustion. It is a simplification to regard the dQ_c as heat addition [57].

For the isochoric process, the internal energy change is proportional to temperature change:

$$dU = nC_v dT \quad (2.11)$$

where n is the number of moles of the gas substance; C_v is the constant-volume molar specific heat; T is the cylinder temperature.

The ideal gas law shows:

$$pV = nRT \quad (2.12)$$

where p is the cylinder pressure, measured by the piezoelectric cylinder-pressure sensor; V is the volume; R is the gas constant.

Combining Eqs. (2.10), (2.11), and (2.12), the heat release rate dQ is expressed as:

$$\begin{aligned} dQ &= dU + dW \\ &= \frac{C_v}{R} d(pV) + p dV \\ &= \frac{C_v + R}{R} p dV + \frac{C_v}{R} V dp \end{aligned} \quad (2.13)$$

The constant volume molar specific heat C_v and constant pressure molar specific heat C_p has:

$$C_p - C_v = R \quad (2.14)$$

which then gives:

$$dQ = \frac{C_p}{C_p - C_v} p dV + \frac{C_v}{C_p - C_v} V dp \quad (2.15)$$

The exponent ratio γ is the ratio of specific heats:

$$\gamma = \frac{C_p}{C_v} \quad (2.16)$$

Then Eq. (2.15) is:

$$dQ = \frac{\gamma}{\gamma - 1} p dV + \frac{1}{\gamma - 1} V dp \quad (2.17)$$

Cylinder geometry

The cylinder volume is calculated as a function of crank angle degrees (CAD, θ):

$$\begin{aligned} V(\theta) &= V_c + \frac{V_d}{2} \left(R_v + 1 - \cos\left(\frac{\pi\theta}{180}\right) - \sqrt{R_v^2 - \sin^2\left(\frac{\pi\theta}{180}\right)} \right) \\ V_c &= \frac{\pi d^2}{4} \frac{s}{r_c - 1} \\ V_d &= \frac{\pi d^2}{4} s \\ R_v &= \frac{2l}{s} \end{aligned} \quad (2.18)$$

where V_c is the clearance volume; V_d is the displacement volume; r_c is the effective compression ratio; d is the piston diameter; s is the crankshaft diameter, which equals to the stroke length; l is the connecting rod length.

Temperature

Viewing the in-cylinder condition at intake valve closing (IVC) as the initial condition, the in-cylinder temperature is given by the ideal gas law:

$$\frac{pV}{T} = \frac{p_{IVC} V_{IVC}}{T_{IVC}} \quad (2.19)$$

where p_{IVC} , V_{IVC} , and T_{IVC} are the pressure, volume, and temperature at intake valve closing. The T_{IVC} is assumed equal to the inlet temperature at IVC.

Ratio of specific heats

The exponent ratio γ changes with both temperature T and gas composition [94]. Nevertheless, a simplified approach is adopted in this work. The effect of gas composition is ignored, and γ is expressed as:

$$\gamma = \gamma_0 - 0.0813 \cdot \frac{T - 300}{1000} \quad (2.20)$$

where γ_0 can be determined according to Heywood [78], which is 1.3736 in this work.

Combustion phases

The accumulated heat-release Q_c is computed by calculating the integral of Eq. (2.17). The variables θ_{CA10} , θ_{CA50} and θ_{CA90} are defined as the crank angle after top dead center (CAD ATDC) where 10%, 50% and 90% of the total heat are released. They are calculated by finding the crank angle degree location where the corresponding ratio of total heat Q_c is released, θ_{CA10} being defined as the start of combustion, θ_{CA50} being the combustion timing and $\theta_{CA90} - \theta_{CA10}$ being the combustion duration.

Load and efficiencies

The gross-indicated and net-indicated mean effective pressure are the normalized work on the piston done by cylinder gas in the closed part of the cycle and the complete cycle, denoted as p_{IMEPg} and p_{IMEPn} , respectively. The closed part is the duration between the intake valve closing and exhaust valve opening (EVO). They are calculated by taking integral using measured cylinder pressure and calculated cylinder volume:

$$\begin{aligned} p_{IMEPg} &= \frac{1}{V_d} \int_{IVC}^{EVO} p dV \\ p_{IMEPn} &= \frac{1}{V_d} \oint p dV \end{aligned} \quad (2.21)$$

The fuel-conversion efficiencies then calculated by:

$$\eta_g = \frac{p_{\text{IMEPg}} V_d}{m_f Q_{\text{LHV}}} \quad (2.22)$$

$$\eta_n = \frac{p_{\text{IMEPn}} V_d}{m_f Q_{\text{LHV}}}$$

where η_g and η_n are the gross efficiency and net efficiency; m_f is the fuel amount injected into the cylinder; Q_{LHV} is the fuel lower heating value. η_n considers the pumping loss.

Together with combustion phasing, load and efficiencies are the standard choices of the control targets and feedback variables.

2.3.2 Gas system models

The gas system layout used in the experiment is shown in Fig. 2.3.

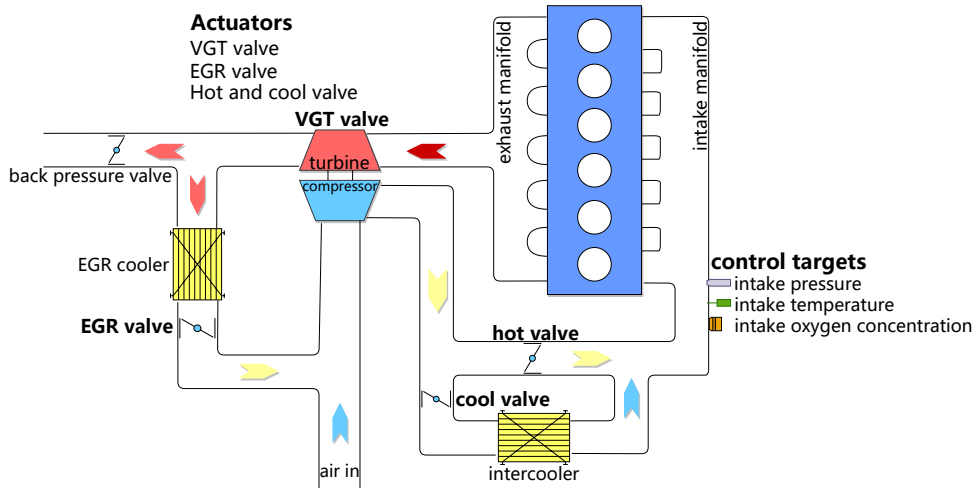


Figure 2.3: Engine gas system layout. The engine is boosted by a variable-geometry turbocharger (VGT). Low pressure exhaust gas recirculation (EGR) is supplied.

The air came from the atmosphere compressed by the VGT. Then the air went partly through the intercooler and partly the direct path, with path opening determined by the cool and hot valves. After combustion, the exhaust expanded through the turbine controlled by the VGT valve, which drove the compressor to compress intake air. Part of the exhaust entered the low-

pressure EGR path, whose mass flow was related to the position of the EGR valve.

The target of this section is to build models suitable for control purposes describing the relationship between actuators EGR, VGT, hot and cool valves to inlet conditions including intake temperature, pressure, and oxygen concentration.

Intake oxygen concentration

The intake oxygen concentration was measured by a wideband zirconia sensor mounted in the intake manifold. The wideband sensor, also called the universal exhaust gas oxygen (UEGO) sensor, utilized a planar zirconia element and an electrochemical gas pump to eliminate the lean-rich cycling characteristics of narrow-band sensors [175]. The measured oxygen concentration value was not the actual oxygen concentration in the gas, but a function depending on the oxygen partial pressure which influences the pump current.

A simplified relationship of the measured oxygen concentration is:

$$O_{2\text{in}} = K_{O_2} p_{O_2} + \text{offset} \quad (2.23)$$

where $O_{2\text{in}}$ is the measured intake oxygen concentration in percentage; K_{O_2} is the coefficient needed to be determined; offset is a constant value; p_{O_2} is the oxygen partial pressure in the gas, which can be expressed as:

$$p_{O_2} = \frac{p_{\text{in}}}{T_{\text{in}}} \left(\frac{w_{\text{air}}}{w_{\text{air}} + w_{\text{EGR}}} \right) O_{2\text{air}} \quad (2.24)$$

where p_{in} , T_{in} are the intake pressure and temperature; $O_{2\text{air}}$ is the oxygen percentage at atmosphere; w_{air} and w_{EGR} are the air and EGR mass flow. Here the mass is used instead of moles, between which a constant proportional conversion relation exists. The conversion coefficient is viewed as part of the K_{O_2} coefficient. The reason for using this expression is that mass flow is consistent with the following process models.

By differentiation, we get:

$$\begin{aligned} dO_{2\text{in}} = & K_{O_2} \frac{1}{T_{\text{in}}} \left(\frac{w_{\text{air}}}{w_{\text{air}} + w_{\text{EGR}}} \right) O_{2\text{air}} dp_{\text{in}} \\ & + K_{O_2} \frac{p_{\text{in}}}{T_{\text{in}}} \left(\frac{-w_{\text{air}}}{(w_{\text{air}} + w_{\text{EGR}})^2} \right) O_{2\text{air}} dw_{\text{EGR}} \end{aligned} \quad (2.25)$$

which is used for oxygen concentration variation prediction and suitable for control purposes.

The variable dp_{in} is detailed in the next subsection. For the mass flow modeling, the methods in this work are inspired by [163], and w_{EGR} is modeled as compressible flow through changing area:

$$dw_{\text{EGR}} = \frac{A_{\text{em}} p_t \Phi_{\text{EGR}}}{\sqrt{T_t} R_e} du_{\text{EGR}} \quad (2.26)$$

where p_t and T_t are the pressure and temperature of the exhaust gas after the turbine; A_{em} is the maximum nominal EGR flow area; Φ_{EGR} is the coefficient related to the pressure ratio between the pressure after and before the EGR valve; u_{EGR} is the normalized EGR valve opening; R_e is the exhaust gas constant.

The variable u_{EGR} is defined by:

$$u_{\text{EGR}} = 1 - e^{-K_{\text{EGR}} \theta_{\text{EGR}}} \quad (2.27)$$

where K_{EGR} is the calibrated coefficient; θ_{EGR} is the actual EGR valve opening.

The variable Φ_{EGR} is:

$$\begin{aligned} \Phi_{\text{EGR}} &= 1 - \left(\frac{1 - \phi_{\text{EGR}}}{1 - \phi_{\text{opt}}} - 1 \right)^2 \\ \phi_{\text{opt}} &= \left(\frac{2}{\gamma_e + 1} \right)^{\frac{\gamma_e}{\gamma_e - 1}} \\ \phi_{\text{EGR}} &= \begin{cases} \phi_{\text{opt}}, & \frac{p_{\text{EGR}}}{p_t} < \phi_{\text{opt}} \\ \frac{p_{\text{EGR}}}{p_t}, & \phi_{\text{opt}} \leq \frac{p_{\text{EGR}}}{p_t} \leq 1 \\ 1, & 1 < \frac{p_{\text{EGR}}}{p_t} \end{cases} \end{aligned} \quad (2.28)$$

where ϕ_{EGR} is the pressure ratio; ϕ_{opt} is the optimal pressure ratio; γ_e is the exhaust gas heat capacity; p_{EGR} is the pressure after the EGR valve and p_t is the pressure after VGT, before the EGR valve.

Intake pressure

From the ideal gas law, the differential of intake pressure satisfies:

$$dp_{\text{in}} = \frac{R_a}{V_{\text{in}}} T_{\text{in}} dm + \frac{R_a}{V_{\text{in}}} m dT_{\text{in}} \quad (2.29)$$

where p_{in} , V_{in} and T_{in} are the intake pressure, intake manifold volume and intake temperature; R_a is the intake gas constant; m is the gas mass in intake manifold.

The variable dT_{in} is described in the next subsection. For dm , the following relation holds:

$$dm = (w_c - w_{\text{ei}})dt \quad (2.30)$$

where w_c is the compressor mass flow and w_{ei} is the mass flow into the cylinder; dt is the time step length chosen according to the application scenario. For simplicity, assuming at the start of the time step that $w_c = w_{\text{ei}}$ and that w_{ei} is constant during one time step, then the intake mass changes is only caused by the compressor mass flow changes dw_c , which gives:

$$dm = dw_c dt \quad (2.31)$$

The variable dw_c is modeled as:

$$dw_c = K_c dn_t \quad (2.32)$$

$$K_c = \frac{p_{\text{amb}} \pi R_c^3 \phi_c}{R_a T_{\text{amb}}} \quad (2.33)$$

where p_{amb} and T_{amb} are ambient pressure and temperature; R_c is the compressor blade radius; ϕ_c is the volumetric flow coefficient which is simplified as a constant in this work; n_t is the turbocharger speed.

The variable dn_t can be modeled as:

$$dn_t = \frac{P_t \eta_m - P_c}{n_t J_t} dt \quad (2.34)$$

where P_t and P_c are the turbocharger and compressor power; η_m is the mechanical efficiency, a constant; J_t is the rotating inertia of the turbocharger.

Similar to the simplification of Eq. (2.30), assuming $P_t \eta_m = P_c$ at the start and P_c constant during the time step, Eq. (2.34) becomes:

$$dn_t = \frac{\eta_m}{n_t J_t} dP_t dt \quad (2.35)$$

The variable dP_t is:

$$dP_t = c_{\text{pe}}(T_{\text{ex}} - T_t)dw_t \quad (2.36)$$

where T_{ex} is the exhaust manifold temperature and c_{pe} is the heat capacity of the exhaust gas; w_t is the turbine mass flow.

According to Eq. (2.26), dw_t is given by:

$$dw_t = \frac{A_{vm} p_{ex} \phi_t}{\sqrt{T_{ex} R_e}} du_{VGT} \quad (2.37)$$

$$u_{VGT} = 1 - e^{-K_{VGT} \theta_{VGT}} \quad (2.38)$$

where p_{ex} and T_{ex} are the pressure and temperature of the exhaust manifold gas; A_{vm} is the maximum nominal VGT flow area; u_{VGT} is the normalized VGT valve opening with K_{VGT} as coefficient need to be calibrated; θ_{VGT} is the actual VGT valve opening; ϕ_t is the turbocharger volumetric flow coefficient:

$$\phi_t = \sqrt{1 - \left(\frac{p_t}{p_{ex}}\right)^{k_t}} \quad (2.39)$$

where k_t is a constant.

Intake temperature

The air enters both the direct path and the path with an intercooler. The gas leaving the intercooler is assumed to have the same temperature as the intercooler coolant. The intake gas temperature is the mix of two paths:

$$T_{in} = \frac{u_{hot}}{u_{hot} + u_{cool}} T_{hot} + \frac{u_{cool}}{u_{hot} + u_{cool}} T_{cool} \quad (2.40)$$

where T_{hot} is the gas temperature after compressor and T_{cool} is the gas temperature after intercooler; u_{hot} is the normalized effective area:

$$u_{hot} = 1 - \cos\left(\theta_{hot} \frac{\pi}{180}\right) \quad (2.41)$$

The same is true for u_{cool} .

To keep the total effective area constant, we enforce:

$$u_{hot} + u_{cool} = 1 \quad (2.42)$$

Then take the differential of (2.40), we get:

$$dT_{in} = (T_{hot} - T_{cool}) du_{hot} \quad (2.43)$$

Validation

The proposed models were validated with the engine running data. Figure 2.4 shows the model prediction performance in the VGT valve θ_{VGT} changing scenario, where the EGR, hot, and cool valve were kept constant from which we can see that increasing VGT opening would increase not only the intake pressure but also the measured oxygen concentration. This was because of the characteristic of the wideband oxygen sensor, whose pump current was proportional to partial oxygen pressure. The twenty-steps-ahead prediction of the model showed an agreement with the true value and outperforms the null prediction, which simply used the current value as the prediction. The VGT opening increase also raised the intake temperature, which was the unmodelled dynamics. In this case, the model prediction was the same as the null prediction.

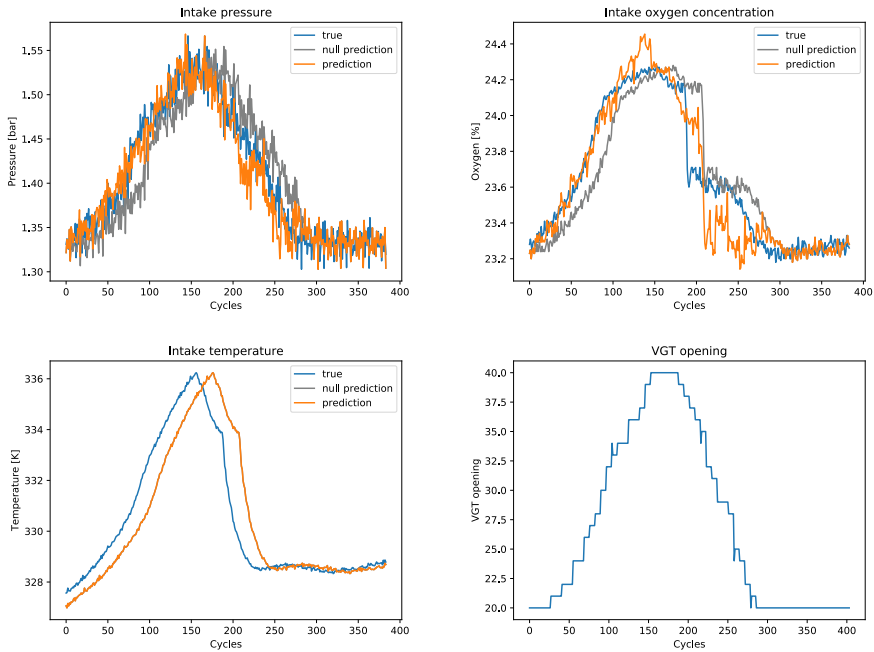


Figure 2.4: Model performance in VGT opening transient

Figure 2.5 shows the twenty-steps-ahead prediction when the hot valve θ_{hot} and cool valve θ_{cool} were changing while EGR and VGT valves were set constant. The change of intake temperature affected the intake temperature, measured oxygen concentration, and intake pressure at the same time. This relation was reflected in the model through the dependency between $dO_{2\text{in}}$,

dp_{in} and dT_{in} . The model showed good consistency to the true value as compared to the null prediction.

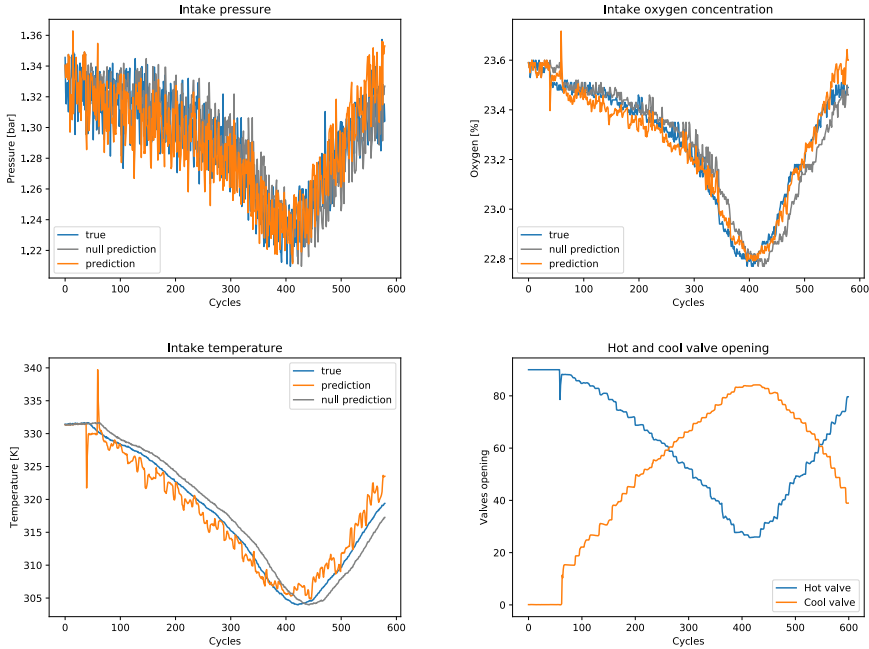


Figure 2.5: Model performance in hot and cool valve transient

Figure 2.6 is the ten-steps-ahead prediction with EGR valve θ_{EGR} and VGT valve θ_{VGT} changing at the same time. Although unmatched dynamics and noises decreased the conformity around cycles 120, 280, and 520 for oxygen concentration, the model made an overall good prediction. Besides, at the cost of model accuracy, the proposed models generated simple linear forms that were desirable for control applications.

Discussion

This work built a gas system model to describe the intake pressure, temperature, and oxygen concentration with the consideration of the EGR and VGT. The performance was validated on a Scania D13 heavy-duty engine. Wahlström and Eriksson gave a thorough gas system model [163] and this work made several simplifications to have a more concise model which is suitable for control application. This avoids the unmeasured state and additional filter in MPC formulation in [178]. Previous work about EGR

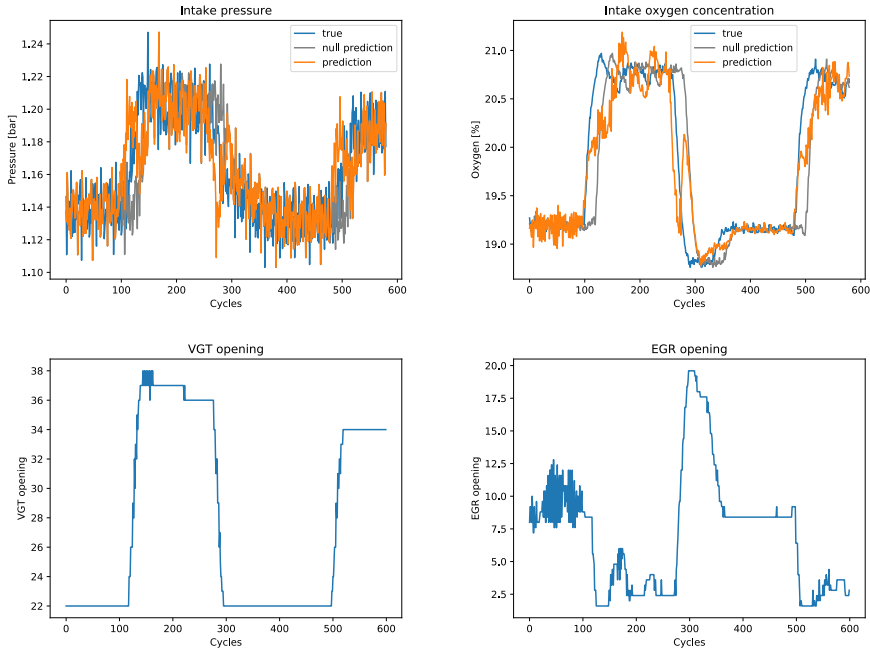


Figure 2.6: Model performance in VGT and EGR opening transient

modeling normally ignored the oxygen sensor characteristic [181], while this work captured the UEGO sensor features and elaborated its relationship to pressure. One drawback of this work was that the transportation delay was not considered. The gas system dynamics were much slower than that of the combustion process, thus the transportation delay should be taken into account when the model was integrated for combustion control.

2.3.3 Ignition delay model

Introduction

This section includes the physical-based model and data-based model for ignition delay and their comparison. The data-based model adopted here is the neural network and Gaussian processes with different structures.

Arrhenius-like expressions are widely adopted in the physical-based ignition delay modeling [82]. It gives the dependence of the chemical reaction rate on temperature, pressure, and reactants concentration. Applications of these

kinds of modeling can be found in [55], [76], [82].

For data-based modeling, a neural network, which has drawn great attention nowadays, is a standard choice. Choi and Chen adopted neural networks to model the ignition delay for fast prediction of the start of combustion in an HCCI engine [43]. Wang et al. applied radial basis function (RBF) network to model the nonlinearities in the SI engine [166]. Zhai et al. utilized a diagonal recurrent neural network for engine modeling in the air-fuel ratio control application [182].

The Gaussian process is another choice that is able to give a measure of uncertainty of the prediction when predicting. Berger et al. analyzed the GP for stationary black-box engine modeling versus other machine learning models [31]. Tietze used GP for model-based calibration of engine control units [158].

Other commonly chosen machine learning methods include support vector machine (SVM) and tree-based models like decision tree under the C4.5 algorithm, whose applications can be found in engine modeling and diagnosis areas [150], [160], [161].

Physical-based model

The ignition delay τ in milliseconds is defined as the time between the start of injection θ_{SOI} and the start of combustion θ_{CA10} . The start of injection θ_{SOI} is the crank angle where the solenoid injector opens. Pilot injections were adopted in this work for promoting combustion and noise reduction. The start of injection θ_{SOI} refers to the main injection timing.

The variable τ being calculated by:

$$\tau = \frac{\theta_{\text{CA10}} - \theta_{\text{SOI}}}{0.006N_s} \quad (2.44)$$

where N_s is the engine speed, with the unit of revolutions per minute, rpm.

The ignition delay τ was estimated using an Arrhenius-type model:

$$\tau = c_1 \exp\left(\frac{c_2}{T}\right) \bar{O}_2^{c_3} \bar{p}^{c_4} \quad (2.45)$$

where c_1 , c_3 , and c_4 are fuel dependent empirical parameters; $c_2 = E_a/R$ where E_a is the apparent activation energy and R is the universal gas constant. For simplicity, the E_a/R in general Arrhenius-type model was represented

by c_2 . The variables $\bar{T}, \bar{O}_2, \bar{p}$ are the mean cylinder temperature, oxygen concentration and pressure between θ_{SOI} and θ_{CA10} .

The adiabatic relation is assumed to hold during this period:

$$pV^\gamma = C \quad (2.46)$$

The in-cylinder pressure p during θ_{SOI} to θ_{CA10} was estimated as:

$$p = p_{\text{IVC}} \left(\frac{V_{\text{IVC}}}{V} \right)^\gamma \quad (2.47)$$

where p_{IVC} is the measured intake pressure at IVC, and V_{IVC} is the cylinder volume at IVC.

The in-cylinder temperature T was computed using the intake manifold temperature at IVC, which gives:

$$T = T_{\text{IVC}} \frac{pV}{p_{\text{IVC}}V_{\text{IVC}}} = T_{\text{IVC}} \left(\frac{V_{\text{IVC}}}{V} \right)^{\gamma-1} \quad (2.48)$$

where T_{IVC} is the measured intake manifold temperature and at IVC.

The oxygen concentration in cylinder was calculated as follows:

$$O_2 = O_{2\text{IVC}} \frac{V_{\text{IVC}}}{V} \quad (2.49)$$

where $O_{2\text{IVC}}$ is the measured intake manifold oxygen concentration in percentage at IVC.

This gives the expression for τ :

$$\tau = c_1 \exp \left(\frac{c_2}{T_{\text{IVC}}T_{\text{co}}} \right) (O_{2\text{IVC}}O_{2\text{co}})^{c_3} (p_{\text{IVC}}p_{\text{co}})^{c_4} \quad (2.50)$$

where the co in subscripts is short for coefficient; the variables $T_{\text{co}}, O_{2\text{co}},$ and p_{co} are:

$$\begin{aligned} T_{\text{co}} &= \frac{\int_{\theta_{\text{SOI}}}^{\theta_{\text{SOI}}+\tau} \left(\frac{V_{\text{IVC}}}{V(\theta)} \right)^{\gamma-1} d\theta}{\int_{\theta_{\text{SOI}}}^{\theta_{\text{SOI}}+\tau} d\theta} \\ O_{2\text{co}} &= \frac{\int_{\theta_{\text{SOI}}}^{\theta_{\text{SOI}}+\tau} \frac{V_{\text{IVC}}}{V(\theta)} d\theta}{\int_{\theta_{\text{SOI}}}^{\theta_{\text{SOI}}+\tau} d\theta} \\ p_{\text{co}} &= \frac{\int_{\theta_{\text{SOI}}}^{\theta_{\text{SOI}}+\tau} \left(\frac{V_{\text{IVC}}}{V(\theta)} \right)^\gamma d\theta}{\int_{\theta_{\text{SOI}}}^{\theta_{\text{SOI}}+\tau} d\theta} \end{aligned} \quad (2.51)$$

The τ in the integration limit was set to the last cycle value when calculating.

Data-based models

The data-based models used for ignition delay modeling are the Gaussian process and neural network described in Sec. 2.2.

Model validation

The data set for model validation was composed of different operation condition data. The fuel choices range from diesel, gasoline/n-heptane mixture to ethanol/n-heptane mixture fuel; the engine speed varied from 1200 rpm to 1500 rpm and the p_{IMEPg} changed from 5 to 8 bar. The detailed experiment set-up can be found in Chapter 4. There were total 14000 data points. The data set was shuffled and divided into five folds. Cross-validation, which takes one fold each round as the test set and other folds as train set and repeats for all sets, was applied to measure the model performance. The results are shown in Table 2.1.

The specifications of GP are the kernel function choice. The specifications of NN refer to the network structure. For example, (3, 64, 256, 64, 1) means that the NN input layer has three nodes and the output layer has one node, and NN has three hidden layers with 64, 256, and 64 nodes, respectively.

The physical model had the worst performance due to a limited number of parameters and model imperfection. Besides, adding new inputs to the

Table 2.1: Model performance comparison

Model	Specifications	Inputs (Features)	RMSE (Error)
Physical	None	p_{in}, T_{in}, O_{2in}	0.429 (24.44%)
GP	Matérn 5/2	p_{in}, T_{in}, O_{2in}	0.192 (10.95%)
	Matérn 5/2	$p_{in}, T_{in}, O_{2in}, p_{IMEPg}, N_s$	0.027 (9.31%)
NN	Matérn 5/2	$p_{in}, T_{in}, O_{2in}, p_{IMEPg}, N_s, \theta_{SOI}$	0.089 (5.06%)
	(3, 10, 1)	p_{in}, T_{in}, O_{2in}	0.343 (19.58%)
	(3, 10, 20, 10, 1)	p_{in}, T_{in}, O_{2in}	0.227 (12.92%)
	(3, 64, 256, 64, 1)	p_{in}, T_{in}, O_{2in}	0.178 (10.17%)
	(5, 64, 256, 64, 1)	$p_{in}, T_{in}, O_{2in}, p_{IMEPg}, N_s$	0.144 (8.19%)
	(6, 64, 256, 64, 1)	$p_{in}, T_{in}, O_{2in}, p_{IMEPg}, N_s, \theta_{SOI}$	0.093 (5.28%)
	(6, 64, 128, 256, 512, 512, 256, 128, 64, 1)	$p_{in}, T_{in}, O_{2in}, p_{IMEPg}, N_s, \theta_{SOI}$	0.090 (5.13%)

physical model required modeling efforts by human experts, whereas the data-based models were more flexible to include relevant inputs as features that won't change the basic structure much. For GP models, adding more features would increase the performance effectively. The same improvement could be seen in NN from network structure (3, 64, 256, 64, 1), (5, 64, 256, 64, 1) to (6, 64, 256, 64, 1). On the other hand, a more complicated network structure would improve the performance, as shown in the three features case with NN structure from (3, 10, 1), (3, 10, 20, 10, 1) to (3, 64, 256, 64, 1) since a complicated structure had a stronger representation ability. But after a certain NN complexity limit, the accuracy improvement was negligible. With the same features, GP behaved competitively to NN.

Discussion

This section only concerned modeling with collected offline data. A more meaningful approach should be the online adaptation performance in real-time.

Although data-based modeling often had higher accuracy in prediction, it encountered some difficulties in the control application. The extrapolation ability of data-based methods might be worse than that of physical models, which was one key drawback. Besides, the nonlinearity of the data-based model required nonlinear optimization techniques which put more computational burden on the controller. However, its powerful representation ability and flexible modeling approach made it an interesting idea for applications.

2.4 Fuel cell model

2.4.1 Physical-based PEFC model

It can be time-consuming and rather difficult to conduct experimental measurements within a PEFC system since the phenomena and reactions inside fuel cells are quite complicated. Thus, a reliable and qualified model can be used as an efficient tool to study specific aspects of a PEFC system for different applications [122], [172]. A PEFC system model is developed in this section.

The PEFC model adopted here was based on previously proposed semi-

empirical models, which have the capabilities to illuminate the electrochemical behavior of a fuel cell without offering deep apprehension of the underlying phenomena [53]. Besides, the PEFC model was on the system level with the length scale being above centimeters. The main consideration was the macro performances of the PEFC system. The details of fluid flow in the porous area, the temperature distribution on the nanometer scale, and the reaction area distribution were not investigated. The water generated in the cathode may involve a two-phase flow pattern, which was beyond the scope of this work. The water can be drained from the system and was not considered. Here we assumed the ideal gas law held for the reactant gases.

Through a pair of redox reactions, the PEFC converted the chemical energy from hydrogen fuel and oxygen into electricity with only heat and water as byproducts. It was typical that output voltage was usually less than the ideal value because of some losses that occurred inside the fuel cells [44], [185]. To get a higher voltage, a number of cells were usually combined in series, and the net output voltage of a PEFC was given as follows [90]:

$$V_{\text{FC}} = n_{\text{cell}}(E_n - V_a - V_o - V_c) \quad (2.52)$$

where V_{FC} , n_{cell} , E_n , V_a , V_o and V_c denote output voltage of the fuel cell system, cell numbers, reversible voltage, activation voltage drop, ohmic voltage drop and mass transport voltage drop.

The reversible voltage E_n was calculated based on the Nernst equation [90]:

$$\begin{aligned} E_n = & 1.229 - 0.85 \cdot 10^{-3}(T_s - 298.15) \\ & + 4.3085 \cdot 10^{-5}T_s (\ln(P_{\text{H}_2}) + \ln(0.5P_{\text{O}_2})) \end{aligned} \quad (2.53)$$

where T_s , P_{H_2} and P_{O_2} are stack temperature, hydrogen pressure and oxygen pressure.

The activation voltage drop V_a occurred due to the conversion of products into reactants on both anode and cathode, and it was defined as in [90]:

$$V_a = -(\xi_1 + \xi_2 T_s + \xi_3 T_s \ln(C_{\text{O}_2}) + \xi_4 T_s \ln(I)) \quad (2.54)$$

$$C_{\text{O}_2} = \frac{P_{\text{O}_2}}{5.08 \cdot 10^6 \exp(\frac{-498}{T_s})} \quad (2.55)$$

where ξ is the parametric coefficient [117], C_{O_2} is the oxygen concentration at the cathode catalytic interface and I is the current.

The ohmic voltage drop V_o came from the resistance of the electrons transfer and protons transfer. It was given as [90]:

$$V_o = I(R_m + R_C) \quad (2.56)$$

$$R_m = \frac{\rho_m l}{A} \quad (2.57)$$

$$\rho_m = \frac{181.6 \left(1 + 0.03i + 0.062i^{2.5} \left(\frac{T_s}{303} \right)^2 \right)}{(\lambda - 0.643 - 3i) \exp \left(4.18 \left(\frac{T_s - 303}{T_s} \right) \right)} \quad (2.58)$$

where R_m , R_C , ρ_m , l , A , i , λ represent membrane resistance, electronic resistance, membrane resistivity, membrane thickness, membrane active area, actual current density and adjustable parameter dependent on membrane water content.

The mass transport voltage drop V_c was because of the mass transfer which affects the reactant and product concentrations within the catalyst layer and it was determined as [90]:

$$V_c = -\beta \ln(1 - i/J_{\max}) \quad (2.59)$$

where β is the system parameter related to the fuel cell operating condition, J_{\max} denotes the maximum current density.

The dynamic behavior of a PEFC was largely affected by a charge double layer phenomenon. The charge layer on the interface electrode/electrolyte acted as an electrical capacitor. There was always a delay for the charge layer to follow the voltage changes. This delay only affected the activation and mass transport voltage drop, which can be described as the following equations [44]:

$$\frac{dV_{ac}}{dt} = \frac{I}{C} - \frac{V_{ac}}{R_a C} \quad (2.60)$$

$$R_a = \frac{V_a + V_c}{I} \quad (2.61)$$

where V_{ac} , C and R_a denote the voltage drop combing the activation drop and concentration drop, the electrical capacitance and the equivalent resistance. Thus, the output voltage of the PEFC can be rewritten as:

$$V_{FC} = n_{\text{cell}}(E_n - V_{ac} - V_o) \quad (2.62)$$

Figure 2.7 gives an illustration of the equivalent circuit model of the PEFC.

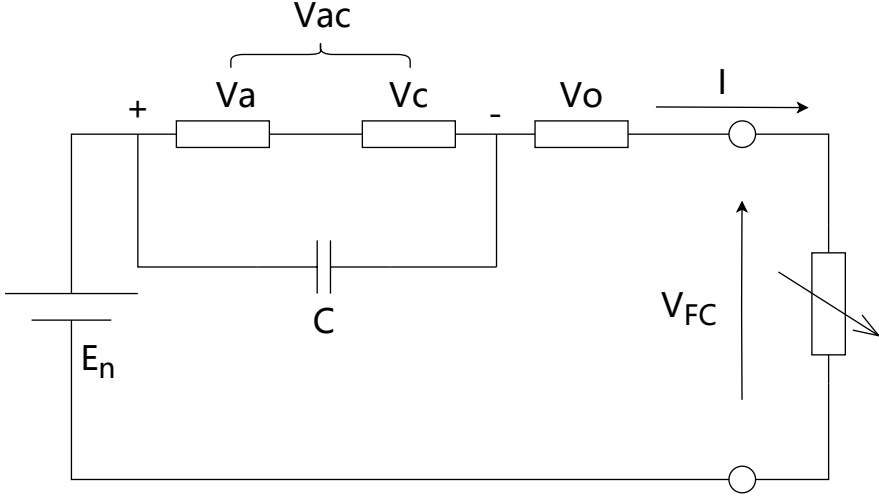


Figure 2.7: Equivalent circuit model of the PEFC [85].

All the reactant gases in this study were considered as ideal gases. The inputs to the fuel cell were the hydrogen volumetric flow rate Q_{H_2} and air volumetric flow rate Q_{air} . In the anode volume, hydrogen was delivered as fuel to the channel. Its mass-flow rate can be calculated as follows based on the mass conservation principle [146]:

$$m_{H_2,in} = \frac{1}{60000} \rho_{H_2} Q_{H_2} \quad (2.63)$$

$$\frac{dm_{H_2}}{dt} = \dot{m}_{H_2,in} - \dot{m}_{H_2,rea} - \dot{m}_{H_2,out} \quad (2.64)$$

$$\dot{m}_{H_2,rea} = \frac{NI}{2F} M_{H_2} \quad (2.65)$$

$$\dot{m}_{H_2,out} = k_a (P_{H_2} - P_{amb}) M_{H_2} \quad (2.66)$$

where ρ_{H_2} , m_{H_2} , $\dot{m}_{H_2,in}$, $\dot{m}_{H_2,rea}$, $\dot{m}_{H_2,out}$, M_{H_2} , k_a and P_{amb} are hydrogen density, hydrogen mass in the anode volume, inlet hydrogen mass-flow rate, hydrogen reaction mass-flow rate, outlet hydrogen mass-flow rate, hydrogen molar mass, anode flow constant and ambient pressure.

In the cathode volume, the air was delivered to the channel. Similar to the anode volume, the oxygen and nitrogen mass-flow rate can be calculated as

follows [146]:

$$m_{\text{O}_2,\text{in}} = \frac{0.21}{60000} \rho_{\text{O}_2} Q_{\text{air}} \quad (2.67)$$

$$m_{\text{N}_2,\text{in}} = \frac{0.79}{60000} \rho_{\text{N}_2} Q_{\text{air}} \quad (2.68)$$

$$\frac{dm_{\text{O}_2}}{dt} = \dot{m}_{\text{O}_2,\text{in}} - \dot{m}_{\text{O}_2,\text{rea}} - \dot{m}_{\text{O}_2,\text{out}} \quad (2.69)$$

$$\dot{m}_{\text{O}_2,\text{rea}} = \frac{NI}{4F} M_{\text{O}_2} \quad (2.70)$$

$$\dot{m}_{\text{O}_2,\text{out}} = k_c \frac{m_{\text{O}_2}}{m_{\text{O}_2} + m_{\text{N}_2}} (P_{\text{ca}} - P_{\text{amb}}) M_{\text{O}_2} \quad (2.71)$$

$$\frac{dm_{\text{N}_2}}{dt} = \dot{m}_{\text{N}_2,\text{in}} - \dot{m}_{\text{N}_2,\text{out}} \quad (2.72)$$

$$\dot{m}_{\text{N}_2,\text{out}} = k_c \frac{m_{\text{N}_2}}{m_{\text{O}_2} + m_{\text{N}_2}} (P_{\text{ca}} - P_{\text{amb}}) M_{\text{N}_2} \quad (2.73)$$

where ρ_{O_2} , ρ_{N_2} , m_{O_2} , $\dot{m}_{\text{O}_2,\text{in}}$, $\dot{m}_{\text{O}_2,\text{rea}}$, $\dot{m}_{\text{O}_2,\text{out}}$, M_{O_2} , m_{N_2} , $\dot{m}_{\text{N}_2,\text{in}}$, $\dot{m}_{\text{N}_2,\text{out}}$, k_c and P_{ca} are oxygen density, nitrogen density, oxygen mass in the cathode volume, inlet oxygen mass-flow rate, reacted oxygen mass-flow rate, outlet oxygen mass-flow rate, oxygen molar mass, nitrogen mass in the cathode channel, inlet nitrogen mass-flow rate, outlet nitrogen mass-flow rate, cathode flow constant and cathode pressure.

PEFC system performances under different operating conditions

The PEFC system model developed in this study was based on the commercial stacked PEFC-NedStackPS6 [90]. All operating parameters needed for the PEFC system are shown in Table 2.2. The performances of the PEFC system under various different operating conditions were investigated. Figure 2.8(a) gives the changes of the PEFC system behavior with the hydrogen flow rate varied from 100 and 400 lpm (liters per minute). Figure 2.8(b) presents the changes of the PEFC system performance with the air flow rates increased from 300 to 700 lpm. The changes of the reactant gas flow rates were made the same as in the Monem model [9] for later comparison. From Fig. 2.8, it can be clearly seen that the increase of hydrogen and air flow rate both slightly improved the PEFC system's voltage. Moreover, the model here showed good agreement with the Monem model when the current was in the range between 0 and 180 A. Above 180 A, the output voltage of the model dropped more than the Monem model [9], which agreed more with the fuel cell polarization

Table 2.2: Parameters used in the PEFC system model.

Parameter	Value
n_{cell}	65
ξ_1	-1.023071
ξ_2	3.4760e-3
ξ_3	7.7883354e-5
ξ_4	-9.54e-5
R_C [Ω]	1.62e-4
λ	15.03229
β [V]	0.0136
l [μm]	178
A [cm^2]	240
J_{max} [A/cm^2]	0.918
M_{H_2} [g/mol]	2
M_{O_2} [g/mol]	32
k_c [$\text{mol s}^{-1}\text{atm}^{-1}$]	0.065
k_a [$\text{mol s}^{-1}\text{atm}^{-1}$]	0.065
T [K]	332-342
Q_{H_2} [lpm]	100-400
Q_{air} [lpm]	300-700
ρ_{H_2} [kg/m^3]	0.0706
ρ_{O_2} [kg/m^3]	1.121
ρ_{N_2} [kg/m^3]	0.988

behavior. At a high current range, the voltage declined faster to the limiting current because the output voltage of the fuel-cell system was mainly affected by the mass transport polarization [54]. The performance difference of the PEFC system between the model here and the Monem model was mainly because of the adoption of different equations of concentration over potential. To clarify, in the Monem model, the voltage increase under the air flow rate from 300 to 700 lpm was very small, which almost overlapped, making it difficult to capture. Thus, in Fig. 2.8(b), only one line is showed for his model.

2.4.2 Gaussian process model

In the last section, a detailed physical fuel cell system model was elaborated, which was assumed to be the true system dynamics. In order to model errors

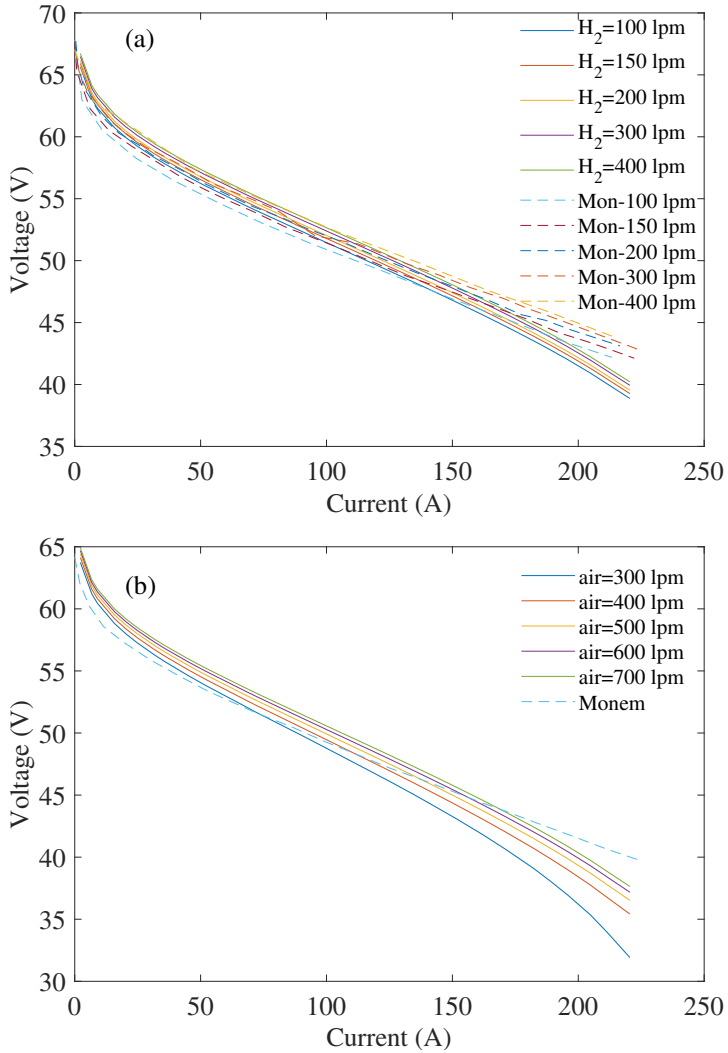


Figure 2.8: Dynamic behavior of PEFC system.

in measurement, Gaussian measurement noises were added to voltage V_{FC} and hydrogen pressure P_{H_2} . The task was to build a suitable Gaussian process model to describe the fuel cell dynamics with collected system data from the detailed physical model.

The Gaussian process model predicts two system states based on three system inputs. The inputs are the control actions, hydrogen volumetric flow rate Q_{H_2} , air volumetric flow rate Q_{air} , and the current I ; the states are the values to be predicted, the fuel cell output voltage V_{FC} and the hydrogen pressure

P_{H_2} . It should be noticed that the current I is the workload and can not be manipulated by the controller. The fuel cell voltage is the control target which should be kept at a constant reference value. The hydrogen pressure needs to be kept below a certain limit, such as 2.5 atm, to ensure safety.

The target of GP modeling was to build a function \mathbf{f} that describes the fuel cell dynamics in the time update:

$$\mathbf{x}^{k+1} = \mathbf{f}(\mathbf{u}^k, \mathbf{x}^k) \quad (2.74)$$

where

$$\begin{aligned} \mathbf{u}^k &= [Q_{\text{H}_2}^k \ Q_{\text{air}}^k \ I^k]^T \\ \mathbf{x}^k &= [V_{\text{FC}}^k \ P_{\text{H}_2}^k]^T \end{aligned} \quad (2.75)$$

the variable \mathbf{u}^k is the model inputs at time step k ; \mathbf{x}^{k+1} is the system states at time step $k + 1$ and \mathbf{x}^k is the measured system states at time step k .

However, the Gaussian process doesn't support multi-dimensional regression natively. One simple solution is to assume the multi-dimensional states are independent of each other and build a Gaussian process for each state with the same inputs. Equation (2.74) then becomes two Gaussian processes f_V and f_P :

$$\begin{aligned} V_{\text{FC}}^{k+1} &= f_V(\mathbf{u}^k, V_{\text{FC}}^k) \\ P_{\text{H}_2}^{k+1} &= f_P(\mathbf{u}^k, P_{\text{H}_2}^k) \end{aligned} \quad (2.76)$$

To collect the training data points for the Gaussian process, Latin hypercube sampling (LHS) was applied to the inputs Q_{H_2} , Q_{air} and the current I . The interval between time steps was 0.5 s. In total, 1000 training data points were collected.

The kernel type for the two Gaussian processes was the addition of an isotropic squared exponential kernel (Gaussian kernel) and an automatic relevance determination (ARD) squared exponential kernel. The parameters of the GP model were chosen by maximizing the log-likelihood function described by Eq. (2.8). This optimization problem is normally nonlinear and nonconvex. Here it was solved using the limited-memory Broyden–Fletcher–Goldfarb–Shanno (L-BFGS) algorithm [105].

After training, the GP model was validated with testing data points. The testing data points were collected by applying another set of LHS sampling

inputs to the fuel cell Simulink model. A total of 300 test points were collected. The prediction result is shown in Fig. 2.9. The blue line is the true value, and the orange line the one-step prediction by the GP model. The orange shaded area is the one σ confidence interval, the prediction value plus/minus one prediction standard deviation (one σ).

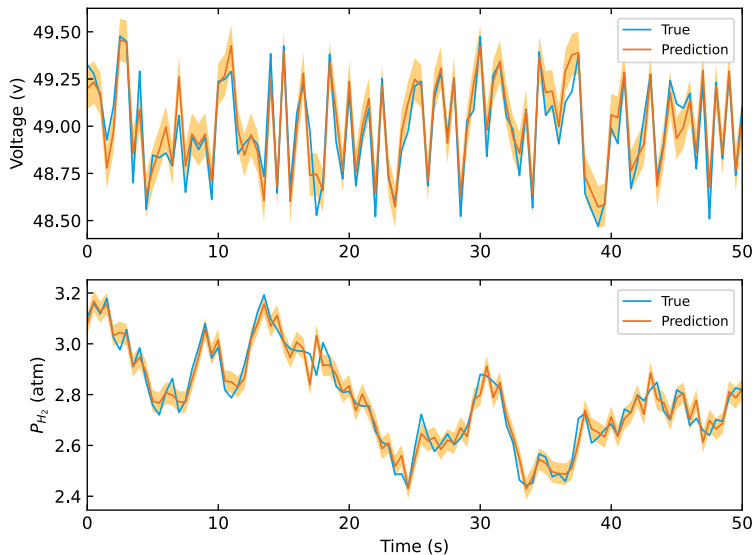


Figure 2.9: Gaussian process test results.

It can be seen that the GP model was able to predict the V_{FC} and P_{H_2} behavior of the fuel cell correctly. The variance calculated by GP was a reflection of the model prediction confidence. The prediction band was wider in the region where the test point was distant from the training points and the GP had a lower prediction accuracy. In most cases, the prediction band could cover the true value.

This chapter is a brief introduction to the control methods and estimation methods used in this thesis.

3.1 Control methods

3.1.1 PI control

The proportional-integral (PI) controller is the most commonly used control method in industry applications [21]. The discrete form of PI controller is given by

$$u^{k+1} = K_P e^k + K_I \sum_{i=0}^{k-1} e^i \quad (3.1)$$

where u is the controller output; e is the control error, the difference between the actual and desired value of the target variable; k indicates the time steps; K_P and K_I are the corresponding gains. The PI controller is a special case of the PID controller when turning off the derivative term. This is fairly common in industrial practice where the derivative part would be sensitive to noise. The discrete form in Eq. (3.1) is a forward-Euler approximation of the continuous PI controller.

The PI controller is widely used because of its simplicity in implementing and tuning. In this work, the PI controller was adopted for many tasks in engine control, such as the control of the gross indicated mean effective pressure (IMEPg) by adjusting main injection duration and common rail pressure control with an inlet-metering valve. The PI controller was also used for fuel cell voltage control by manipulating the intake hydrogen and air flow rate.

3.1.2 Model predictive control

Model predictive control (MPC) is an advanced optimal control method that is suitable for multi-input multi-output problems while satisfying a set of constraints [113]. It solves an optimization problem each time step concerning a prediction horizon H_p and control horizon H_u , getting a sequence of inputs for tracking the control references. Only the inputs corresponding to the first time step in the sequence are applied to the system and this process is repeated for the next step.

In this thesis, the system being considered is modeled as a discrete-time system with states $\mathbf{x} \in \mathbb{R}^n$, inputs $\mathbf{u} \in \mathbb{R}^m$ and outputs $\mathbf{y} \in \mathbb{R}^p$ satisfying:

$$\begin{aligned} \mathbf{x}^{k+1} &= \mathbf{A}\mathbf{x}^k + \mathbf{B}\mathbf{u}^k \\ \mathbf{y}^k &= \mathbf{C}\mathbf{x}^k \end{aligned} \tag{3.2}$$

where k indicates the sample index; $\mathbf{A} \in \mathbb{R}^{n \times n}$, $\mathbf{B} \in \mathbb{R}^{n \times m}$, and $\mathbf{C} \in \mathbb{R}^{p \times n}$ are system matrices. This state-space model is a special case of the function g in (1.1) in Sec. 1.4.

The control target is to have the system output \mathbf{y} follow the references \mathbf{r} , which is incorporated into the cost function. One example of an MPC optimization problem is the minimization:

$$\min_{\mathbf{u}^0, \mathbf{u}^1, \dots, \mathbf{u}^{H_u-1}} \mathbf{J}(\mathbf{u}^k) = \sum_{k=1}^{H_p} \left\| \mathbf{y}^k - \mathbf{r} \right\|_{Q^2} + \sum_{k=0}^{H_u-1} \left\| \mathbf{u}^k \right\|_{R^2} \tag{3.3}$$

subject to:

$$\begin{aligned}
\mathbf{x}^{k+1} &= \mathbf{A}\mathbf{x}^k + \mathbf{B}\mathbf{u}^k \\
\mathbf{y}^k &= \mathbf{C}\mathbf{x}^k \\
\mathbf{u}_{\text{lb}} &\leq \mathbf{u}^k \leq \mathbf{u}_{\text{ub}} \\
\mathbf{x}_{\text{lb}} &\leq \mathbf{x}^k \leq \mathbf{x}_{\text{ub}} \\
\mathbf{x}^0 &= \mathbf{x}_{\text{init}} \\
k &= 0, 1, \dots, H_p
\end{aligned} \tag{3.4}$$

where H_p and H_u are prediction and control horizon lengths; k in the superscript refers to the time step; \mathbf{Q} and \mathbf{R} are weight tuning parameters for reference tracking and control inputs; \mathbf{u}_{lb} , \mathbf{u}_{ub} , \mathbf{x}_{lb} , and \mathbf{x}_{ub} are the lower bounds and upper bounds of inputs \mathbf{u} and states \mathbf{x} ; \mathbf{x}_{init} is the latest measured or estimated value, the state feedback.

This quadratic programming (QP) problem will be solved each time step to get the control inputs, and only the first solved control inputs \mathbf{u}^0 is applied to the system. The QP problem is a well-researched optimization problem [38] and several mature solvers and software are available. Due to its convex nature, the solution time is short enough for real-time control applications. In this thesis, the QP problem was solved by Interior-Point Optimizer (IPOPT) [162].

3.2 Estimation method

The state estimation is to estimate the states \mathbf{x} according to measured outputs \mathbf{y} . For our case where the system is considered linear, a Kalman filter (KF) was used, which is the optimal linear filter under the assumptions of perfect modeling, Gaussian noises, and known noise covariances [89]. For a nonlinear system model situation, the extended Kalman filter (EKF) [87] or particle filter [107] is commonly chosen.

The state-space model (3.2) with Gaussian noises:

$$\begin{aligned}
\mathbf{x}^{k+1} &= \mathbf{A}^k \mathbf{x}^k + \mathbf{B}^k \mathbf{u}^k + \mathbf{v}^k \\
\mathbf{y}^k &= \mathbf{C}^k \mathbf{x}^k + \mathbf{e}^k
\end{aligned} \tag{3.5}$$

is considered for filtering. The noise \mathbf{v}^k and \mathbf{e}^k are zero-mean white noise with known covariances:

$$\begin{aligned}\mathbf{v}^k &\sim N(0, \mathbf{Q}) \\ \mathbf{e}^k &\sim N(0, \mathbf{R})\end{aligned}\tag{3.6}$$

where \mathbf{Q} and \mathbf{R} are the covariance matrices. In absence of covariance information, the covariance matrices are often substituted with diagonal positive definite matrices, meaning that noise components are assumed to be independent.

With the noting of $\hat{\mathbf{x}}^{k|k-1}$ as the prediction of $\hat{\mathbf{x}}^k$ with the knowledge of \mathbf{x}^{k-1} , the detailed steps of the Kalman filter are:

Algorithm 1: Kalman filter

```

1 Initialize  $\hat{\mathbf{x}}^{0|0}$ ,  $\mathbf{P}^{0|0}$ , and  $k = 1$ ;
2 repeat
3   Predict:
4      $\hat{\mathbf{x}}^{k|k-1} = \mathbf{A}^k \hat{\mathbf{x}}^{k-1|k-1} + \mathbf{B}^k \mathbf{u}^{k-1}$ 
5      $\mathbf{P}^{k|k-1} = \mathbf{A}^k \mathbf{P}^{k-1|k-1} (\mathbf{A}^k)^T + \mathbf{Q}$ 
6   Update:
7      $\mathbf{S}^k = \mathbf{C}^k \mathbf{P}^{k|k-1} (\mathbf{C}^k)^T + \mathbf{R}$ 
8      $\mathbf{K}^k = \mathbf{P}^{k|k-1} (\mathbf{C}^k)^T (\mathbf{S}^k)^{-1}$ 
9      $\hat{\mathbf{x}}^{k|k} = \hat{\mathbf{x}}^{k|k-1} + \mathbf{K}^k (\mathbf{y}^k - \mathbf{C}^k \hat{\mathbf{x}}^{k|k-1})$ 
10     $\mathbf{P}^{k|k} = (\mathbf{I} - \mathbf{K}^k \mathbf{C}^k) \mathbf{P}^{k|k-1}$ 
11     $k = k + 1$ 
12 until stop;
```

4.1 Flex-fuel CI engine

The engine related experiments in this thesis were conducted on a Scania D13 heavy-duty compression-ignition engine. The experiment apparatus also included the measurement system and control system.

4.1.1 Engine

The engine shown in Fig. 4.1 has the specifications exhibited in Table 4.1.

The engine gas system was modified to meet the experimental requirements. A long-route low-pressure EGR system was added and used in the experiments. The engine also had an original short-route EGR, but it was not used, thus not described in Fig. 2.3 and Fig. 4.2. The turbocharger hardware was provided by BorgWarner and was matched for the long-route EGR. A fast thermal management system was installed in the inlet path to control the inlet temperature which consists of two paths, one of which is cooled by the intercooler. Figure 4.2 shows a schematic diagram of the overall test-cell structure.



Figure 4.1: Scania D13 heavy-duty compression-ignition engine.

Table 4.1: Engine specifications.

Name	Value
Displaced volume	12.74 dm ³
Cylinder number	6
Stroke	160 mm
Bore	130 mm
Connecting Rod	235 mm
Compression ratio	18:1
Number of Valves	4
Maximum power	360 kW

4.1.2 Measurement system

Figure 4.2 presents most sensor locations.

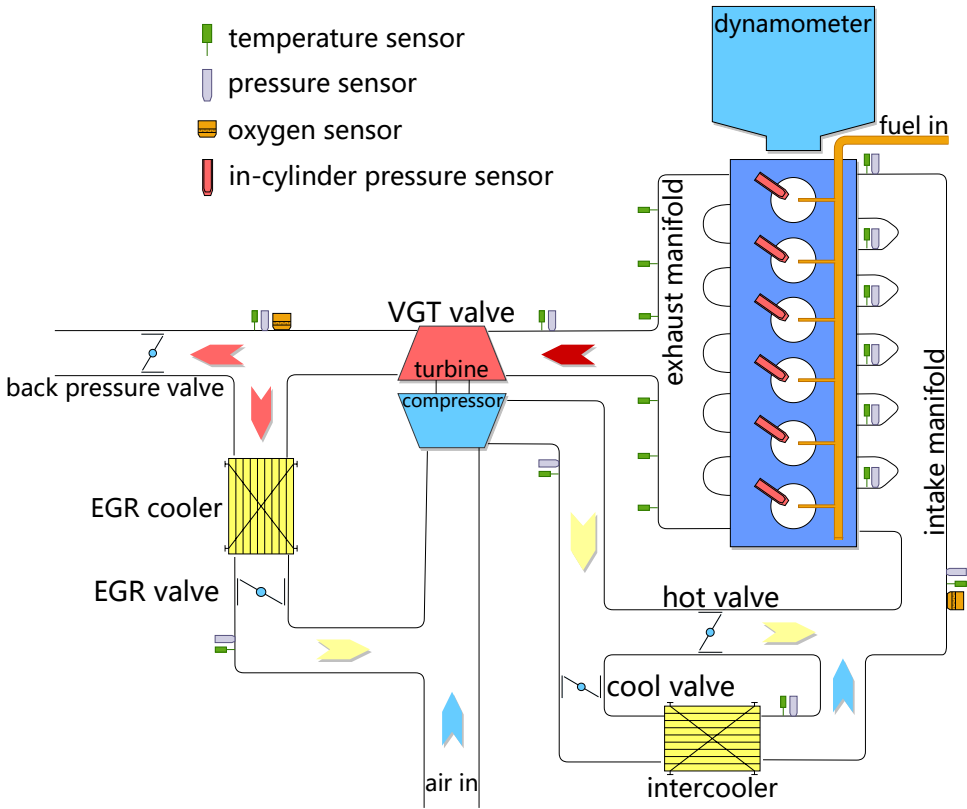


Figure 4.2: Schematic drawing of the test-cell structure. Valves, sensor types and locations are marked in the diagram.

Sampling

A Leine & Linde encoder [1] enabled the crank-angle based sampling which emits 5 pulses per CAD. The measurement of cylinder pressure, engine torque, and injector current were triggered by the crank-angle signal, while other sensors were triggered cycle by cycle.

In-cylinder pressure sensor

Water-cooled Kistler 7061B piezoelectric pressure transducers [2] were mounted in each cylinder for the measurement of in-cylinder pressure, triggered every 0.2 CAD.

Gas system pressure and temperature sensors

The pressure sensors were Keller PAA-23S absolute pressure sensors [3] with a response time of milliseconds. The temperature was measured by K-type thermocouples with response time in seconds. The various locations of the pressure and temperature sensors are detailed in Figure 4.2, which covers almost every pipe in the gas system.

Oxygen sensors

Two Bosch LSU 4.9 wideband zirconia oxygen sensors [4] were mounted in the exhaust manifold after the turbine and in the intake manifold before cylinders.

Common-rail pressure sensor

The common-rail pressure was measured by a pressure sensor in the common-rail volume.

Air and fuel flow

A Bronkhorst hot-film air-mass flow meter installed before the compressor was used to measure the air-mass flow, while a Bronkhorst mini CORI-FLOW M15 mass-flow meter [5] installed before the fuel system was used for the measurement of the fuel-mass flow.

Engine speed and torque

The electric motor dynamometer integrated with a force sensor was used for the detection of engine speed and torque.

4.1.3 Fuel

The fuels for the experiments included diesel, the mixture of 80 volume % Swedish 95 octane pump gasoline and 20 volume % n-heptane, and the mixture of 80 volume % pure ethanol and 20 volume % n-heptane. The three fuel species are shown in Table 4.2.

Table 4.2: Fuel species.

Fuel number	Diesel	Gasoline	Ethanol	n-Heptane
1	100%	-	-	-
2	-	80%	-	20%
3	-	-	80%	20%

4.1.4 Control system

Hardware

The control hardware was mainly from National Instruments (NI). An embedded controller PXIe-8135 [6] was installed in a PXIe-1078 chassis, whose central processing unit (CPU) frequency is 2.3 GHz. Two field programmable gate array (FPGA) cards, I/O cards, and a sub-chassis with Drivven hardware drivers managing injectors and valves were also available. A user interface and part of the control logic were running on a separate PC communicating over TCP and UDP.

Software

The control system was programmed by LabVIEW, a graphical language by NI and Julia, an open-source high-level dynamic language designed for high performance [33]. The real-time heat release analysis and most basic control logic were programmed by LabVIEW and executed in an embedded controller. A graphical LabVIEW user interface was operated on a separate host PC with Windows 7 operating system. Advanced control logic including the MPC formation and solving was written by Julia and running on the host PC. This functionality gives more flexibility for developing, testing, and deploying control algorithms offline than using LabVIEW in the embedded controller.

4.2 Fuel cell

The fuel-cell experiments were conducted on the physical model detailed in Sec. 2.4.1 established with Simulink. Figure 4.3 shows the illustration of the Simulink model.

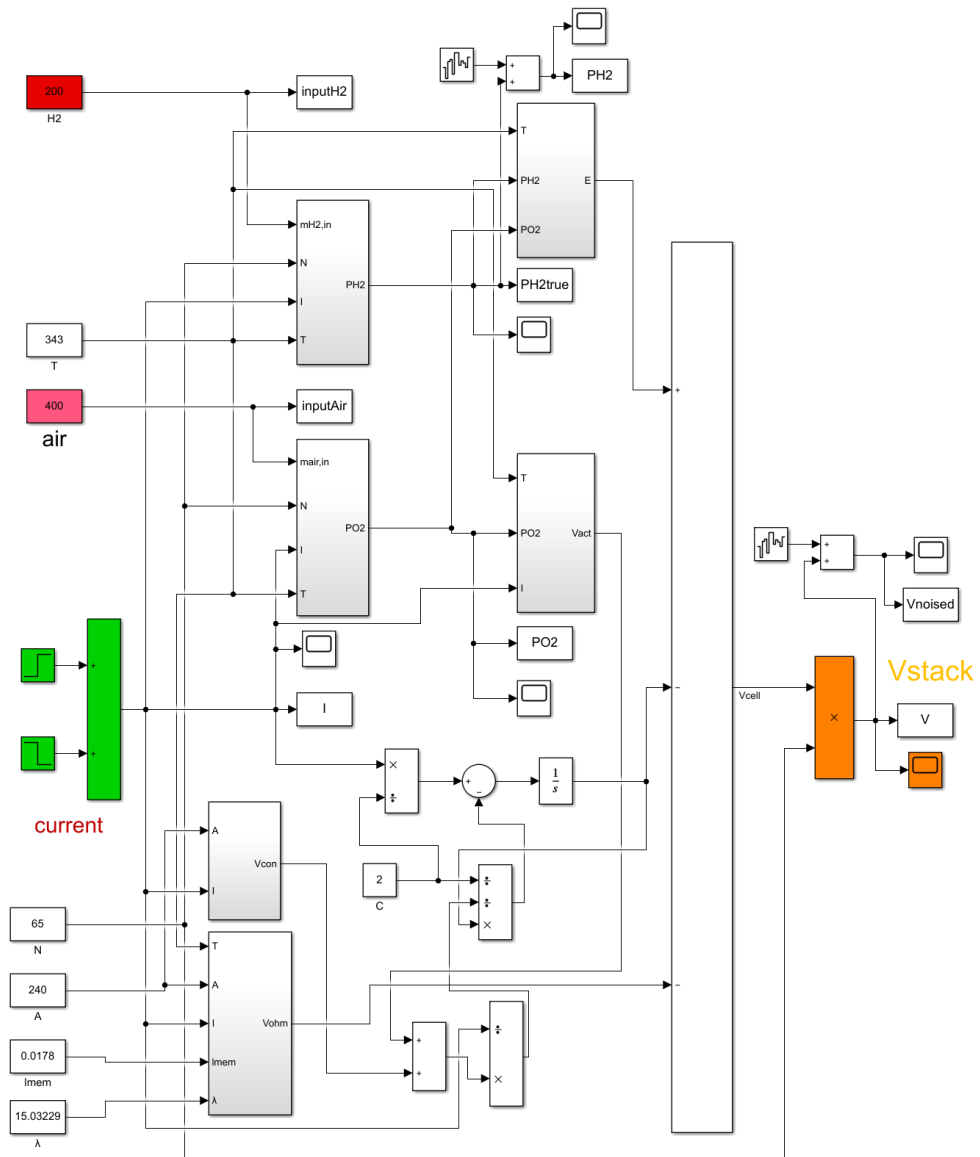


Figure 4.3: Simulink model diagram.

The Simulink model was developed with MATLAB & Simulink R2020a. The controllers were implemented using both MATLAB and Julia.

5.1 Introduction

Four decades have passed since the seminal paper on Dynamic Matrix Control (DMC) appeared [45], which was the first Model Predictive Control (MPC) algorithm. In the pre-MPC era, Propoi applied linear programming to control linear systems with hard constraints [136], showing the idea of MPC. Åström and Wittenmark used self-tuning regulators to control a system with constant and unknown parameters [19]. The appearance of MPC gives systematic methods to handle hard constraints and was welcomed by the industry immediately. Along with the commercial practices, the theoretical foundation of MPC is built, with strict closed-loop stability requirements and performance guarantees [118], [125]. The rapid development of computational power and availability of cheap microprocessors further encourage the usage of MPC in extensive and complicated tasks. Nowadays, MPC is regarded by many as one important control method which has a great impact on industrial control practice, especially in the process control area. MPC is adopted almost in every refinery and petrochemical plant control tasks [98], and also penetrated into a wide variety of industries such as automotive [79] and energy systems [108], [190].

In this chapter, the design and evaluation of MPC based on physical models applied to flex-fuel CI engine and fuel cell control tasks is described. When the state-space model is changing according to current system states during

operation, it could be termed as an adaptive MPC. This is a practical method to deal with system nonlinearity and disturbances like variable fuels.

5.2 Flex-fuel CI engine control

5.2.1 Introduction

Control approaches based on physical models have been applied in many areas of engine control, especially for various combustion modes useful in the flex-fuel CI engine. Bengtsson et al. showed that MPC is a promising control method for a homogeneous charge compression ignition (HCCI) engine [30]. Blom et al. developed a low-complexity physical model aiming at describing the major thermodynamic and chemical interactions in the course of an engine stroke, and the model was used to synthesize a controller for the combustion phasing control in an HCCI engine [35]. Albin et al., Ingesson et al., Yin et al. applied MPC to partially premixed combustion (PPC) combustion control [14], [81], [179]. Raut et al. utilized MPC for combustion phasing and load control of a reactivity controlled compression ignition (RCCI) engine [140].

Adaptive MPC has been adopted to compensate for the model error, unmodeled dynamics, noise, and system variation in engine control applications. McKinley and Alleyne used adaptive MPC as a solution to rapid and unpredictable changes of selective catalytic reduction (SCR) in broad operating conditions [119]. Optimal adaptive predictive control has been applied by Nenchev and Hans to an SI engine to track the error dynamics [130]. Yildiz et al. developed an adaptive control approach for the SI engine idle speed control problem to improve performance [177].

This section illustrates an adaptive model predictive control approach to control the flex-fuel CI engine combustion process with mutable, unknown fuel contents. Due to the dynamically changing environment, the learning ability, also called adaptivity, of the model is necessary to track the time-varying fuel properties and its influence on the engine. The high variations of renewable fuel characteristics also put demands on controller adaptivity. The learning ability is achieved by estimating the time-varying parameters in the grey box model of ignition delay in a real-time manner by the Kalman filter detailed in Chapter 3. The ignition delay model is the physical model in Sec. 2.3.3 with parameters c_1 , c_2 , c_3 and c_4 . The parameters are the reflection of the fuel features. The control targets are the combustion phasing θ_{CA50} and the ignition delay τ . The combustion phasing and ignition delay influence

engine efficiency, emission, noise, etc. [78]. Since combustion phasing and ignition delay are intimately coupled, the fuel injection system and air system need to be combined. The actuators are injection timings, the exhaust gas recirculation (EGR) system, and the variable-geometry turbocharger (VGT), EGR and VGT being used to manipulate the intake oxygen concentration and intake pressure. Model predictive control (MPC) is a suitable design for the multiple input/output system with actuator constraints [113].

5.2.2 System modeling

Ignition delay model

The ignition delay model is the physical-based model from Sec. 2.3.3. The ignition delay τ in milliseconds is the time between the start of injection θ_{SOI} and the start of combustion θ_{CA10} . One pilot injection was adopted in this scenario for promoting combustion and noise reduction. The start of injection θ_{SOI} refers to the main injection timing; τ is calculated by:

$$\tau = \frac{\theta_{\text{CA10}} - \theta_{\text{SOI}}}{0.006N_s} \quad (5.1)$$

where θ_{SOI} is the crank angle at the start of the injector current impulse and N_s is the engine speed, with the unit of revolutions per minute, rpm.

For control applications, it is necessary to model the θ_{CA50} and τ . The variable θ_{CA50} can be computed using:

$$\theta_{\text{CA50}} = \theta_{\text{SOI}} + 0.006N_s\tau + \theta_{\text{CA10-50}} \quad (5.2)$$

where $\theta_{\text{CA10-50}}$ is the crank angle difference between θ_{CA10} and θ_{CA50} . Here it was assumed that the chosen actuators, injection timing, EGR, and VGT valve opening did not influence $\theta_{\text{CA10-50}}$. This assumption will not degrade the controller performance much since the main contribution of θ_{CA50} was from the injection timing θ_{SOI} and ignition delay τ .

The ignition delay τ was estimated using an Arrhenius-type model [178]:

$$\tau = c_1 \exp\left(\frac{c_2}{T}\right) \bar{O}_2^{c_3} \bar{p}^{c_4} \quad (5.3)$$

where c_1 , c_3 , and c_4 are fuel dependent empirical parameters. $c_2 = E_a/R$ where E_a is the apparent activation energy and R is the universal gas constant. For simplicity, the E_a/R in the general Arrhenius-type model was represented

by c_2 . \bar{T} , \bar{O}_2 , \bar{p} are the mean cylinder temperature, oxygen concentration and pressure between θ_{SOI} and θ_{CA10} .

Assuming the adiabatic relation holds during this period, the ignition delay τ is finally expressed as:

$$\tau = c_1 \exp\left(\frac{c_2}{T_{\text{IVC}} T_{\text{co}}}\right) (O_{2\text{IVC}} O_{2\text{co}})^{c_3} (p_{\text{IVC}} p_{\text{co}})^{c_4} \quad (5.4)$$

where the co in subscripts is short for coefficient; the variables T_{co} , $O_{2\text{co}}$, and p_{co} are:

$$\begin{aligned} T_{\text{co}} &= \frac{\int_{\theta_{\text{SOI}}}^{\theta_{\text{SOI}}+\tau} \left(\frac{V_{\text{IVC}}}{V(\theta)}\right)^{\gamma-1} d\theta}{\int_{\theta_{\text{SOI}}}^{\theta_{\text{SOI}}+\tau} d\theta} \\ O_{2\text{co}} &= \frac{\int_{\theta_{\text{SOI}}}^{\theta_{\text{SOI}}+\tau} \frac{V_{\text{IVC}}}{V(\theta)} d\theta}{\int_{\theta_{\text{SOI}}}^{\theta_{\text{SOI}}+\tau} d\theta} \\ p_{\text{co}} &= \frac{\int_{\theta_{\text{SOI}}}^{\theta_{\text{SOI}}+\tau} \left(\frac{V_{\text{IVC}}}{V(\theta)}\right)^{\gamma} d\theta}{\int_{\theta_{\text{SOI}}}^{\theta_{\text{SOI}}+\tau} d\theta} \end{aligned} \quad (5.5)$$

The τ in the integration limit was set to the last cycle value when calculating. The detailed steps are in Sec. 2.3.3.

Gas system model

In this chapter, the relationships between the intake oxygen concentration, pressure at IVC and EGR, VGT valve opening were determined by experiments, as shown in Fig. 5.1.

The EGR valve opening was assumed to have no effect on intake pressure. In the intake manifold, one oxygen sensor was mounted before all cylinders and six pressure sensors for each cylinder were installed. The pressure variations between cylinders were neglected here, i.e., all cylinders used the same intake pressure to VGT valve opening relationship in Fig. 5.1.

5.2.3 Adaptive MPC design

Real-time parameter estimation

In our control application, the ignition delay was most prone to be influenced by mutable fuel contents. The variable θ_{CA50} was then affected according to

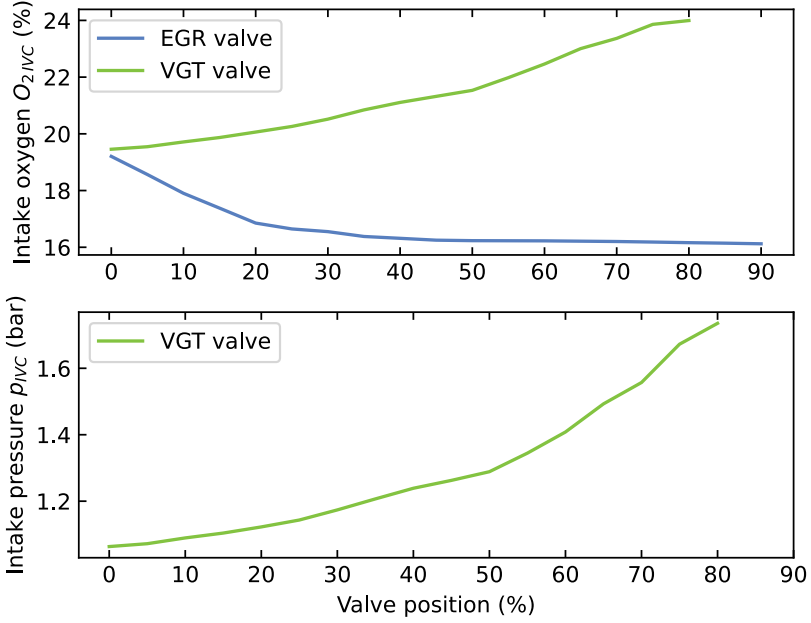


Figure 5.1: Intake oxygen O_{2IVC} and pressure p_{IVC} as a function EGR and VGT valve positions

Eq. (5.2). To fulfill the control task, the ignition delay model parameters of Eq. (5.4) need to be estimated and updated online with real-time data.

Taking natural logarithm of both sides in Eq. (5.4), we get:

$$\ln(\tau) = \ln(c_1) + \frac{c_2}{T_{IVC}T_{co}} + c_3 \ln(O_{2IVC}O_{2co}) + c_4 \ln(p_{IVC}p_{co}) \quad (5.6)$$

which can be described by the state-space equation:

$$\begin{bmatrix} \ln(c_1^{k+1}) \\ c_2^{k+1} \\ c_3^{k+1} \\ c_4^{k+1} \end{bmatrix} = \begin{bmatrix} \ln(c_1^k) \\ c_2^k \\ c_3^k \\ c_4^k \end{bmatrix} + \mathbf{v}^k \quad (5.7)$$

$$\ln(\tau^k) = \begin{bmatrix} 1 \\ 1/T_{IVC}^k T_{co}^k \\ \ln(O_{2IVC}^k O_{2co}^k) \\ \ln(p_{IVC}^k p_{co}^k) \end{bmatrix}^T \begin{bmatrix} \ln(c_1^k) \\ c_2^k \\ c_3^k \\ c_4^k \end{bmatrix} + e^k$$

where the k in superscript represents the cycle number; \mathbf{v}^k and e^k are the process noise and the observation noise.

The classic Kalman filter is then used to estimate the state vector:

$$\begin{bmatrix} \ln(c_1) \\ c_2 \\ c_3 \\ c_4 \end{bmatrix} \quad (5.8)$$

For more details about the Kalman filter and its application in real-time identification, please see [89] and [86].

Since the fuel contents were varying during this process, the estimated parameters would not converge to certain constant values. Whereas there were no theoretical proofs for the stability of the interconnected MPC, state estimation, and parameter estimation, no significant stability problem appeared in our experiments.

State-space model

The cycle-to-cycle dynamics for each cylinder between control targets θ_{CA50} and τ and control inputs the start of injection θ_{SOI} , the EGR valve position θ_{EGR} and the VGT valve position θ_{VGT} can be written as:

$$\begin{aligned} \theta_{CA50_i}^{k+1} &= \theta_{CA50_i}^k + \begin{bmatrix} \frac{\partial \theta_{CA50_i}}{\partial \theta_{SOI_i}} & \frac{\partial \theta_{CA50_i}}{\partial \theta_{EGR}} & \frac{\partial \theta_{CA50_i}}{\partial \theta_{VGT}} \end{bmatrix} \begin{bmatrix} d\theta_{SOI_i}^k \\ d\theta_{EGR}^k \\ d\theta_{VGT}^k \end{bmatrix} \\ \tau_i^{k+1} &= \tau_i^k + \begin{bmatrix} \frac{\partial \tau_i}{\partial \theta_{SOI_i}} & \frac{\partial \tau_i}{\partial \theta_{EGR}} & \frac{\partial \tau_i}{\partial \theta_{VGT}} \end{bmatrix} \begin{bmatrix} d\theta_{SOI_i}^k \\ d\theta_{EGR}^k \\ d\theta_{VGT}^k \end{bmatrix} \end{aligned} \quad (5.9)$$

where the i in subscript represents the cylinder number, and the k in superscript represents the cycle number. It should be noticed that the injection timing θ_{SOI} was adjusted per cylinder, while the θ_{EGR} and θ_{VGT} were the same for all cylinders.

The linearized, discrete-time, state-space model of each cylinder used for

control is written as:

$$\begin{aligned} \mathbf{x}^{k+1} &= \mathbf{A}\mathbf{x}^k + \mathbf{B}\mathbf{u}^k \\ \mathbf{y}^k &= \mathbf{C}\mathbf{x}^k \end{aligned} \quad (5.10)$$

where the state vector \mathbf{x}^k at sample index k is:

$$\mathbf{x}^k = \begin{bmatrix} \theta_{\text{CA50}}^k \\ \tau^k \\ \theta_{\text{SOI}}^k \\ \theta_{\text{EGR}}^k \\ \theta_{\text{VGT}}^k \end{bmatrix} \quad (5.11)$$

with input:

$$\mathbf{u}^k = \begin{bmatrix} d\theta_{\text{SOI}}^k \\ d\theta_{\text{EGR}}^k \\ d\theta_{\text{VGT}}^k \end{bmatrix} \quad (5.12)$$

and output:

$$\mathbf{y}^k = \begin{bmatrix} \theta_{\text{CA50}}^k \\ \tau^k \end{bmatrix} \quad (5.13)$$

and state-space matrices:

$$\begin{aligned} \mathbf{A} &= \mathbf{I}_{5 \times 5} \\ \mathbf{B} &= \begin{bmatrix} \frac{\partial \theta_{\text{CA50}}}{\partial \theta_{\text{SOI}}} & \frac{\partial \theta_{\text{CA50}}}{\partial \theta_{\text{EGR}}} & \frac{\partial \theta_{\text{CA50}}}{\partial \theta_{\text{VGT}}} \\ \frac{\partial \tau}{\partial \theta_{\text{SOI}}} & \frac{\partial \tau}{\partial \theta_{\text{EGR}}} & \frac{\partial \tau}{\partial \theta_{\text{VGT}}} \\ 1 & 0 & 0 \\ 0 & 1 & 0 \\ 0 & 0 & 1 \end{bmatrix} \\ \mathbf{C} &= \begin{bmatrix} 1 & 0 & 0 & 0 & 0 \\ 0 & 1 & 0 & 0 & 0 \end{bmatrix} \end{aligned} \quad (5.14)$$

The actuator increments were selected as the system inputs. Consequently, θ_{SOI}^k , θ_{EGR}^k , and θ_{VGT}^k were added into the state vector to help set constraints on them.

According to Eq. (5.2), we get:

$$\begin{aligned}
\frac{\partial \theta_{CA50}}{\partial \theta_{SOI}} &= 1 \\
\frac{\partial \theta_{CA50}}{\partial \theta_{EGR}} &= 0.006 N_s \frac{\partial \tau}{\partial \theta_{SOI}} \\
\frac{\partial \theta_{CA50}}{\partial \theta_{VGT}} &= 0.006 N_s \frac{\partial \tau}{\partial \theta_{VGT}}
\end{aligned} \tag{5.15}$$

The partial derivatives of τ with respect to θ_{SOI} , O_{2IVC} , and p_{IVC} are obtained from Eq. (5.4). Although the θ_{SOI} is in the integration limit, its influence on the ignition delay τ is neglected for simplicity. We have:

$$\begin{aligned}
\frac{\partial \tau}{\partial \theta_{SOI}} &= 0 \\
\frac{\partial \tau}{\partial \theta_{EGR}} &= \frac{\partial \tau}{\partial O_{2IVC}} \frac{\partial O_{2IVC}}{\partial \theta_{EGR}} \\
\frac{\partial \tau}{\partial \theta_{VGT}} &= \frac{\partial \tau}{\partial O_{2IVC}} \frac{\partial O_{2IVC}}{\partial \theta_{VGT}} + \frac{\partial \tau}{\partial p_{IVC}} \frac{\partial p_{IVC}}{\partial \theta_{VGT}}
\end{aligned} \tag{5.16}$$

As stated in Sec. 5.2.2, EGR had no influence on intake pressure, which means $\partial p_{IVC} / \partial \theta_{EGR} = 0$. The value of $\partial O_{2IVC} / \partial \theta_{EGR}$, $\partial O_{2IVC} / \partial \theta_{VGT}$, and $\partial p_{IVC} / \partial \theta_{VGT}$ are estimated from the slopes in Fig. 5.1.

MPC design

At each time step, the parameters $\ln(c_1)$, c_2 , c_3 , and c_4 are estimated first by Kalman filter with state-space model represented by Eq. (5.7). Then, based on the state-space model (5.10), a quadratic programming (QP) problem will be solved to obtain optimal control inputs:

$$\min_{\mathbf{u}^0, \mathbf{u}^1, \dots, \mathbf{u}^{H_u-1}} \mathbf{J}(\mathbf{u}^k) = \sum_{k=1}^{H_p} \left\| \mathbf{y}^k - \mathbf{r} \right\|_Q^2 + \sum_{k=0}^{H_u-1} \left\| \mathbf{u}^k \right\|_R^2 + \left\| \begin{bmatrix} \theta_{EGR}^1 \\ \theta_{VGT}^1 \end{bmatrix} \right\|_S^2 \tag{5.17}$$

subject to:

$$\begin{aligned}
\mathbf{x}^{k+1} &= \mathbf{A}\mathbf{x}^k + \mathbf{B}\mathbf{u}^k \\
\mathbf{y}^k &= \mathbf{C}\mathbf{x}^k \\
\mathbf{u}_{lb} &\leq \mathbf{u}^k \leq \mathbf{u}_{ub} \\
\mathbf{x}_{lb} &\leq \mathbf{x}^k \leq \mathbf{x}_{ub} \\
\mathbf{x}^0 &= \mathbf{x}_{init} \\
k &= 0, 1, \dots, H_p
\end{aligned} \tag{5.18}$$

where H_p and H_u are prediction and control horizon; k in the superscript represents the time step, and $k = 0$ refers to the current time step; \mathbf{r} is the control reference; \mathbf{Q} , \mathbf{R} and \mathbf{S} are weight tuning parameters for reference tracking, control inputs and valve positions; \mathbf{u}_{lb} , \mathbf{u}_{ub} , \mathbf{x}_{lb} , and \mathbf{x}_{ub} are the lower bounds and upper bounds of inputs \mathbf{u} and states \mathbf{x} ; \mathbf{x}_{init} is the latest measured value, the state feedback.

For current time step, MPC will only apply the first solved control inputs \mathbf{u}^0 to the system. Then it will estimate parameters $\ln(c_1)$, c_2 , c_3 , and c_4 again, and reformulate the QP problem and get a new solution in next time step. This procedure will be repeated for every time step. This process is also known as receding horizon control.

For each cylinder, this MPC problem was formulated and solved independently. The solution θ_{SOI} was applied per cylinder, and the average of solved θ_{EGR} and θ_{VGT} was applied to the EGR and VGT valves. The variation magnitude of the calculated θ_{EGR} and θ_{VGT} in cylinders are shown in Fig. 5.4. Both controls agreed well between the different cylinders which made the approach suitable.

An illustration of the overall adaptive MPC design is shown in Fig. 5.2.

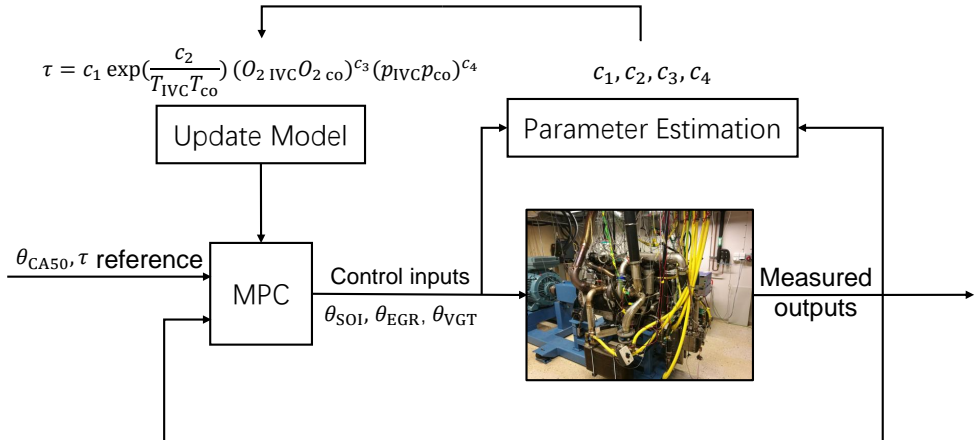


Figure 5.2: Adaptive MPC design.

5.2.4 Experimental set-up

The control plant was a six-cylinder heavy-duty Scania D13 engine. The engine specifications and control system are detailed in Chapter 4. However, due to the sixth cylinder was malfunctioning during this chapter work, only cylinders one to five were used in the experiments. The fuel for the experiments was diesel, the mixture of 80 volume % Swedish 95 octane pump gasoline and 20 volume % n-heptane, and the mixture of 80 volume % pure ethanol and 20 volume % n-heptane. The n-heptane was added to avoid misfire since the cetane numbers of gasoline and ethanol are significantly lower than the diesel fuel. Another potential solution was the use of an intake air heater [100].

5.2.5 Experimental results

Two fuel transition scenarios were conducted: the transition from diesel to the gasoline/n-heptane mixture and the transition from the gasoline/n-heptane mixture to the ethanol/n-heptane mixture. Each transition took approximately 30 to 40 minutes. The transition was done by turning off one fuel pipe and turning on the other fuel pipe. This procedure was applied to simulate the situation that after running for some distance with one fuel, the user stops the car and fills the tank with another kind of fuel. The focus was on the gradual transition in the engine from one fuel to the newly added fuel since many studies have investigated the steady fuel situation.

Diesel to gasoline/n-heptane mixture

During this transition, the gross indicated mean effective pressure (IMEPg) was kept at 5 bar controlled by a proportional-integral (PI) controller. The engine speed was 1200 rpm.

Figure 5.3 shows the controller behavior at the beginning of the diesel to gasoline/n-heptane transition. When the combustion timing θ_{CA50} target increased, the injection timing θ_{SOI} was retarded to track the reference. The ignition delay τ was mainly manipulated by valve position θ_{EGR} and θ_{VGT} . When the τ target increased, the VGT valve position θ_{VGT} was increased to raise the intake oxygen concentration and pressure, and the EGR valve position θ_{EGR} were decreased since the lower the EGR, the higher the intake oxygen concentration. The gas system dynamics were slower compared with

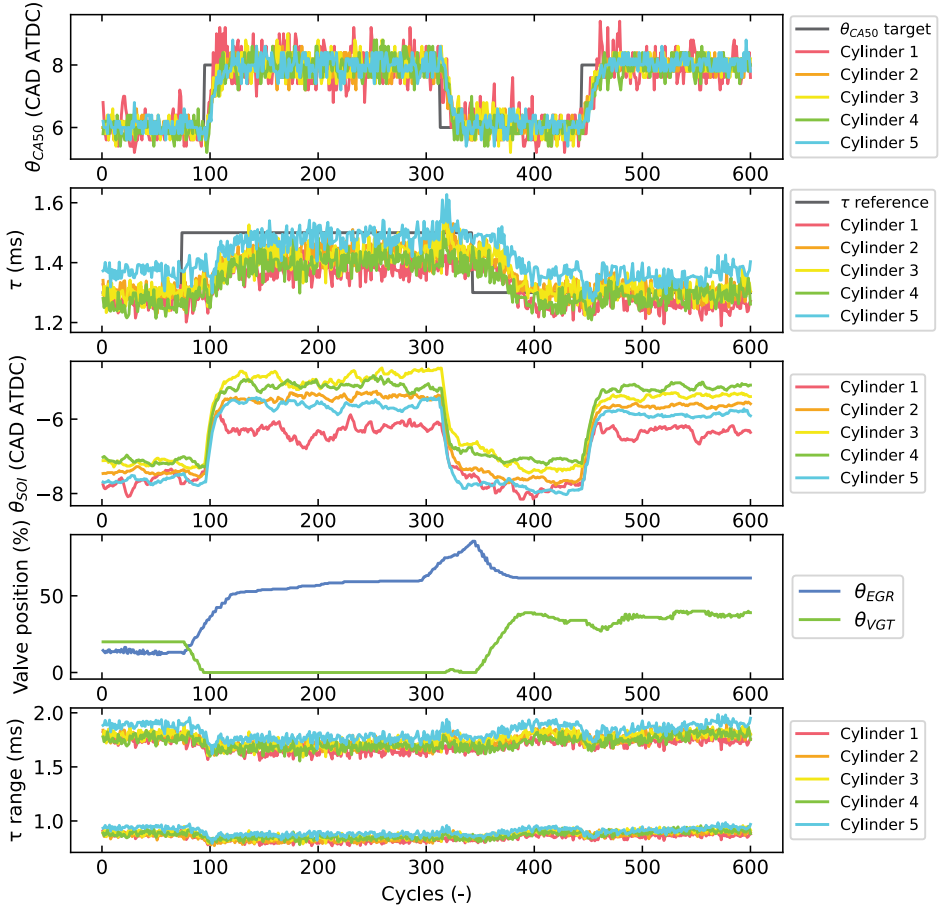


Figure 5.3: Controller behavior at the start of diesel to gasoline/n-heptane transition. θ_{CA50} is the combustion timing, the CAD where 50% total heat are released; τ is the ignition delay; θ_{SOI} is the CAD of start of main injection; θ_{EGR} and θ_{VGT} are EGR and VGT valves opening. The same applies to the rest figures of this chapter.

the injection system, and the tracking speed of ignition delay τ was slower than that of combustion timing θ_{CA50} . Figure 5.4 shows the calculated θ_{EGR} and θ_{VGT} in five cylinders, and their mean values were applied to EGR and VGT valves.

When considering ignition delay τ , the control inputs (θ_{EGR} , θ_{VGT}) number were less than the control outputs (5 cylinder τ) number. This resulted in higher variance in τ than θ_{CA50} . In Fig. 5.3, the high cylinder-to-cylinder τ variation of cylinder 5 further degraded the τ control performance.

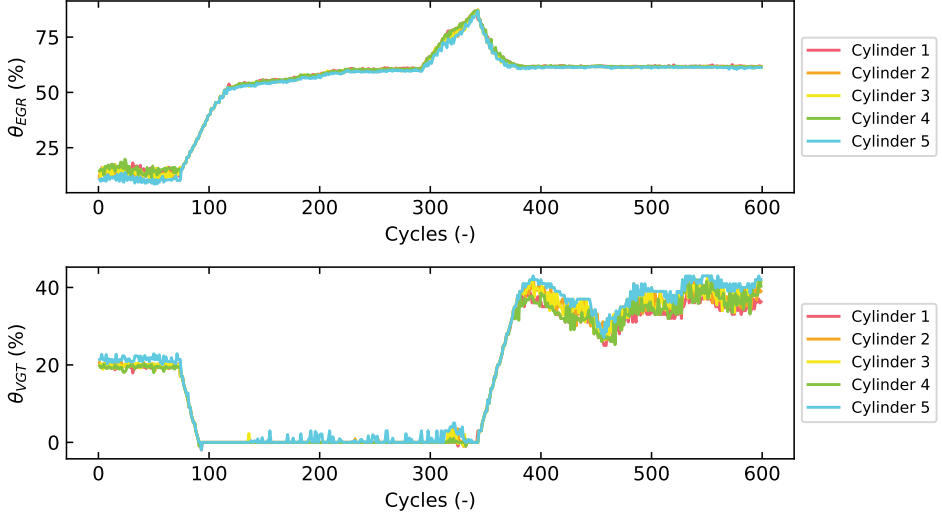


Figure 5.4: Calculated θ_{EGR} and θ_{VGT} in five cylinders.

At cycles 100 to 300 in Fig. 5.3, the τ didn't achieve the set point. Notice that the θ_{EGR} was already 0 and θ_{VGT} was in a high position, which means current τ was the highest τ the controller could reach. The punishment term in cost function (5.17) stopped the θ_{EGR} from increasing further. This is because at this moment the engine fuel system was still the easy-ignited diesel.

The τ range calculated from estimated c_1, c_2, c_3, c_4 and Eq. (5.4) can reflect the change of fuel characteristics. The τ range was composed of the possible τ minimum, the τ of Eq. (5.4) in $O_{2\text{IVC}} = 24.00\%$ and $p_{\text{IVC}} = 1.73$ bar which corresponded to $\theta_{\text{EGR}} = 0\%$ and $\theta_{\text{VGT}} = 80\%$, and the possible τ maximum, the τ of Eq. (5.4) in $O_{2\text{IVC}} = 16.12\%$ and $p_{\text{IVC}} = 1.06$ bar which corresponded to $\theta_{\text{EGR}} = 90\%$ and $\theta_{\text{VGT}} = 0\%$. As we can see next, during the fuel transition, the possible τ range also varied in the same trend which served as an indicator for fuel properties.

Figure 5.5 shows the controller behavior in the middle of the transition, approximately 15 minutes after the fuel pipe switch. Here the possible τ maximum was around 2.6 ms, bigger than that in Fig. 5.3, which was around 1.9 ms.

Figure 5.6 shows the controller behavior in the end of the transition, approximately 40 minutes after the fuel pipe switch. At that moment the possible τ maximum was around 5 ms. There was a clear difference in the τ

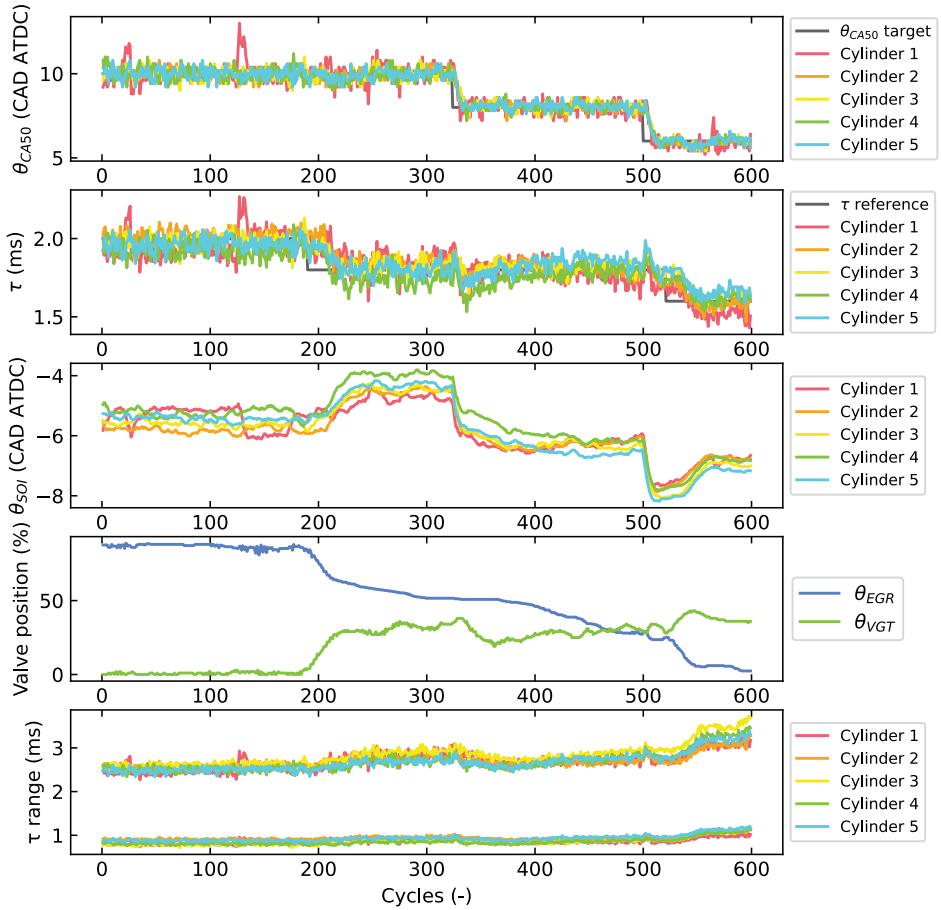


Figure 5.5: Controller behavior in the middle of diesel to gasoline/n-heptane transition

range, especially the possible τ maximum. The more gasoline there was in the engine fuel system, the higher the possible τ maximum.

Figures 5.5 and 5.6 also show the adaptive MPC performance at different fuel transition stages. The performance was comparable with that in Fig. 5.3. But to keep the similar τ value, such as at the cycle 100 in Fig. 5.5 and the cycle 100 in Fig. 5.6, the actuator values θ_{EGR} and θ_{VGT} were totally different due to the fuel properties change.

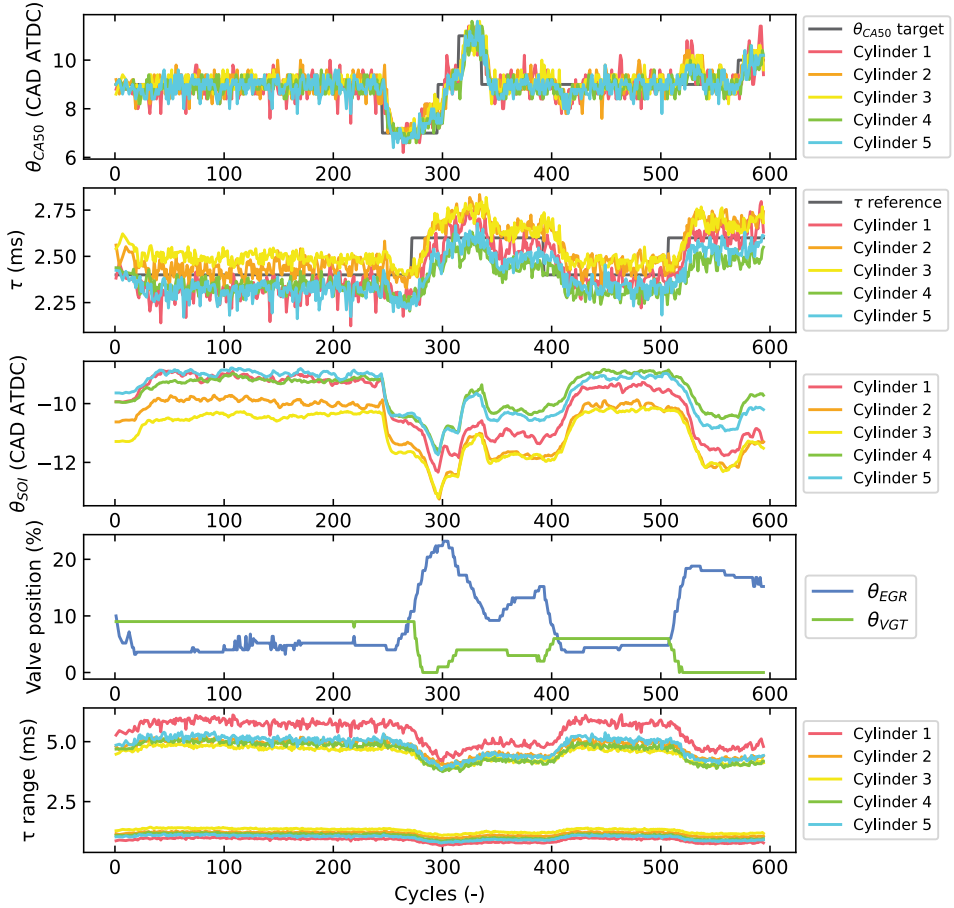


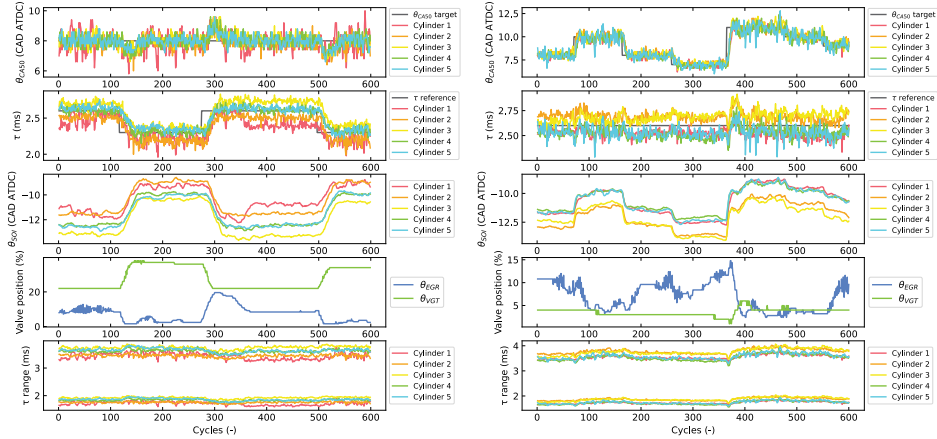
Figure 5.6: Controller behavior in the end of diesel to gasoline/n-heptane transition

Gasoline/n-heptane mixture to ethanol/n-heptane mixture

During this transition, the IMEP_g was still kept at 5 bar. Figures 5.7(a) and 5.7(b) show the τ reference transient and θ_{CA50} reference transient performance respectively at engine speed 1200 rpm. Figure 5.8 shows the performance in the engine speed N_s transient scenario.

In the transition from gasoline/n-heptane mixture to the ethanol/n-heptane mixture, the τ didn't change much. This is because gasoline and ethanol have similar cetane number and ignition properties. In this case, the τ range failed to be an indicator of the fuel transition process.

Observing from Figs. 5.3 and 5.5-5.8, the cylinder-to-cylinder ignition delay



(a) Ignition delay τ transient, 6 minutes after the fuel pipe switch (b) θ_{CA50} transient, 16 minutes after the fuel pipe switch

Figure 5.7: Controller behavior in gasoline/n-heptane to ethanol/n-heptane transition

τ variations varied for different scenarios. This might be another problem introduced by mutable fuel contents.

5.2.6 Discussion

This section proposed an adaptive MPC to control the transient combustion process of the flex-fuel engine under the changing fuel situation.

The ignition delay was a key indicator of the fuel properties inside the engine. Since the ignition delay was also changing with mutable fuels, an adaptive model was used to describe the ignition delay. An Arrhenius-type model with four parameters was built, where the parameters are estimated online with the Kalman filter. This gave MPC the ability to adapt to the time-varying fuel properties. Based on the estimated parameters, the possible ignition delay range could be calculated and was a good reflection of the fuel characteristic. The constant model used in [81], [82] was not suitable for the flex-fuel engine application. Besides, this ignition delay model got rid of the *ad-hoc* term which lacked interpretability in the combustion model in [178].

The adaptive MPC performance was validated in the fuel transition scenarios, from diesel to gasoline mixture, and then to ethanol mixture. The adaptivity was because of the mutable fuel properties. Other adaptive MPC shown in [130], [166] used the adaptivity to adjust to the unchanged engine nonlinearity

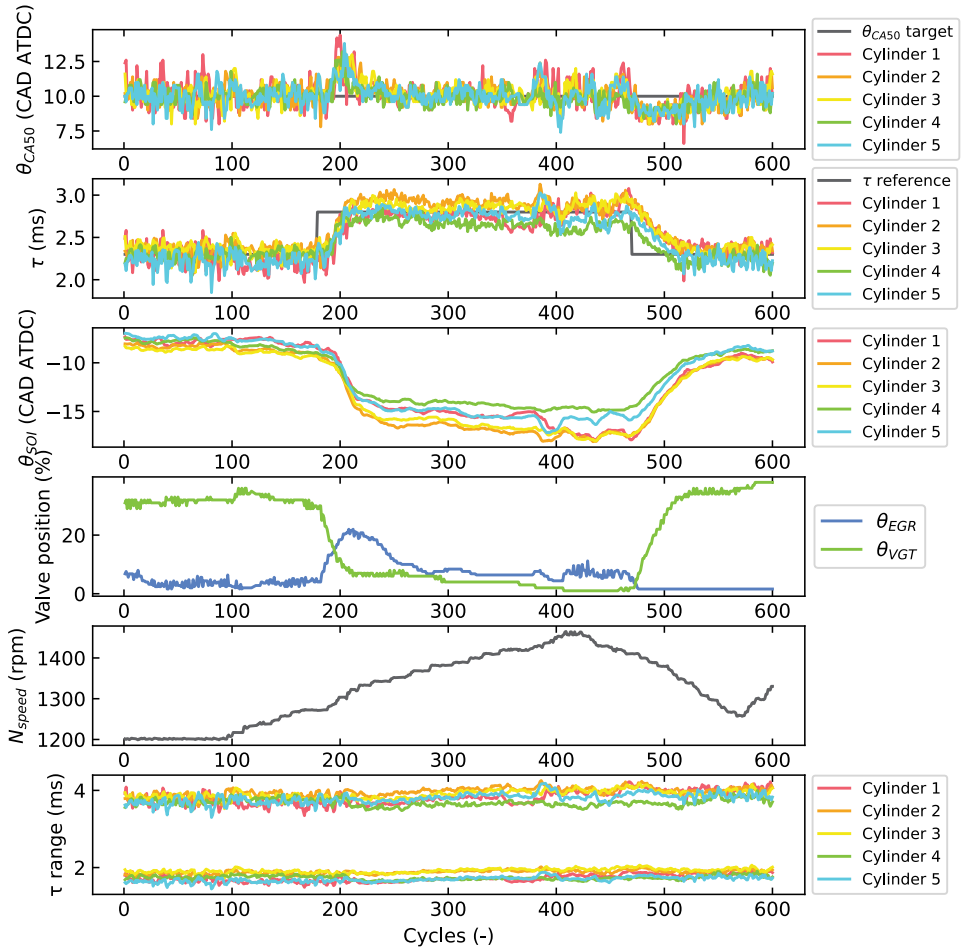


Figure 5.8: N_s transient, 25 minutes after the fuel pipe switch during gasoline/n-heptane to ethanol/n-heptane transition

online. The integration of the gas system and combustion process gave a more concise and less computationally demanding structure as compared to the MPC formulation in [178]. However, instead of the static relation between valve positions and intake manifold gas states in a small operating range, a dynamic gas system model could possibly improve the performance. It also gave the possibility of including gas exchange efficiency in the cost function.

This was the first work about the flex-fuel CI engine control to the author’s knowledge. The flex-fuel CI engine was a new concept suitable for commercial vehicles like trucks, and it could run with broader fuel choices and combustion

modes than the flex-fuel SI engine. Widely used in Brazil [39], the flex-fuel SI engine operated with two fuel species, gasoline and ethanol. Thus the controller might just need to detect ethanol concentration and apply corresponding control strategy as shown in [12], [92], whereas the fuel in flex-fuel CI engine could be a mixture of more than three different fuels, and the control strategy needed to deal with the mutable fuel property directly.

The MPC framework gave a simple way to prioritize the system output behavior. It considered interaction effects. The input constraints and the cost of using EGR and VGT were incorporated. The mean of the calculated θ_{EGR} and θ_{VGT} of five cylinders were applied to EGR and VGT valves. Whereas it will be better if all cylinders required the same EGR and VGT opening, the variation was acceptable to take an average as shown in Fig. 5.4.

The experimental engine used in this work was initially designed for diesel usage. Though some modifications had been made, the engine was still not able to run with pure gasoline or ethanol, thus the addition of n-heptane was necessary for a successful ignition. Potential hardware solutions to this problem included the usage of intake air heater [100] and ethanol compatible injectors. Besides, the pollution level was not investigated, which was another limitation. This was an important practical concern regarding the strict regulations on emissions.

5.2.7 Conclusion

An adaptive MPC approach was proposed to control the flex-fuel multi-cylinder heavy-duty CI engine. The controller was validated in the diesel to gasoline mixture transition and gasoline mixture to ethanol mixture transition. The innovations in this work include:

1. Control of flex-fuel CI engine instead of the SI engine.
2. The fuel choice is not limited to two specific fuel species.
3. Fuel species is unknown in advance for the controller, which is not the case for contemporary flex-fuel controllers.

5.3 Fuel cell control

5.3.1 Introduction

To ensure reliable operation as a power source, a polymer electrolyte fuel cell (PEFC) system should be able to supply steady voltage in its applications despite any disturbance to the working load, which is an important demand in electrical equipment use [95], [165]. Efficient and robust control strategies are considered as one of the key solutions to ensure the fuel cell system's high-reliability [97]. Significant numbers of research contributions have been conducted to develop solid and powerful control algorithms for PEFC systems to provide a steady output voltage. Yang et al. designed an adaptive controller to stabilize the fuel cell system's voltage by changing the air flow rate under system variations [176]. It was found that the adaptive controller effectively can achieve the desired reference values subject to external disturbances. Wang et al. employed H_∞ solid control strategy to improve the PEFC system's stability, finding that the controller was found effective to control the output voltage at the desired value under different loading conditions by adjusting the air flow rate [165]. In another paper, also by Wang et al., multivariable H_∞ controllers were proposed to provide steady output response by controlling both the air and hydrogen flow rates [164]. Chen increased the relative stability of a PEFC system by controlling the hydrogen and oxygen input flow rates using the designed state feedback controller [42]. Woo and Benziger incorporated a standard PID feedback controller in a PEFC system to achieve desired power output by limiting the hydrogen feed [171]. Fragiaco and Piraino kept the PEFC system working in a steady-state using a hybrid control algorithm which combined a fuzzy logic controller and an error minimization control method [56]. Narjiss et al. proposed a digital signal process controller to regulate the PEFC system's voltage and current, making it more suitable for transport application [129]. The above-mentioned studies have developed various well-qualified control methods to stabilize the PEFC system's performance. However, there are still some limitations that can be improved in future studies. For one thing, most previous control systems were only limited to one single input, the effects of other factors in the fuel cell system were neglected; for another, there is still some time delays and oscillation regarding the control performance. Reliable and highly efficient control algorithms are still much in need.

Due to its high complexity, strong nonlinearity, and especially series of constraints on the operation parameters [147], the PEFC system requires

much more advanced and robust control algorithms to ensure its reliable and safe operation. As an advanced process control method, model predictive control (MPC) controller usually excels in solving control schemes with multi-input variables and a set of constraints [27], [61], [145], which makes it especially suitable for the PEFC system's control application. MPC controllers have been widely used in PEFC systems. Vahidi et al. formulated distribution of current demand between the fuel cell and the auxiliary source using a constrained optimization MPC framework to avoid stack starvation and damage [159]. The results showed that the reactant deficit during sudden increases in stack power was reduced from 50% in stand-alone architecture to less than 1% in the hybrid configuration. Wang and Kim studied the modeling and air flow control for a PEFC using MPC [167]. It was found that the proposed MPC presents superior performance compared with the proportional-integral control result. Chatrattanawet et al. proposed both a traditional MPC and a novel robust linear time-varying MPC for PEFC control and found out the novel MPC can ensure the PEFC system's stable operation [40]. Mengi designed three different MPC-based hybrid controllers to investigate the elimination of reactive power in a medium-scale PEFC system and found out PI^λ-MPC controller presented the best performance [121]. He et al. proposed an MPC controller to enhance a PEFC system's operation by regulating its hydrogen circulation [72]. Zhang et al. implemented an MPC controller in an open cathode PEFC system to manipulate its stack temperature at the desired value despite the changes on the working load [183]. Goshtasbi and Ersal developed a linear time-varying MPC framework for an automotive PEFC system to resist its degradation [61]. Hahn et al. proposed an MPC-based operation strategy to control an automotive fuel cell air system [67]. It proved that the MPC approach had the potential of reducing the hydrogen consumption by 3% while decreasing the risk of harmful operation conditions compared with a validated map-based operation strategy.

The problem here is to regulate the fuel cell output voltage by controlling its hydrogen flow rate and air flow rates simultaneously while under the safety requirements and the workload disturbance. The safety constraints include the hydrogen pressure limits and input change rates limit. The workload is current. An MPC controller was designed to fulfill this multi-input single-output (MISO) task. The model used in MPC is a physical model simplified from the detailed system model.

5.3.2 System modeling

The system modeling for control purposes was a simplification and linearization of the model elaborated in Sec. 2.4.1. Differentiating both sides of Eq. (2.62):

$$\dot{V}_{\text{FC}} = n_{\text{cell}}(\dot{E}_n - \dot{V}_{\text{ac}} - \dot{V}_o) \quad (5.19)$$

where V_{FC} , n_{cell} , E_n , V_{ac} , and V_o denote output voltage of the fuel cell system, cell numbers, reversible voltage, voltage drop combining the activation drop and concentration drop, and ohmic voltage drop.

Here \dot{E}_n is a differentiation of Eq. (2.53) assuming the stack temperature T_{stack} is a constant value of 343K during one prediction horizon:

$$\dot{E}_n = k_1 \frac{1}{P_{\text{H}_2}} \dot{P}_{\text{H}_2} + \frac{k_1}{2} \frac{1}{P_{\text{O}_2}} \dot{P}_{\text{O}_2} \quad (5.20)$$

$$k_1 = 4.308 \cdot 10^{-5} \cdot 343 \quad (5.21)$$

where P_{H_2} and P_{O_2} are the hydrogen pressure and oxygen pressure; k_1 is a coefficient.

Combining Eqs. (2.63) to (2.73), \dot{P}_{H_2} , \dot{P}_{O_2} , and \dot{P}_{N_2} are expressed as:

$$\dot{P}_{\text{H}_2} = \frac{k_2}{0.005} \left(k_3 Q_{\text{H}_2} - 0.065 P_{\text{H}_2} + 0.065 - \frac{65I}{2 \cdot 96485} \right) \quad (5.22)$$

$$\dot{P}_{\text{O}_2} = \frac{k_2}{0.01} \left(k_4 Q_{\text{air}} - \frac{0.065 m_{\text{O}_2}}{m_{\text{O}_2} + m_{\text{N}_2}} P_{\text{N}_2} + \frac{0.065 m_{\text{O}_2}}{m_{\text{O}_2} + m_{\text{N}_2}} - \frac{65I}{4 \cdot 96485} \right) \quad (5.23)$$

$$\dot{P}_{\text{N}_2} = \frac{k_2}{0.01} \left(k_5 Q_{\text{air}} - \frac{0.065 m_{\text{N}_2}}{m_{\text{O}_2} + m_{\text{N}_2}} P_{\text{O}_2} - \frac{0.065 m_{\text{N}_2}}{m_{\text{O}_2} + m_{\text{N}_2}} P_{\text{N}_2} + \frac{0.065 m_{\text{N}_2}}{m_{\text{O}_2} + m_{\text{N}_2}} \right) \quad (5.24)$$

with coefficients:

$$k_2 = 0.0821 \cdot 10^{-3} \cdot 343 \quad (5.25)$$

$$k_3 = \frac{0.0706}{2 \cdot 60} \quad (5.26)$$

$$k_4 = 0.21 \cdot \frac{1.121}{2 \cdot 60} \quad (5.27)$$

$$k_5 = 0.79 \cdot \frac{0.988}{28 \cdot 60} \quad (5.28)$$

where I is the current; P_{N_2} is the nitrogen pressure; Q_{H_2} and Q_{air} are the inlet hydrogen volumetric flow rate and inlet air volumetric flow rate; m_{O_2} and m_{N_2} are the oxygen mass in the cathode volume and nitrogen mass in the cathode channel; k_2 , k_3 , k_4 , and k_5 are constant coefficients.

The derivative \dot{V}_o is simplified as:

$$\dot{V}_o = I \cdot \dot{R}_m = 0 \quad (5.29)$$

where R_m is the membrane resistance. The current I and R_m were assumed to be constant during the prediction horizon. Combining the Eqs. (5.19) to (5.29) gives the state-space model detailed in the next section.

5.3.3 Adaptive MPC design

State-space model

The linearized continuous-time state-space model is written as:

$$\begin{aligned} \dot{\mathbf{x}} &= \mathbf{A}\mathbf{x} + \mathbf{B}\mathbf{u} \\ \mathbf{y} &= \mathbf{C}\mathbf{x} \end{aligned} \quad (5.30)$$

The state vector \mathbf{x} is:

$$\mathbf{x} = \begin{bmatrix} V_{\text{FC}} \\ V_{\text{ac}} \\ P_{\text{H}_2} \\ P_{\text{O}_2} \\ P_{\text{N}_2} \\ 1 \end{bmatrix} \quad (5.31)$$

The physical unit for V_{FC} and V_{ac} is Volt, V; the unit for P_{H_2} , P_{O_2} and P_{N_2} is atm. The constant 1 in the state vector is to enforce integral action, taking into account the constant terms in Eqs. (5.22) to (5.24). The m_{O_2} , m_{N_2} and I are viewed as constant value during prediction horizon.

The input \mathbf{u} is:

$$\mathbf{u} = \begin{bmatrix} Q_{\text{H}_2} \\ Q_{\text{air}} \end{bmatrix} \quad (5.32)$$

The physical unit for inputs is liters per minute, lpm.

The output \mathbf{y} is:

$$\mathbf{y} = \begin{bmatrix} V_{\text{FC}} \end{bmatrix} \quad (5.33)$$

the state-space matrices are:

$$\mathbf{A} = \begin{bmatrix} 0 & \frac{65}{2R_d} & A_{13} & A_{14} & A_{15} & A_{16} \\ 0 & -\frac{1}{2R_d} & 0 & 0 & 0 & \frac{I}{2} \\ 0 & 0 & \frac{-0.065k_2}{0.005} & 0 & 0 & A_{36} \\ 0 & 0 & 0 & \frac{k_2}{0.01} \left(-\frac{0.065m_{O_2}}{m_{O_2}+m_{N_2}} \right) & \frac{k_2}{0.01} \left(-\frac{0.065m_{O_2}}{m_{O_2}+m_{N_2}} \right) & A_{46} \\ 0 & 0 & 0 & \frac{k_2}{0.01} \left(-\frac{0.065m_{N_2}}{m_{O_2}+m_{N_2}} \right) & \frac{k_2}{0.01} \left(-\frac{0.065m_{N_2}}{m_{O_2}+m_{N_2}} \right) & A_{56} \\ 0 & 0 & 0 & 0 & 0 & 0 \end{bmatrix} \quad (5.34)$$

$$\mathbf{B} = \begin{bmatrix} \frac{65k_1k_2k_3}{0.005P_{H_2}} & \frac{k_1k_2k_4}{0.002P_{O_2}} \\ 0 & 0 \\ \frac{k_2k_3}{0.005} & 0 \\ 0 & \frac{k_2k_4}{0.01} \\ 0 & \frac{k_2k_5}{0.01} \\ 0 & 0 \end{bmatrix} \quad (5.35)$$

$$\mathbf{C} = [1 \ 0 \ 0 \ 0 \ 0 \ 0] \quad (5.36)$$

here

$$\begin{aligned} A_{13} &= \frac{65k_1}{P_{H_2}} \cdot \frac{-0.065k_2}{0.005} \\ A_{14} &= A_{15} = \frac{65k_1}{2P_{O_2}} \cdot \frac{k_2}{0.01} \left(-\frac{0.065m_{O_2}}{m_{O_2}+m_{N_2}} \right) \\ A_{16} &= \frac{65k_1k_2}{0.005P_{H_2}} \left(0.065 - \frac{65I}{2.96485} \right) + \frac{65k_1k_2}{0.02P_{O_2}} \left(\frac{0.065m_{O_2}}{m_{O_2}+m_{N_2}} - \frac{65I}{4.96485} \right) - \frac{65I}{2} \\ A_{36} &= \frac{k_2}{0.005} \left(0.065 - \frac{65I}{2.96485} \right) \\ A_{46} &= \frac{k_2}{0.01} \left(\frac{0.065m_{O_2}}{m_{O_2}+m_{N_2}} - \frac{65I}{4.96485} \right) \\ A_{56} &= \frac{k_2}{0.01} \left(\frac{0.065m_{N_2}}{m_{O_2}+m_{N_2}} \right) \end{aligned} \quad (5.37)$$

For the variables in matrix A like m_{O_2} and m_{N_2} , their value were assumed to be constant during the prediction horizon. In other words, the matrix A didn't change when solving the optimization problem.

MPC design

A Quadratic Programming (QP) problem will be solved at each time step to obtain the optimal control inputs:

$$\min_{\mathbf{u}^0, \mathbf{u}^1, \dots, \mathbf{u}^{H_u-1}} \mathbf{J}(\mathbf{u}^k) = \sum_{k=1}^{H_p} \left\| \mathbf{y}^k - \mathbf{r} \right\|_{\mathbf{Q}}^2 + \sum_{k=0}^{H_u-1} \left\| \mathbf{u}^k \right\|_{\mathbf{R}}^2 + \rho \sum_{k=1}^{H_p} \left\| \boldsymbol{\epsilon}^k \right\|^2 \quad (5.38)$$

subject to:

$$\begin{aligned} \mathbf{x}^{k+1} &= \mathbf{A}^d \mathbf{x}^k + \mathbf{B}^d \mathbf{u}^k \\ \mathbf{y}^k &= \mathbf{C}^d \mathbf{x}^k \\ \mathbf{u}_{\text{lb}} &\leq \mathbf{u}^k \leq \mathbf{u}_{\text{ub}} \\ d\mathbf{u}_{\text{lb}} &\leq \mathbf{u}^k - \mathbf{u}^{k-1} \leq d\mathbf{u}_{\text{ub}} \\ \mathbf{x}_{\text{lb}} &\leq \mathbf{x}^k \leq \mathbf{x}_{\text{ub}} + \boldsymbol{\epsilon}^k \\ \mathbf{0} &\leq \boldsymbol{\epsilon}^k \\ \mathbf{u}^{-1} &= \mathbf{u}_{\text{init}} \\ \mathbf{x}^0 &= \mathbf{x}_{\text{init}} \\ k &= 0, 1, \dots, H_p \end{aligned} \quad (5.39)$$

where \mathbf{A}^d , \mathbf{B}^d , and \mathbf{C}^d are state-space matrices in discrete-time; H_p and H_u are prediction and control horizon; k in the superscript represents the time step, and $k = 0$ refers to the initial time step; \mathbf{r} is the control reference; \mathbf{Q} and \mathbf{R} are weight tuning parameters for reference tracking and control inputs; \mathbf{u}_{lb} , \mathbf{u}_{ub} , \mathbf{x}_{lb} , and \mathbf{x}_{ub} are the lower bounds and upper bounds of inputs \mathbf{u} and states \mathbf{x} ; $d\mathbf{u}_{\text{lb}}$ and $d\mathbf{u}_{\text{ub}}$ are the lower bounds and upper bounds of inputs change rate; \mathbf{u}_{init} is latest applied control inputs and \mathbf{x}_{init} is the latest measured value, the state feedback; $\boldsymbol{\epsilon}$ is the slack variable introduced to soft constraints and ρ is a nonnegative scalar to control the magnitude of penalizing soft constraint violations. To remove the constraints, it is straight forward to remove corresponding inequality clauses in Eq. (5.39) and the slack variable punishment term in Eq. (5.38).

The slack variable $\boldsymbol{\epsilon}$ is to deal with the possibility of infeasibility by hard constraints and model imperfection. It is defined that their value is non-zero only if the constraints are violated. Then the violations are highly penalized in cost function by a large enough ρ to let the optimizer have a strong incentive to keep $\boldsymbol{\epsilon}$ at zero. Besides the quadratic penalty for the constraint violations, the 1-norm (sum of violations) or the ∞ -norm (maximum violation) are also possible choices [113].

In the fuel cell problem, the state constraint was the limitation of the hydrogen pressure P_{H_2} . The hydrogen pressure in the pipe should be under a certain value to ensure safety, which was 2.5 atm here. Only slack variables for state upper bounds were introduced. The input Q_{H_2} was limited between 100 and 400 lpm and Q_{air} was limited within 300 to 700 lpm. The change rate of the inputs was constrained within -40 to 20 lpm.

The time step for the MPC controller was 0.5 s. The QP problem mentioned above was solved every 0.5 s and the first of the solved input sequences was applied to the fuel cell plant.

5.3.4 Experimental set-up

The experiment was conducted on the established Simulink model detailed in Sec. 2.4.1. Gaussian measurement noises were added to voltage V_{FC} and hydrogen pressure P_{H_2} . Two test scenarios were chosen, one was the typical step disturbance applied on the working load, the current; the other was a mixture of slope and step working load changes. Two kinds of controllers, the classical PID and MPC were applied to the fuel cell voltage control problem. Figure 5.9 shows the diagram of the PID control process.

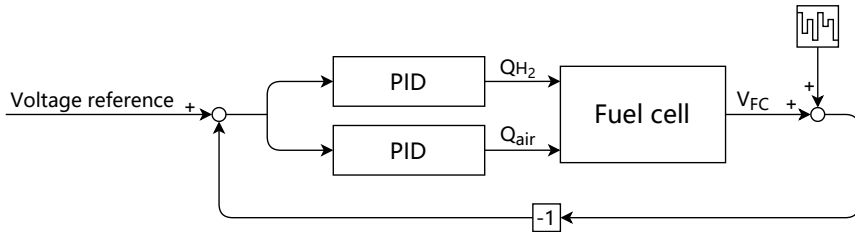


Figure 5.9: PID control process

Two separate PID controllers were built to regulate two inputs, the hydrogen volumetric flow rate Q_{H_2} and air volumetric flow rate Q_{air} .

Figure 5.10 gives the illustration of the MPC control process.

During the experiment, the PID controller acted continuously during the process and the MPC acted every 0.5 s.

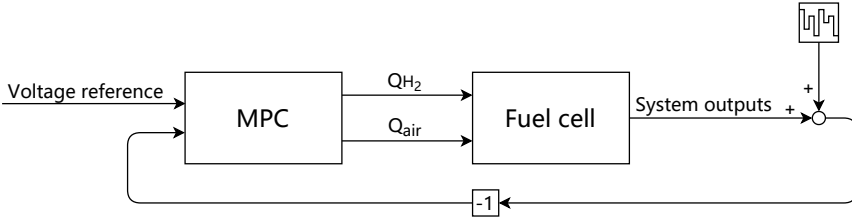


Figure 5.10: MPC control process

5.3.5 Experimental results

Firstly, the PID controller was compared with the MPC controller without the input change rate and P_{H_2} constraints. Since PID control can not handle the constraints explicitly as MPC, this gave an equitable comparison. Secondly, input change rate and state constraints were activated in MPC and the results were shown.

In the MPC parameter settings, the weight for the control target was 400; the weight for the manipulated variables (inputs) was 0.001; the weight for the input change rate was 0.3; the prediction horizon was 20 and the control horizon was 10. In the PID control settings, the proportional gain K_P and integral gain K_I for hydrogen flow rate control were 210 and 80; the K_P and K_I for air flow rate control were 210 and 30. The derivative gain was 0. The parameters were chosen that the controllers reacted fast while keeping the system stable. The input change rate was limited by added constraints in one of the test scenarios.

PID and MPC

Figure 5.11 shows the control performance of PID and MPC with the current load being interrupted by one sudden increase and one sudden decrease step. Figure 5.12 shows the corresponding hydrogen pressure P_{H_2} and control inputs Q_{H_2} and Q_{air} behavior. Figure 5.13 presents the instantaneous fuel cell power during the process.

When the system started, the output voltage increased from 0 V to 48 V. In this period, the deviation between measured voltage and reference was large, thus the PID and MPC controller both took big moves. After around 5 s, an overshoot occurred, but MPC had a smaller overshoot as compared to the PID controller. The overshoot was 0.41 V for MPC and 0.70 V for PID controller

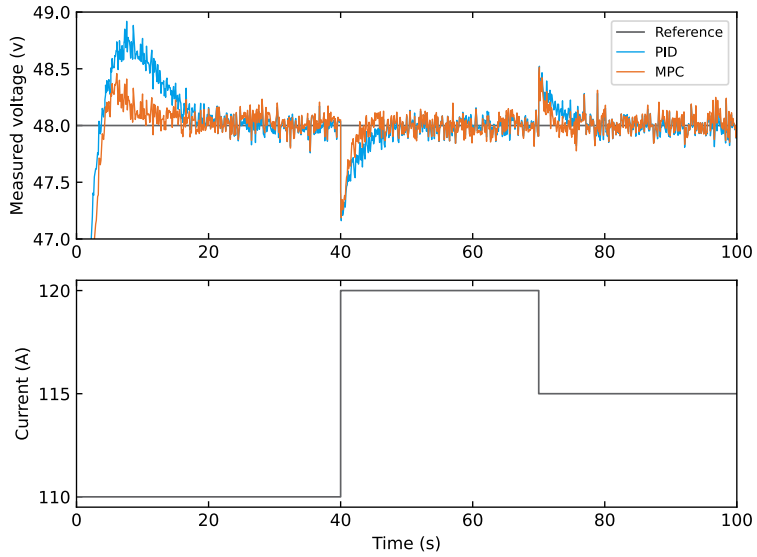


Figure 5.11: Output voltage under the current disturbance for PID and MPC without constraints.

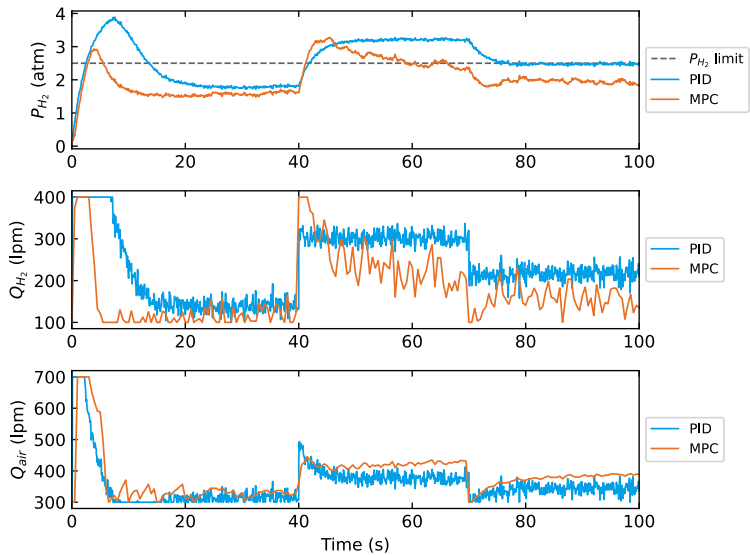


Figure 5.12: Hydrogen pressure and system inputs for PID and MPC without constraints. The P_{H_2} is hydrogen pressure; Inputs Q_{H_2} and Q_{air} are hydrogen volumetric flow rate and air volumetric flow rate.

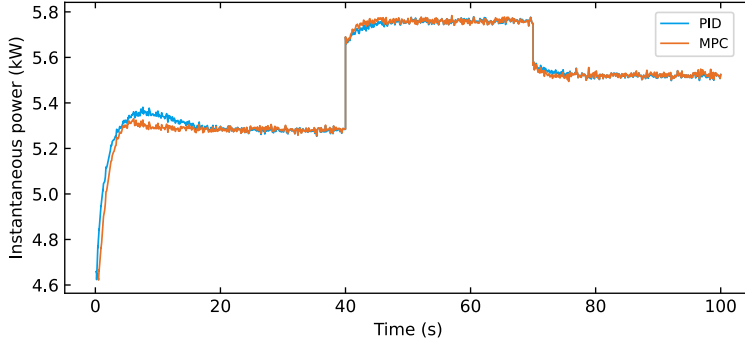


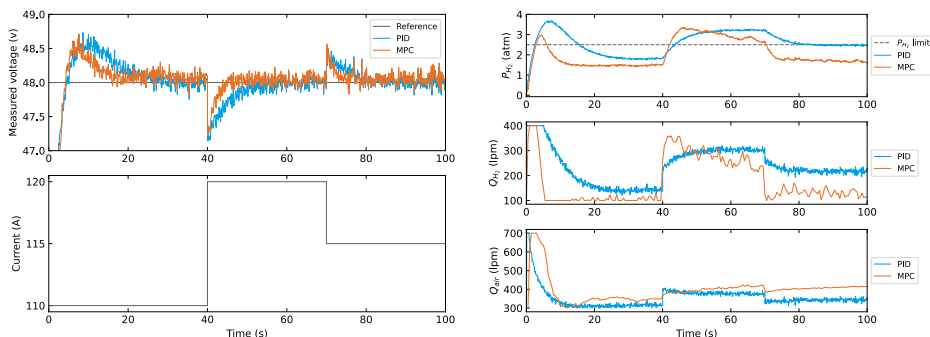
Figure 5.13: Instantaneous fuel cell power.

in terms of true system voltage. At 40 s, the current load jumped from 110 A to 120 A. According to the polarization theory, the output voltage of the PEFC system will drop with this increased current load. To resist the voltage drop, controllers adjusted the hydrogen and air flow rates to a higher level to increase the hydrogen and oxygen pressure at the anode and cathode volume and increased the voltage. In this process, the MPC responded quicker than the PID controller. To arrive at 47.9 V again, the MPC took 2.5 s and the PID controller took 5.0 s. Similarly, when the current dropped to 115 A at 70 s, the controllers decreased Q_{H_2} and Q_{air} to reduce the voltage. The MPC still had a faster response than the PID controller. Both the PID controller and the MPC can keep the PEFC system's output voltage at the desired 48 V, but the MPC showed superior performance with faster response and lower overshoot.

Both the PID controller and the MPC did not consider P_{H_2} and input change rate constraints. Thus in the period around 5 - 15 s and 40 - 70 s, the P_{H_2} went above 2.5 atm. Meanwhile, since the input change rate was not limited and both controllers adopted aggressive settings, the inputs Q_{H_2} and Q_{air} acted swiftly and more sensitively to noise. The input change rate was limited in the next section.

The performance of the controllers when adopting less aggressive parameter settings is shown in Fig 5.14. The weight for the control target in MPC was reduced to 100; the K_P and K_I for hydrogen flow rate control were 100 and 40 and for air flow rate control were 100 and 15 in the PI control settings. In this case, the MPC controller had a similar overshoot with the PID controller, but the MPC still had a faster response. The maximum overshoot for MPC was 0.46 V and for PID controller was 0.55 V. To arrive at 47.9 V again after

step disturbance at 40 s, the MPC took 3.4 s and the PID controller took 10.1 s.



(a) Output voltage and current disturbance. (b) Hydrogen pressure and system inputs.

Figure 5.14: The MPC and PI controllers behavior with less aggressive parameter settings

Figures 5.15 and 5.16 show the PID controller and the MPC performance under slope and step current changes. The result was similar as before. Figure 5.17 exhibits the instantaneous fuel cell power.

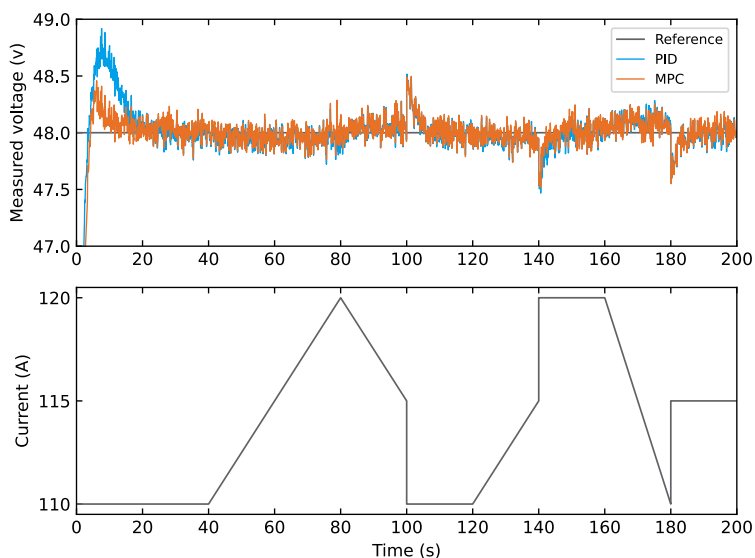


Figure 5.15: Output voltage under the current disturbance for PID and MPC without constraints.

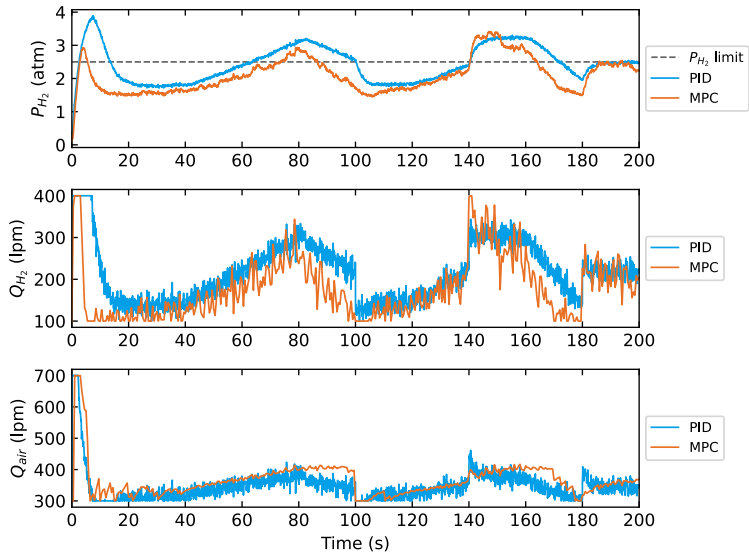


Figure 5.16: Hydrogen pressure and system inputs for PID and MPC without constraints.

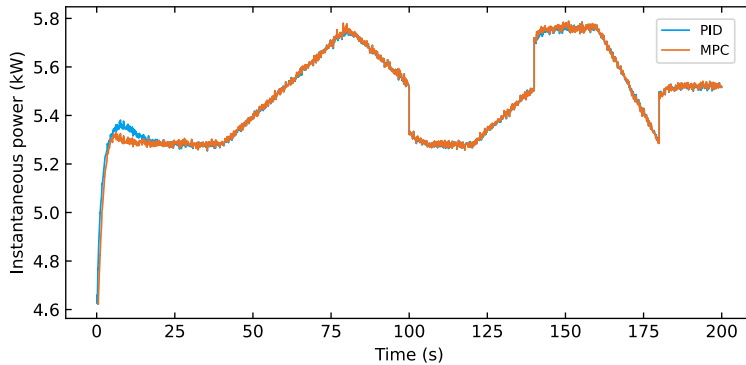


Figure 5.17: Instantaneous fuel cell power.

It can be seen from these two studies that both the PID and MPC controllers can stabilize the output voltage at the reference value despite the working load disturbance and measurement noise, and the MPC outperformed the PID control with faster response and lower overshoot. However, the MPC required more system information as the state measurement for feedback control, whereas the PID control only needed the measured control target value. The PID control had a simpler structure and fewer parameters thus

was easy to design and tune.

MPC with constraints

One major advantage of MPC over PID control is its ability to handle constraints explicitly. The hydrogen pressure P_{H_2} and input Q_{H_2} and Q_{air} change rate limits, the safety consideration, were added to MPC in this section. The results were compared with that of MPC without constraints, as shown in Figs. 5.18 to 5.21.

Figures 5.18 and 5.19 show the MPC with constraints and MPC without constraints performance under working load step changes. Controlled voltage by the MPC with constraints increased slower than that of the MPC without constraints when the system started because the input change rate limits suppressed the rapid inputs rise. The overshoot for the MPC with constraints and the MPC without constraints was 0.42 V and 0.41 V in terms of the true system voltage. Meanwhile, the P_{H_2} of MPC without constraints exceeded 2.5 atm and MPC with constraints successfully kept the P_{H_2} under 2.5 atm. When the current load increased to 120 A at 40 s, both inputs increased, but the change rate limits still acted, thus the MPC with constraints responded slower. It took 5.2 s for MPC with constraints instead of 2.5 s to arrive at 47.9 V in this case. When the P_{H_2} was about to hit the limit at around 45 s, the input Q_{H_2} decreased quickly to ensure safety, while the input Q_{air} did not drop to ensure the voltage following the reference. When current dropped to 115 A at 70 s, the MPC with constraints still acted slower.

Figures 5.20 and 5.21 show the MPC with constraints and MPC without constraints performance under slope and step current changes. The controlled voltage of the MPC with constraints was able to satisfy the P_{H_2} limit all the time and responded slower due to the change rate limit.

5.3.6 Discussion

This section proposed an MPC controller for voltage regulation under safety requirements and current disturbance by adjusting the hydrogen and air volumetric flow rate. The proposed MPC was superior to the PI controller in response time and overshoot in two different parameter settings. The model-based controller accounted for the system future behavior which gave a more precise inputs solution. The controller manipulated the hydrogen and air flow rate at the same time. The simultaneous control of the inputs gave a

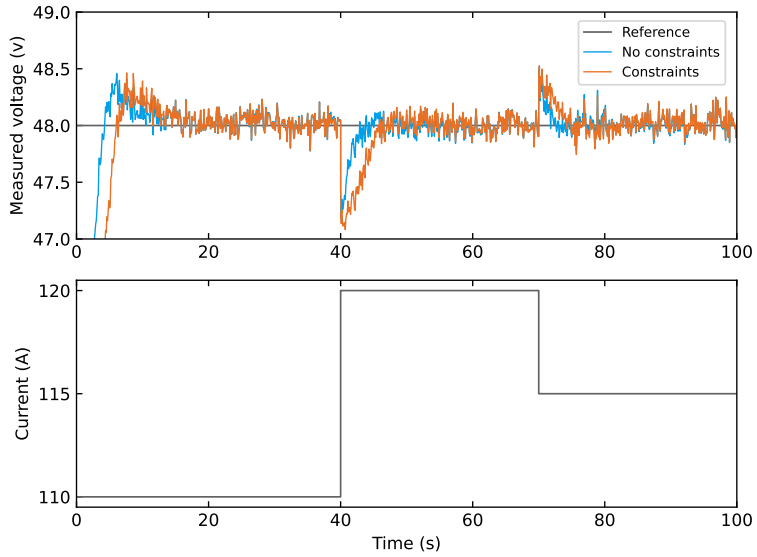


Figure 5.18: Output voltage under the current disturbance for MPC without constraints and MPC with constraints.

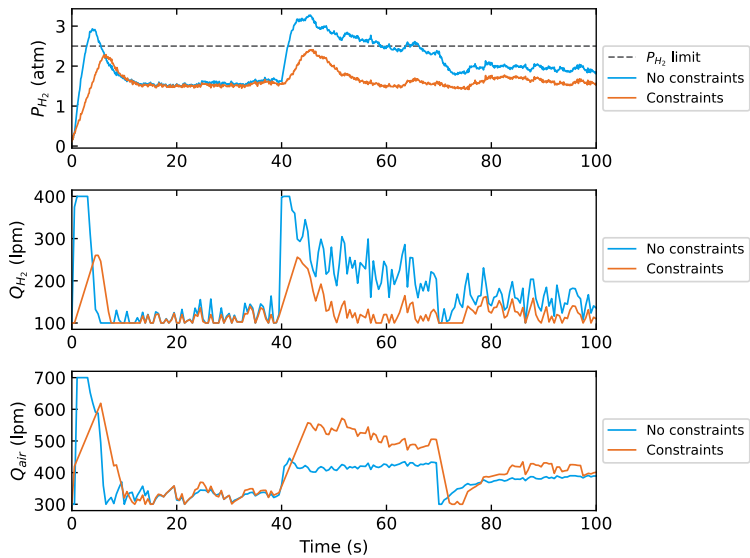


Figure 5.19: Constraint handling and system inputs for MPC without constraints and MPC with constraints.

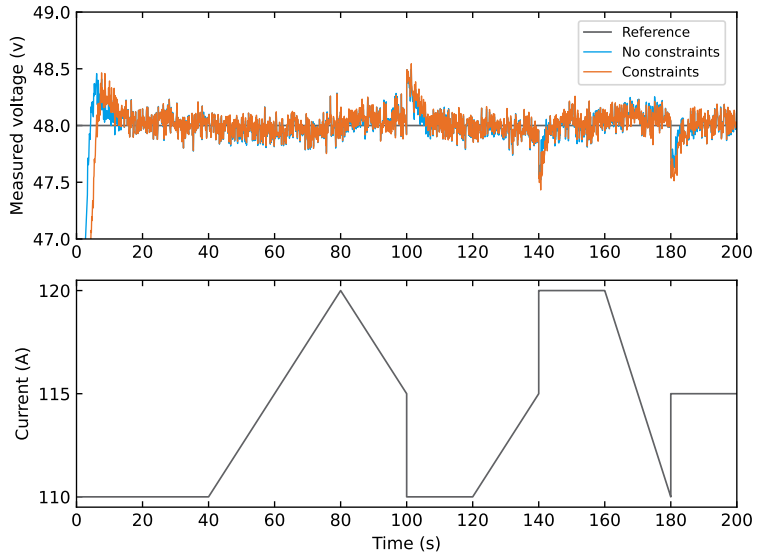


Figure 5.20: Output voltage under the current disturbance for MPC without constraints and MPC with constraints.

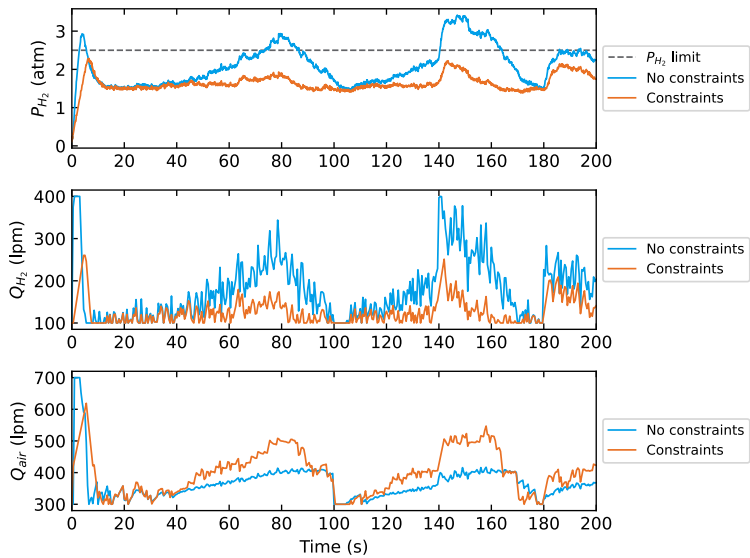


Figure 5.21: Constraint handling and system inputs for MPC without constraints and MPC with constraints.

more practical and broader application scenario. In contrast, the controller designs in [18], [63], [167] only adopted the air flow rate as input. The controller here also considered the safety requirements which included the hydrogen pressure and actuator limits. The hydrogen pressure limit ensured safe operation inside the fuel cell and the inputs change limits was a result of actuator characteristic as well as a safety consideration. The simulation result showed that it successfully fulfilled the voltage regulation task and can handle safety requirements well. Many other MPC designs for fuel cells didn't take those requirements into account, like [62], [133]. It is possible to add constraints to the PI controller. However, the MPC framework provided a systematic way of handling input and output constraints. All constraints were accounted for simultaneously, and it was straightforward to remove and add constraints. The MPC was also flexible when modifying inputs or outputs and adjusting the size of the optimization problems accordingly. The models used for MPC were linear models simplified from detailed system models. The linear property contributed an efficient and fast solver which was easy to implement. The MPC designs in [62], [110], [133], [189] adopted nonlinear models which were undesired in computational power limited cases especially for an embedded controller.

Although the MPC framework had its potential advantages, it required careful tuning to get the desired controller behavior. An accurate model was also needed to achieve superior performance. The modeling process could be tedious and required expert knowledge. Meanwhile, the MPC design in this section required a lot of system information, which could be hard to implement in practice. Though MPC had a better performance, the effectiveness and simple of PID control made it attractive in many cases without constraints. It is also limited that the method was only validated on a Simulink model, while a test on real fuel cell stacks would be much more desirable. The target of the controller was to keep a constant output voltage, and didn't consider the efficiency interval.

The controller here didn't use the hydrogen and air excess ratio to their minimum required flow rates for maintaining current density as the control inputs. However it could be an interesting idea since it was also important to keep excess ratio above a certain value for safe operation [46]. The investigated target was mainly the reaction subsystem of the fuel cell, while there were other subsystems like the thermal, water management, and power electronics subsystems that arose interesting control tasks. For example, the temperature and moisture level maintenance task, which was important to a stable and efficient operation.

5.3.7 Conclusion

A PID controller and an MPC controller were designed to regulate the fuel cell output voltage by controlling the hydrogen and air flow rates at the same time. MPC designs with and without constraints were explored. The controller performances were validated and compared on two different current disturbance situations. The results showed that MPC gave a quicker response and less overshoot than PID control with the help of the system model, and MPC with constraints can handle the safety requirements well.

6.1 Introduction

Besides the adaptive physical-based model control method, the learning and data-based control methods draw more and more attention in recent years with the availability of increasing sensing and computational power as well as the achievements in the machine learning field. MPC gives a reliable way to exploit the data abundance while satisfying the safety constraints, which makes learning-based MPC a preferable approach.

Most of the research address learning for automatic prediction model improvement from recorded data during operation [77]. Kabzan et al. presented a learning-based control approach for autonomous racing, where the vehicle model was improved online based on selected data points [88]. Desaraju et al. applied parametric learning-based MPC methods to improve a quadrotor model over time for robotic systems while considering the approximate prediction uncertainty [48].

Meanwhile, direct usage of machine learning methods based on pre-collected data utilizes its strong representation ability for complicated system modeling. Afram et al. showed the application of neural networks (NN) based MPC on a complicated nonlinear heating, ventilation, and air-conditioning system [11]. Kazemi et al. designed a learning-based stochastic MPC for cooperative adaptive cruise control to handle interfering vehicles with neural networks [91].

Aswani et al. proposed a learning-based MPC framework that combines a physical-based base model and a data-based learning model, trying to combine the robustness of physical models and the prediction performance of data-based models [23]. This approach was adopted by Bouffard et al. in a quadrotor control task to catch a ball thrown with a priori unknown trajectory [37]. Another conceptually learning-based control leverages MPC for constraint fulfillment and safety requirements, and the performance is optimized with a reinforcement learning algorithm [77].

Gaussian process (GP) is a popular nonparametric approach as the learning model due to its ability to provide an assessment of prediction uncertainty. Likar and Kocijan used Gaussian process MPC for the control of a gas-liquid separation plant [104]. A stochastic MPC based on Gaussian processes was applied to the Barcelona drinking water network taking real demand data into account by Wang et al. [168]. Chen et al. utilized Gaussian process model-based control for underactuated balance robot control [41].

In this chapter, the learning-based MPC framework combining a base model and a learning model is adopted for the engine combustion process control, and the Gaussian process MPC is applied to the fuel-cell control task.

6.2 Compression-ignition engine control

6.2.1 Introduction

Learning models and learning control methods are interesting ideas for combustion engine applications which is a highly nonlinear and complicated system. Various works have been done in this area for decades, and this field has become more active recently with encouragement from successes in the machine learning field and hardware developments.

Malikopoulos et al. took the reinforcement learning approach to learn the optimal engine calibration perceiving the driver's driving style in real-time while running a vehicle for fuel economy [115]. Stochastic gradient based extreme learning machines was adopted for stable online learning of a homogeneous charge compression ignition (HCCI) engine by Janakiraman et al. [83]. Liu et al. applied random forest models on the prediction of combustion feedback information for a natural gas spark ignition engine [106]. Badra et al. proposed machine learning grid gradient ascent methods for heavy-duty gasoline compression ignition engine modeling and validated

with engine computational fluid dynamics simulations [26]. In-cylinder flow fields were analyzed with a multilayer perceptron and boosted decision trees to predict a direct injection spark-ignition gasoline engine performance by Hanuschkin et al. [70].

Lenz and Schroeder made use of neural networks for multidimensional nonlinearities identification in closed-loop control of air-to-fuel ratio on a spark-ignition Engine [99]. Recurrent neural network was used by Müller and Schneider for the approximation and control of the engine torque [126]. Javaherian et al. presented an adaptive critic design, one model-free action-dependent heuristic dynamic programming method, for engine torque and air-fuel ratio control [84]. A similar approach was adopted by Shih et al. for engine emission control [153] and by Xue et al. for engine idle speed control [174].

The combination of learning models and MPC is also an active research area. Egan et al. gave usage of the neural network along with physical models in nonlinear model predictive engine control for the spark-ignition engine [49]. Both Moriyasu et al. and Hu et al. adopted the neural network in the MPC design for engine air path system control task [80], [124]. Bergmann et al. showed the nonlinear MPC with Gaussian process regression for heavy-duty turbocharged diesel engine control [32].

However, the lack of extrapolation ability limits the pure data-based black-box model usage in safety-critical control applications and requires careful calibrations and regulations. To resolve this problem, Aswani et al. proposed a learning-based model predictive control (LBMPC) method. In this framework, two models, the physical-based base model and the data-based learning model, are used. It makes use of the base model for constraints handling to ensure safety, and the learning model for prediction to get better performance. Aswani et al. showed that LBMPC can utilize statistical learning to identify richer models of the system in order to improve performance while providing deterministic guarantees on robustness [23].

LBMPC has been widely applied for control challenges with dynamic environments. Aswani et al. adopted the LBMPC to reduce the transient and steady-state electricity consumption in a heating, ventilation, and air conditioning system [24]. Ostafew et al. applied learning-based nonlinear MPC to improve vision-based robot path-tracking in challenging outdoor environments [131]. Rosolia et al. applied LBMPC to autonomous racing, exploiting information from the previous racing laps to improve the control performance [143].

In this chapter, a learning-based MPC is proposed for combustion timing control. Since it was the first application of LBMPC on engine control, a relatively simple control scenario with only diesel fuel was chosen instead of multiple fuel transitions. The control target was only the combustion timing CA50 instead of the CA50 and ignition delay.

6.2.2 System modeling

Learning-based MPC requires two different model parts: the base model and the learning model. The base model is a constant model, usually with clear physical meaning, and used to handle state and input constraints. The learning model is learned and updated online from sensor data by statistical learning and can be used to capture system variations, unmodeled dynamics, and noises. The model definitions here are in the context of one cylinder.

Base model

The process from the injection spray to the end of combustion is intertwined and complicated, including liquid atomization, break-up, mixing, low temperature reaction and high temperature reaction [78]. It was influenced by the fuel-gas mixing and inlet charge conditions. Normally a nonlinear physical ignition-delay model and an empirical combustion model were used to capture this process, but it required time and experiments to calibrate the coefficients in those models for different operating points. This time-consuming process was taken over by the learning model in LBMPC. A constant base model was firstly used to describe the combustion process. The injection strategy was triple injections with two pilot injections and one main injection. It can reduce the pressure-rise rate and give a better fuel economy in comparison to a double injection strategy. The base model:

$$\theta_{CA50} = \theta_{SOI} + \theta_D \quad (6.1)$$

where θ_{CA50} is the crank angle relative to top dead center (TDC) for 50% heat released, the combustion timing; θ_{SOI} is the crank angle of the main injection timing; θ_D is the crank angle dwell between them; θ_D includes the ignition delay and half of the combustion duration and was influenced by load, inlet condition, and so forth. For the base model, θ_D was set to a constant.

Learning model

To capture the trend of θ_D , linear model for θ_D was proposed:

$$\theta_D = \mathbf{w}^T \boldsymbol{\mu} \quad (6.2)$$

where $\boldsymbol{\mu}$ are variables chosen to model the θ_D behavior; \mathbf{w} are the corresponding coefficients, \mathbf{w}^T meaning the transpose of \mathbf{w} . Here the $\boldsymbol{\mu}$ is:

$$\boldsymbol{\mu} = \begin{bmatrix} d_{\text{inj}} \\ p_{\text{IVC}} \\ O_{2\text{IVC}} \end{bmatrix} \quad (6.3)$$

where d_{inj} is the sum of three injection durations; p_{IVC} and $O_{2\text{IVC}}$ are inlet pressure and inlet oxygen concentration at intake valve closing respectively. When the engine is running, the controller updates parameters w using stochastic gradient descent (SGD):

$$\mathbf{w}^{k+1} = \mathbf{w}^k + \alpha(\theta_D^k - (\mathbf{w}^k)^T \boldsymbol{\mu}^k) \boldsymbol{\mu}^k \quad (6.4)$$

where θ_D^k and $\boldsymbol{\mu}^k$ are the measurements of θ_D and $\boldsymbol{\mu}$ at cycle k ; \mathbf{w}^{k+1} and \mathbf{w}^k are coefficients at cycle $k+1$ and k ; α is the learning rate. For different operating intervals, different sets of \mathbf{w} were adopted and updated separately.

6.2.3 Learning-based MPC design

State-space model

A linearized, discrete-time, state-space model of the plant:

$$\begin{aligned} \mathbf{x}_B^{k+1} &= \mathbf{A} \mathbf{x}_B^k + \mathbf{B} \mathbf{u}^k \\ \mathbf{y}^k &= \mathbf{C} \mathbf{x}_B^k \end{aligned} \quad (6.5)$$

where k indicates the time step; \mathbf{x}_B are the system states; \mathbf{u} are system inputs; \mathbf{y} are the system outputs; \mathbf{A} , \mathbf{B} , and \mathbf{C} are constant state-space model parameters. Assuming θ_D is constant, and take differential of Eq. (6.1) respect to engine cycles, yielding the difference equation:

$$d\theta_{\text{CA50}} = d\theta_{\text{SOI}} \quad (6.6)$$

where the $d\theta_{\text{SOI}}$ is set to the plant input, constituting \mathbf{u} in the state-space model, and $d\theta_{\text{CA50}}$ constitutes \mathbf{x}_B . The MPC using only the base model will

be used as a baseline controller for comparison, which will be referred to as MPC in the following part of this section. LBMPC adds learning terms to base state-space model:

$$\mathbf{x}_L^{k+1} = (\mathbf{A} + \mathbf{F})\mathbf{x}_L^k + (\mathbf{B} + \mathbf{H})\mathbf{u}^k \quad (6.7)$$

where \mathbf{x}_L are states of the learning-based state-space model. The added parameters \mathbf{F} , \mathbf{H} are learned and updated online while the controller is running. The θ_D can be modeled by the learning model of Eq. (6.2) online. Taking differential of Eq. (6.1) in consideration of learning model, yields:

$$d\theta_{CA50} = d\theta_{SOI} + d\theta_D \quad (6.8)$$

Integrating the learned $d\theta_D$ into \mathbf{F} gives the learning-based state-space model.

Adopt the following learning-based state-space model:

$$\begin{aligned} \mathbf{x}_L^{k+1} &= (\mathbf{A} + \mathbf{F})\mathbf{x}_L^k + (\mathbf{B} + \mathbf{H})\mathbf{u}^k \\ \mathbf{y}^k &= \mathbf{C}\mathbf{x}_L^k \end{aligned} \quad (6.9)$$

where

$$\mathbf{u} = \begin{bmatrix} d\theta_{SOI1} \\ d\theta_{SOI2} \\ d\theta_{SOI3} \\ d\theta_{SOI4} \\ d\theta_{SOI5} \\ d\theta_{SOI6} \end{bmatrix}, \mathbf{x}_B^0 = \mathbf{x}_L^0 = \begin{bmatrix} \theta_{SOI1} \\ \theta_{SOI2} \\ \theta_{SOI3} \\ \theta_{SOI4} \\ \theta_{SOI5} \\ \theta_{SOI6} \\ 1 \end{bmatrix}, \mathbf{y} = \begin{bmatrix} \theta_{CA501} \\ \theta_{CA502} \\ \theta_{CA503} \\ \theta_{CA504} \\ \theta_{CA505} \\ \theta_{CA506} \end{bmatrix} \quad (6.10)$$

The variable θ_{SOIi} refers to the main injection timing in cylinder i ; θ_{CA50i} is the combustion timing of cylinder i . \mathbf{x}_B^0 and \mathbf{x}_L^0 are the initial states of the state-space models.

$$\begin{aligned} \mathbf{A}_{7 \times 7} &= \begin{bmatrix} 1 & & 0 \\ & \ddots & \vdots \\ & & 1 \\ 0 & \dots & 0 \end{bmatrix}, \quad \mathbf{B}_{7 \times 6} = \begin{bmatrix} 1 & & & & & \\ & \ddots & & & & \\ & & & & & 1 \\ 0 & \dots & 0 & & & \end{bmatrix} \\ \mathbf{F}_{7 \times 6} &= \beta \cdot \begin{bmatrix} 0 & \dots & 0 & d\theta_{D1} \\ & & & d\theta_{D2} \\ \vdots & & \vdots & d\theta_{D3} \\ & & & d\theta_{D4} \\ & & & d\theta_{D5} \\ & & & d\theta_{D6} \\ 0 & \dots & 0 & 0 \end{bmatrix}, \quad \mathbf{C}_{6 \times 7} = \begin{bmatrix} 1 & & & & & & 0 \\ & \ddots & & & & & \\ & & & & & & \\ & & & & & & \\ & & \ddots & & & & \vdots \\ & & & & 1 & & 0 \end{bmatrix} \end{aligned} \quad (6.11)$$

where subscript of matrices indicates the matrix dimension. θ_{Di} is the i -th cylinder θ_D , calculated by Eq. (6.2); \mathbf{H} is a 7×6 zero matrix; β adjusts the

strength of the learning process; $\beta = 0$ means that the learning model takes no effect in LBMPC. By setting β to 0 or not, one can switch between the base state-space model and the learning-based state-space model.

LBMPC design

At each time step, a quadratic programming (QP) problem will be solved to obtain optimal control inputs:

$$\min_{\mathbf{u}^0, \mathbf{u}^1, \dots, \mathbf{u}^{H_u-1}} \mathbf{J}(\mathbf{u}^k) = \sum_{k=1}^{H_p} \left\| \mathbf{y}^k - \mathbf{r} \right\|_{\mathbf{Q}}^2 + \sum_{k=0}^{H_u-1} \left\| \mathbf{u}^k \right\|_{\mathbf{R}}^2 \quad (6.12)$$

subject to:

$$\begin{aligned} \mathbf{x}_B^{k+1} &= \mathbf{A}\mathbf{x}_B^k + \mathbf{B}\mathbf{u}^k \\ \mathbf{x}_L^{k+1} &= (\mathbf{A} + \mathbf{F})\mathbf{x}_L^k + (\mathbf{B} + \mathbf{H})\mathbf{u}^k \\ \mathbf{y}^k &= \mathbf{C}\mathbf{x}^k \\ \mathbf{u}_{\text{lb}} &\leq \mathbf{u}^k \leq \mathbf{u}_{\text{ub}} \\ \mathbf{x}_{\text{lb}} &\leq \mathbf{x}_B^k \leq \mathbf{x}_{\text{ub}} \\ \mathbf{x}_L^0 &= \mathbf{x}_B^0 = \mathbf{x}_{\text{init}} \\ k &= 0, 1, \dots, H_p \end{aligned} \quad (6.13)$$

where \mathbf{r} are the references; \mathbf{Q} , \mathbf{R} are weight-tuning-parameters for reference tracking and control inputs; \mathbf{x}_{init} are the initial states at present time step; \mathbf{u}_{lb} , \mathbf{u}_{ub} , \mathbf{x}_{lb} , and \mathbf{x}_{ub} are the lower bounds and upper bounds of inputs \mathbf{u} and states \mathbf{x}_B ; H_p and H_u are the predictive horizon and control horizon; k in the superscript represents the time step, and $k = 0$ refers to the current time step.

It should be noticed that the base model was used to satisfy constraints, while the learned model was utilized for prediction to get better performance. This is the main insight of LBMPC, where safety and performance are decoupled in an optimization framework by maintaining two models of the system. The LBMPC probabilistically converges to an MPC computed using true system dynamics if the system is sufficiently excited [23].

6.2.4 Experimental results

The experimental set-up is detailed in Chapter 4. In this experiment, only diesel fuel was used.

To evaluate the learning-based MPC controller performance, tests were carried out in the following scenarios: MPC and LBMPC comparison in load transient, load and θ_{CA50} reference transient, LBMPC in load, θ_{CA50} and speed transient. A triple injection strategy with two pilot injections and one main injection was applied in those tests. The two pilot injections timing and duration were set constant in experiments. For each running, all coefficients \mathbf{w} were set to 0 in the beginning. Then MPC with the base model ran for one sequence. During this process, coefficients \mathbf{w} were updated continuously. The coefficients \mathbf{w} can converge within 50 cycles for one operating interval, as shown in Fig. 6.1. After running one sequence with MPC, LBMPC was applied.

In load transient, the engine speed was 1200 rpm, and load transient is generated by changing main injection duration, varied from 0.6 ms to 0.9 ms. The result is shown in Fig. 6.2. As load increases or decreases, the combustion timing will retard or advance respectively without system inputs, causing an impact on combustion timing. The controller will advance or retard the injection timing to keep combustion timing constant. As compared to the MPC controller, LBMPC can respond more agile, keeping the impact lower

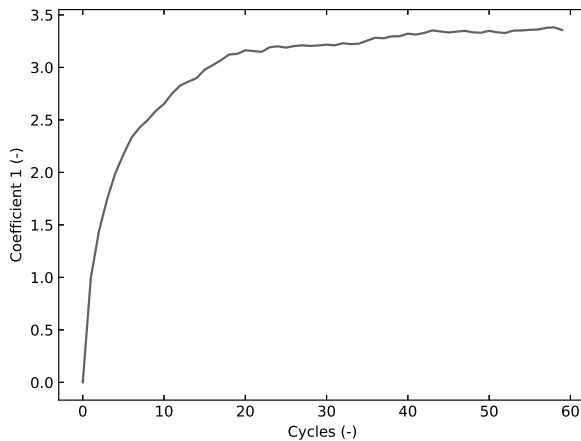


Figure 6.1: Coefficient update.

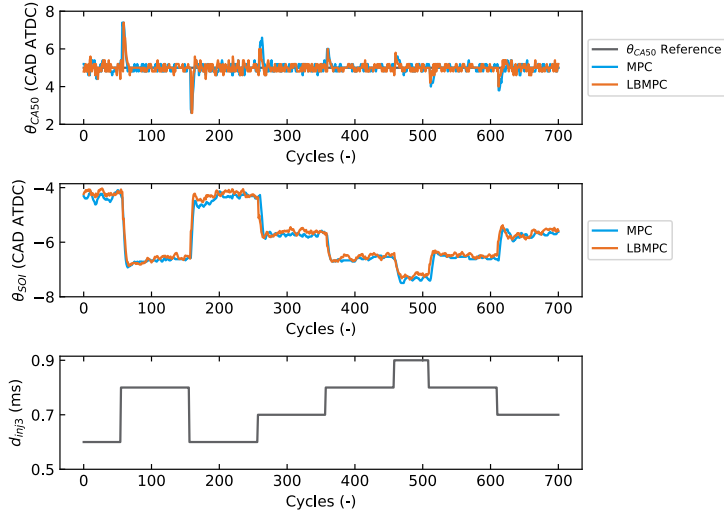


Figure 6.2: Controller performance in load transient.

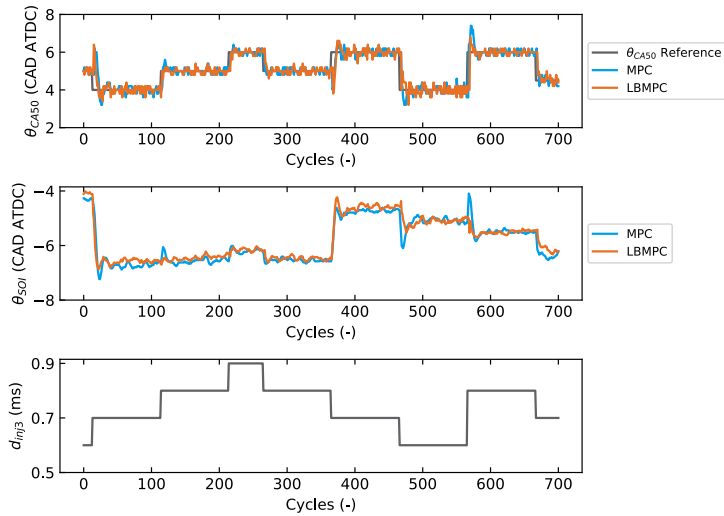


Figure 6.3: Controller performance in load and θ_{CA50} reference transient.

and achieving reference tracking faster.

In load and θ_{CA50} reference transient, combustion timing reference varied from 4 CAD ATDC to 7 CAD ATDC, and the main injection duration varied from 0.6 ms to 0.9 ms. The engine speed was kept constant at 1200 rpm. The result is shown in Fig. 6.3. Both MPC and LBMPC can track the reference

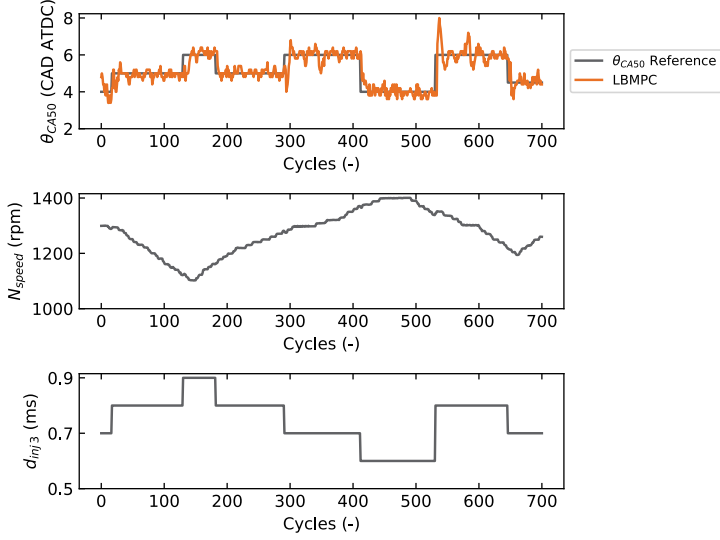


Figure 6.4: Controller performance in load, θ_{CA50} reference and speed transient.

signal quickly, within 2 cycles. But LBMPC can better handle the transient situations by using the learned transient information. This resulted in a significant reduction in overshoot and gave a faster response. Meanwhile, LBMPC had lower variances in steady-state conditions.

In Fig. 6.4, the engine speed varied from 1100 rpm to 1400 rpm, and load and θ_{CA50} reference settings were the same as the previous scenario. LBMPC controller can track the reference combustion timing signal well in this case.

6.2.5 Discussion

The proposed LBMPC method utilized a base model and a learning model to decouple the safety and performance requirements. The LBMPC was successfully applied to the engine combustion phasing control. The performance was validated on a heavy-duty engine running with diesel. It showed superior performance over MPC in terms of faster response and lower overshoot. The separation of safety and performance by two models gave a flexible framework, where many different learning models could be incorporated as needed [23]. There were also other learning-based approaches for engine control as shown in [32], [80], [170], but it was the first application of the adopted LBMPC framework in the engine control field. Previous work

on the same experimental engine applied MPC to the combustion control problem [81], [179], while this method added a new learning model which can improve the performance online. The novel structure of LBMPC also provided possibilities of application on more complicated cases such as the fuel transition scenario in a flex-fuel engine.

The limitation of this work is the validation scenario was relatively simple and didn't show its behavior in a fuel transition situation. Though simpler methods can be found in this specific scenario, this application showed the potential of the LBMPC method.

6.2.6 Conclusion

This chapter introduced a learning-based model predictive control method applied to multi-cylinder engine combustion timing control. The base model and learning model were introduced to satisfy constraints and improve performance accordingly. A quadratic programming problem with constraints was formed to control the combustion timing. MPC and LBMPC were detailed, and their performances are compared. The experimental results confirmed that LBMPC responded faster and had a lower overshoot comparing with MPC.

6.3 Fuel cell control

6.3.1 Introduction

The learning methods and learning control methods are also attractive to fuel cell applications due to its nonlinearity and complexity. Mehrpooya et al. trained a two-hidden-layer neural network to predict fuel cell steady-state performance with experimentally collected data with different inlet humidity, temperature, and oxygen and hydrogen flow rates [120]. Han and Chung adopted both neural network and SVM to describe the fuel cell polarization curve and compared their performances [68]. Bicer et al. utilized neural network for fuel cell dynamics prediction trained on data collected from MATLAB simulation [34]. A nonparametric Gaussian process regression model was used by He and Ma to capture the nonlinear relationship between operating conditions and output voltage in the microbial fuel cell. A simple online learning strategy was also proposed to recursively update the model hyper-parameters [73]. Zhu and Chen applied Gaussian process state-space models to analyze the degradation of fuel cells, and incorporated prediction confidence interval to improve the inference accuracy [188]. Zhang et al. constructed Gaussian process regression model to predict the methane conversion rate in a solid oxide fuel cell [184].

There are also some research efforts focusing on learning control methods for fuel cell applications. El-Sharkh et al. applied neural networks based active and reactive power controller to a stand-alone PEFC output power management problem [149]. Gheisarnejad et al. adopted a deep deterministic policy gradient method to adjust the coefficients of baseline PI controller adaptively by online learning for oxygen excess ratio regulation of PEFC [60]. This work used model-free features of reinforcement learning. Zhou et al. devised a predictive energy management policy for fuel-cell/battery-based PHEVs with MPC control framework, where speed prediction is enhanced by online learning Markov predictor [187].

The problem here is to control the fuel cell voltage under safety constraints and workload disturbance. Different from Sec. 5.3, the detailed system model is unknown to the controller and only collected system data is available. Gaussian processes are used to build a system model from collected data. An MPC controller based on the linearized Gaussian process model is proposed to fulfill the control task.

6.3.2 System modeling

The procedures and specifications of building Gaussian processes are detailed in Sec. 2.4.2. Two Gaussian processes f_V and f_P were obtained to describe the fuel cell dynamics:

$$\begin{aligned} V_{\text{FC}}^{k+1} &= f_V(\mathbf{u}^k, V_{\text{FC}}^k) \\ P_{\text{H}_2}^{k+1} &= f_P(\mathbf{u}^k, P_{\text{H}_2}^k) \end{aligned} \quad (6.14)$$

where

$$\mathbf{u}^k = [Q_{\text{H}_2}^k \quad Q_{\text{air}}^k \quad I^k]^T \quad (6.15)$$

the k in superscript represents the time step; V_{FC} is the fuel cell voltage, the control target; P_{H_2} is the hydrogen pressure which needs to be kept below a certain limit to ensure safety; the variable \mathbf{u} is the model inputs; Q_{H_2} and Q_{air} are the hydrogen volumetric flow rate and air volumetric flow rate, the inputs to the system; I is the current, the workload which treated as a disturbance.

6.3.3 Gaussian process MPC design

State-space model

The state-space model for MPC was obtained by linearizing the Gaussian process models. The Gaussian process f_V shown in Eq. (6.14) then becomes:

$$dV_{\text{FC}} = \begin{bmatrix} \frac{\partial f_V}{\partial Q_{\text{H}_2}} & \frac{\partial f_V}{\partial Q_{\text{air}}} & \frac{\partial f_V}{\partial I} \end{bmatrix} \begin{bmatrix} dQ_{\text{H}_2} \\ dQ_{\text{air}} \\ dI \end{bmatrix} \quad (6.16)$$

where the partial derivative is applied to the latest system states, which will update each time step. The partial derivative of the GP with Gaussian kernel can be solved explicitly, but the forward mode automatic differentiation (AD) method [28] was used here for simplicity and flexibility. The same expression is true for the Gaussian process f_P .

The discrete-time state-space model of the fuel cell used for control is written as:

$$\begin{aligned} \mathbf{x}^{k+1} &= \mathbf{A}\mathbf{x}^k + \mathbf{B}\mathbf{u}^k \\ \mathbf{y}^k &= \mathbf{C}\mathbf{x}^k \end{aligned} \quad (6.17)$$

where the state vector \mathbf{x}^k at sample index k is:

$$\mathbf{x}^k = \begin{bmatrix} V_{\text{FC}}^k \\ P_{\text{H}_2}^k \\ dI^k \\ Q_{\text{H}_2}^k \\ Q_{\text{air}}^k \end{bmatrix} \quad (6.18)$$

with input:

$$\mathbf{u}^k = \begin{bmatrix} dQ_{\text{H}_2}^k \\ dQ_{\text{air}}^k \end{bmatrix} \quad (6.19)$$

and output:

$$\mathbf{y}^k = \begin{bmatrix} V_{\text{FC}}^k \end{bmatrix} \quad (6.20)$$

and state-space matrices:

$$\begin{aligned} \mathbf{A} &= \begin{bmatrix} 1 & 0 & \frac{\partial f_V}{\partial I} & 0 & 0 \\ 0 & 1 & \frac{\partial f_P}{\partial I} & 0 & 0 \\ 0 & 0 & 0 & 0 & 0 \\ 0 & 0 & 0 & 1 & 0 \\ 0 & 0 & 0 & 0 & 1 \end{bmatrix} \\ \mathbf{B} &= \begin{bmatrix} \frac{\partial f_V}{\partial Q_{\text{H}_2}} & \frac{\partial f_V}{\partial Q_{\text{air}}} \\ \frac{\partial f_P}{\partial Q_{\text{H}_2}} & \frac{\partial f_P}{\partial Q_{\text{air}}} \\ 0 & 0 \\ 1 & 0 \\ 0 & 1 \end{bmatrix} \\ \mathbf{C} &= \begin{bmatrix} 1 & 0 & 0 & 0 & 0 \end{bmatrix} \end{aligned} \quad (6.21)$$

The actuator increments were selected as the system inputs. Consequently, $Q_{\text{H}_2}^k$ and Q_{air}^k were added into the state vector to help impose appropriate constraints.

MPC design

A Quadratic Programming (QP) problem will be solved at each time step to obtain the optimal control inputs in this MPC problem formulation:

$$\min_{\mathbf{u}^0, \mathbf{u}^1, \dots, \mathbf{u}^{H_u-1}} \mathbf{J}(\mathbf{u}^k) = \sum_{k=1}^{H_p} \left\| \mathbf{y}^k - \mathbf{r} \right\|_{\mathbf{Q}}^2 + \sum_{k=0}^{H_u-1} \left\| \mathbf{u}^k \right\|_{\mathbf{R}}^2 + \rho \sum_{k=1}^{H_p} \left\| \boldsymbol{\epsilon}^k \right\|^2 \quad (6.22)$$

subject to:

$$\begin{aligned} \mathbf{x}^{k+1} &= \mathbf{A}^d \mathbf{x}^k + \mathbf{B}^d \mathbf{u}^k \\ \mathbf{y}^k &= \mathbf{C}^d \mathbf{x}^k \\ \mathbf{u}_{\text{lb}} &\leq \mathbf{u}^k \leq \mathbf{u}_{\text{ub}} \\ d\mathbf{u}_{\text{lb}} &\leq \mathbf{u}^k - \mathbf{u}^{k-1} \leq d\mathbf{u}_{\text{ub}} \\ \mathbf{x}_{\text{lb}} &\leq \mathbf{x}^k \leq \mathbf{x}_{\text{ub}} + \boldsymbol{\epsilon}^k \\ \mathbf{0} &\leq \boldsymbol{\epsilon}^k \\ P_{\text{H}_2}^k &\leq P_{\text{H}_2}^{\text{lim}} + \epsilon^k \\ P_{\text{H}_2}^k &\leq P_{\text{H}_2}^{\text{lim}} + \epsilon^k - \alpha \sigma_p \Delta P_{\text{H}_2} \\ \mathbf{u}^{-1} &= \mathbf{u}_{\text{init}} \\ \mathbf{x}^0 &= \mathbf{x}_{\text{init}} \\ k &= 0, 1, \dots, H_p \end{aligned} \quad (6.23)$$

where H_p and H_u are prediction and control horizon; k in the superscript represents the time step, and $k = 0$ refers to the current time step; \mathbf{r} is the control reference; \mathbf{Q} and \mathbf{R} are weight tuning parameters for reference tracking and control inputs; \mathbf{A}^d , \mathbf{B}^d , and \mathbf{C}^d are state-space matrices \mathbf{A} , \mathbf{B} and \mathbf{C} in discrete-time; \mathbf{u}_{lb} , \mathbf{u}_{ub} , \mathbf{x}_{lb} , and \mathbf{x}_{ub} are the lower bounds and upper bounds of inputs \mathbf{u} and states \mathbf{x} ; $d\mathbf{u}_{\text{lb}}$ and $d\mathbf{u}_{\text{ub}}$ are the lower bounds and upper bounds of inputs change rate; \mathbf{u}_{init} is latest applied control inputs and \mathbf{x}_{init} is the latest measured value, the state feedback; $P_{\text{H}_2}^{\text{lim}}$ is the upper bound of P_{H_2} ; ϵ is the slack variable introduced to soft constraints and ρ is a nonnegative scalar to control the magnitude of penalizing soft constraint violations.

The additional inequality for P_{H_2} as a compensation for model errors is:

$$P_{\text{H}_2}^k \leq P_{\text{H}_2}^{\text{lim}} + \epsilon^k - \alpha \sigma_p \Delta P_{\text{H}_2} \quad (6.24)$$

where σ_p is the prediction variance when making inference with Gaussian process f_p on the data point in the current time step; ΔP_{H_2} is the possible

P_{H_2} move with respect to the possible calculated inputs:

$$\Delta P_{H_2} = \sum_{i=0}^{k-1} (dQ_{H_2}^i \frac{\partial f_P}{\partial Q_{H_2}} + dQ_{air}^i \frac{\partial f_P}{\partial Q_{air}}) \quad (6.25)$$

α is a tuning parameter. This $\alpha\sigma_p\Delta P_{H_2}$ term can be understood from an intuitive point of view. Typically, a bigger possible move will lead to a bigger uncertainty. Thus, a redundancy proportional to the possible movement size and prediction uncertainty in the constraint is desirable to compensate for the model imperfections. Since the P_{H_2} limit is from above, the added constraint in Eq. (6.24) is only meaningful when the possible move is positive.

To be precise, this constraint on $P_{H_2}^k$ is simplified from the stochastic MPC constraint formation. In stochastic MPC, a probabilistic constraint is

$$p(\mathbf{x}^k \leq \mathbf{x}_{ub}) \geq \eta \quad (6.26)$$

where η denotes the confidence level. When η is 0.95, it is:

$$\mathbf{x}^k \leq \mathbf{x}_{ub} - 2\Sigma^k \quad (6.27)$$

where Σ^k is the covariance matrix of \mathbf{x}^k . Here \mathbf{x}^k actually represents its mean value. The Σ^k is estimated from the uncertainty propagation. The specific form for P_{H_2} of Eq. (6.27) is:

$$P_{H_2}^k \leq P_{H_2}^{lim} - 2\sigma_p^k \quad (6.28)$$

For every step in the prediction horizon, the $P_{H_2}^k$ variance is propagated along with the uncertainty in \mathbf{B} matrix.

The linearized form:

$$P_{H_2}^{k+1} = P_{H_2}^k + dQ_{H_2}^k \frac{\partial f_P}{\partial Q_{H_2}} + dQ_{air}^k \frac{\partial f_P}{\partial Q_{air}} \quad (6.29)$$

The variance estimate update is:

$$(\sigma_p^{k+1})^2 = (\sigma_p^k)^2 + (dQ_{H_2}^k)^2 \text{var}\left(\frac{\partial f_P}{\partial Q_{H_2}}\right) + (dQ_{air}^k)^2 \text{var}\left(\frac{\partial f_P}{\partial Q_{air}}\right) \quad (6.30)$$

The variance of the partial derivative taken at the initial step is approximated by:

$$\begin{aligned} \text{var}\left(\frac{\partial f_P}{\partial Q_{H_2}}\right) &= \text{var}\left(\frac{f_P(Q_{H_2} + \delta Q_{H_2}) - f_P(Q_{H_2})}{\delta Q_{H_2}}\right) \\ &= \frac{2}{(\delta Q_{H_2})^2} (\sigma_p)^2 \\ &= \alpha_1 E^2\left\{\frac{\partial f_P}{\partial Q_{H_2}}\right\} (\sigma_p)^2 \end{aligned} \quad (6.31)$$

where $2/(\delta Q_{\text{H}_2})^2$ is assumed to be proportional to $E^2\{\partial f_P/\partial Q_{\text{H}_2}\}$ value with a constant value α_1 . The $E\{\partial f_P/\partial Q_{\text{H}_2}\}$ is actually the $\partial f_P/\partial Q_{\text{H}_2}$ value calculated at the initial time step. Thus, at each time step in the prediction horizon, the variance increases with a magnitude of:

$$\alpha_1(\sigma_p)^2(dQ_{\text{H}_2}^k)^2E^2\left\{\frac{\partial f_P}{\partial Q_{\text{H}_2}}\right\} + \alpha_2(\sigma_p)^2(dQ_{\text{air}}^k)^2E^2\left\{\frac{\partial f_P}{\partial Q_{\text{air}}}\right\} \quad (6.32)$$

Summing over the steps until time step k , and viewing all constant coefficient as the same, gives the total standard error of time step k :

$$\sigma_p^k = \alpha\sigma_p \sum_{i=0}^{k-1} \sqrt{(dQ_{\text{H}_2}^i)^2E^2\left\{\frac{\partial f_P}{\partial Q_{\text{H}_2}}\right\} + (dQ_{\text{air}}^i)^2E^2\left\{\frac{\partial f_P}{\partial Q_{\text{air}}}\right\}} \quad (6.33)$$

All constants are written together as α . But this form is too conservative for constraint handling and requires high computational effort. The root part is approximated as:

$$dQ_{\text{H}_2}^k E\left\{\frac{\partial f_P}{\partial Q_{\text{H}_2}}\right\} + dQ_{\text{air}}^k E\left\{\frac{\partial f_P}{\partial Q_{\text{air}}}\right\} \quad (6.34)$$

Then the Eq. (6.33) becomes

$$\sigma_p^k = \alpha\sigma_p\Delta P_{\text{H}_2} \quad (6.35)$$

where ΔP_{H_2} is shown in the Eq. (6.25). This also gives an intuitive interpretation of the constraint redundancy. Meanwhile, the constant 2 and α are integrated to the coefficient α in the constraints described by Eq. (6.23). This does not necessarily give a 95% confidence level, and α should be tuned according to the performance and safety requirements.

The constraint settings are the same as the settings in Sec. 5.3. The hydrogen pressure in the pipe should be under 2.5 atm to ensure safety. Only slack variable of states upper bounds was added. The input Q_{H_2} was limited between 100 and 400 lpm and Q_{air} was limited within 300 to 700 lpm. The change rate of the inputs was constrained within -40 to 20 lpm.

The time step for the MPC controller was 0.5 s. The QP problem was solved at each step, then the solved $Q_{\text{H}_2} + dQ_{\text{H}_2}$ and $Q_{\text{air}} + dQ_{\text{air}}$ were applied to the fuel cell.

6.3.4 Experimental set-up

The experiment was conducted on the Simulink model detailed in Sec. 2.4.1. This model is viewed as the true system dynamics. Gaussian measurement noises were added to voltage V_{FC} and hydrogen pressure P_{H_2} .

The illustration of the GP MPC control process is:

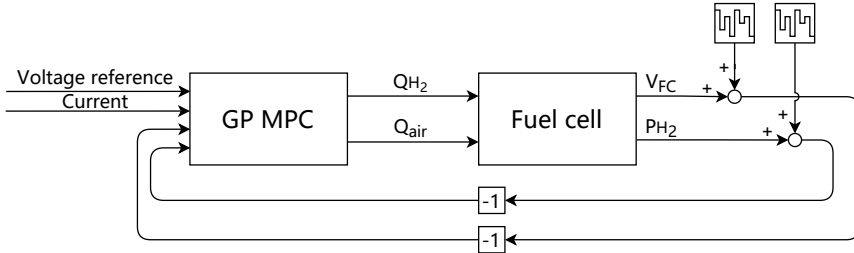


Figure 6.5: GP MPC control process

As compared to the MPC controller shown in Fig. 5.10, the GP MPC only needs the system information of V_{FC} and P_{H_2} , whereas MPC requires other information such as oxygen and nitrogen pressure. This is a desirable aspect in practice.

6.3.5 Experimental results

In the experiments, two test scenarios were chosen, one was the typical step disturbance applied on the working load, the current; the other was a mixture of slope and step working load changes. The performance of GP MPC and MPC with physical models explained in Sec. 5.3 were compared first, then the performance of GP MPC and neural network MPC were compared.

Gaussian process MPC vs MPC

Figure 6.6 shows the GP MPC voltage tracking performance compared with MPC under step workload disturbance, and Fig. 6.7 presents the corresponding P_{H_2} behavior and system inputs. At the beginning of the experiment, the MPC and GP MPC had similar rise-up traces, which were limited by the input change rate constraint. The MPC had a lower overshoot than GP MPC benefiting from the accurate system model. The overshoot for GP MPC was 0.60 V and for MPC was 0.42 V. Both controllers can

successfully satisfy the P_{H_2} safety requirements. When the current increased suddenly, the MPC and GP MPC drove the voltage back to the reference at a similar pace, but MPC responded faster. To arrive at 47.9 V again, MPC took 5.2 s and GP MPC took 6.5 s. It can be clearly seen that the inputs increased following a straight line, indicating the activation of the change rate limits. However, similar to the start of the system, the GP MPC calculated Q_{H_2} increment was rather conservative in comparison with MPC. This is because the added constraint in Eq. (6.24) enforced the controller to take a more cautious action when increasing Q_{H_2} which directly increased the P_{H_2} . In contrast, Q_{air} was adjusted aggressively. When the current suddenly dropped at time 75 s, the MPC and GP MPC had a similar performance in pulling back the voltage. The steady-state tracking behaviors of the two controllers were comparable and the safety constraint was satisfied throughout the process.

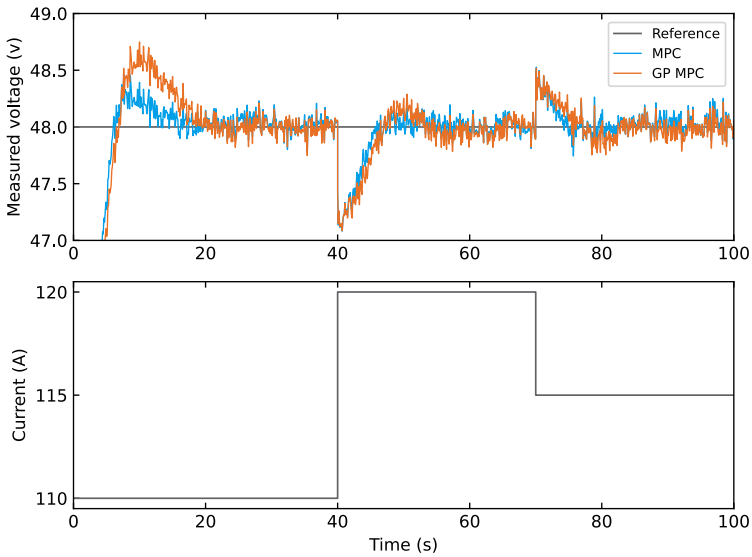


Figure 6.6: Output voltage under the current disturbance.

Figures 6.8 and 6.9 exhibit the GP MPC and MPC behavior under slope and step current changes. The behavior was similar to the step change scenario, and GP MPC and MPC had equivalent performance most of the time. The P_{H_2} constraint was satisfied in all cases.

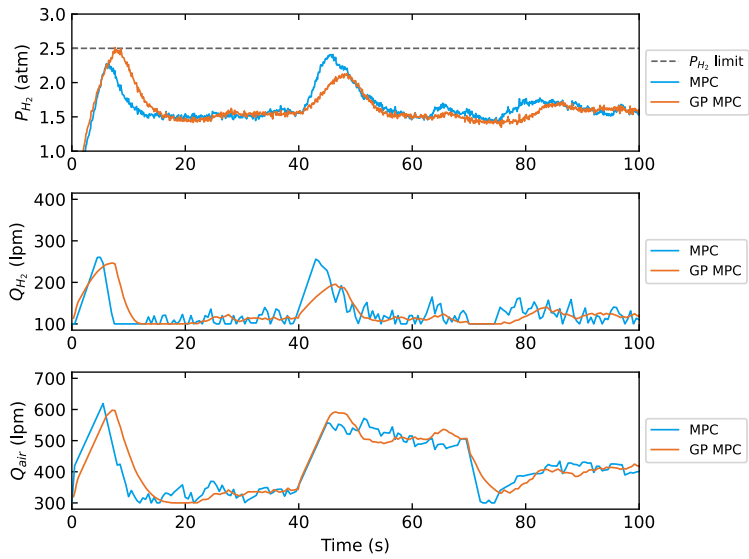


Figure 6.7: Constraint handling and system inputs.

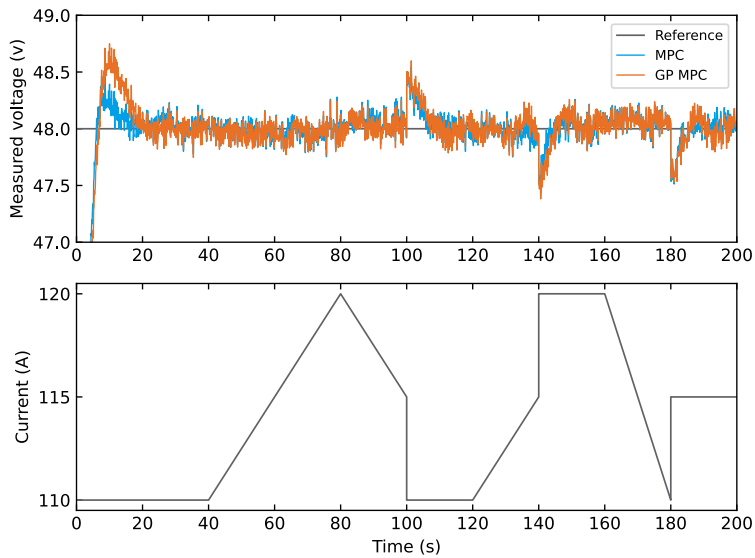


Figure 6.8: Output voltage under the current disturbance.

Gaussian process MPC vs neural network MPC

The neural network MPC was built with a similar procedure to GP MPC. The neural network was trained with the collected data to predict the output

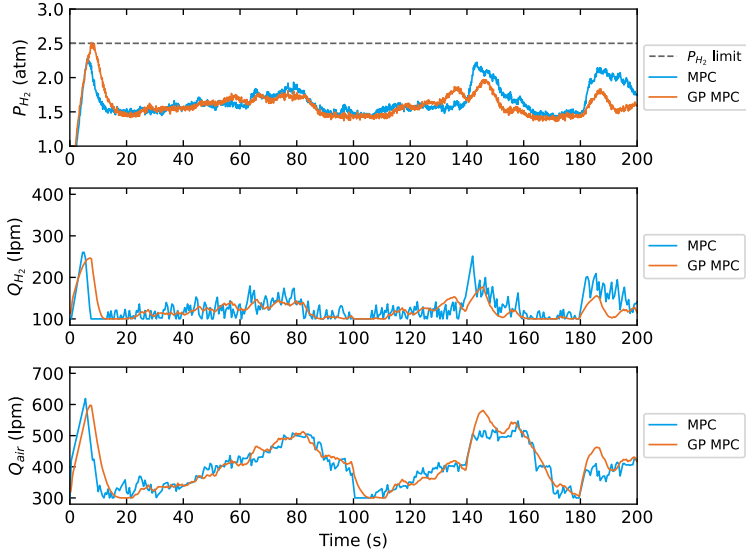


Figure 6.9: Constraint handling and system inputs.

voltage and hydrogen pressure behavior. The difference was that only one neural network was used instead of two Gaussian processes, so it directly worked as the function f in Eq. (2.74). Besides, there were 2000 training points for neural network training instead of 1000 points for the Gaussian process. The network structure was (5, 16, 32, 8, 2), which means that the NN input layer had five nodes and the output layer has two nodes, and NN had three hidden layers with 16, 32, and 8 nodes respectively. After getting the neural network, it was linearized using automatic differentiation to get the state-space model for NN MPC. Since the NN here can not give the prediction variance, the additional inequality of Eq. (6.24) was removed.

The performance of the NN MPC and GP MPC under step disturbance is shown in Fig. 6.10, and Fig. 6.11 gives the corresponding hydrogen pressure P_{H_2} behavior and system inputs. It can be seen that GP MPC drove the voltage back to the reference faster than NN MPC after system start-up, around 10-30 s. The overshoot for NN MPC and GP MPC were close. In terms of the voltage without noise, the overshoot for NN MPC was 0.57 V and for GP MPC it was 0.60 V. After a sudden current increase at 40 s, GP MPC responded slower than NN MPC. To arrive at 47.9 V again, GP MPC took 6.5 s and NN MPC took 5.5 s. The slower response was due to the conservative increment of hydrogen flow rate Q_{H_2} as the result of the additional inequality of Eq. (6.24), although it contributed to the constraint satisfaction of GP

MPC. In contrast, the NN MPC violated the hydrogen pressure constraint with a small peak. When the current suddenly dropped at time 75 s, the NN MPC and GP MPC had a similar performance in pulling back the voltage. The steady-state tracking behaviors of the two controllers were comparable and the safety constraint was satisfied throughout the remaining process.

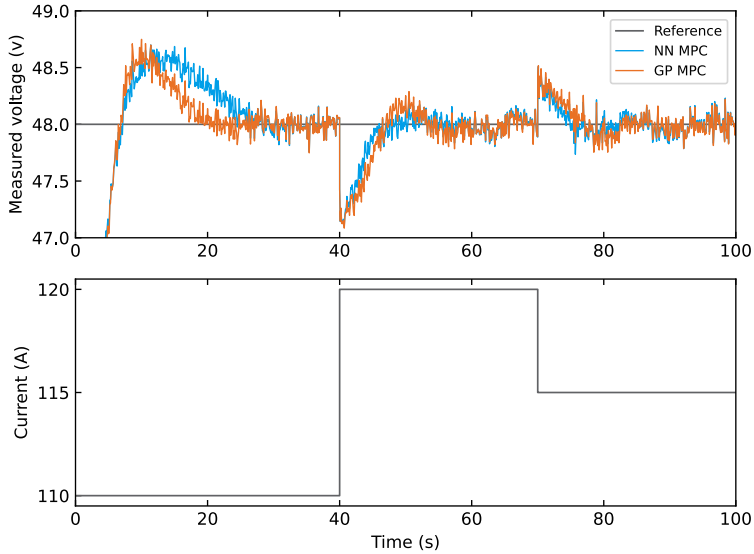


Figure 6.10: Output voltage under the current disturbance.

Figures 6.12 and 6.13 exhibit the GP MPC and NN MPC behavior under a mixture of slope and step current changes. The behavior was similar to the step change scenario. The overshoots after the system start-up were close for the NN MPC and GP MPC. The NN MPC violated the hydrogen pressure constraint with a small peak in this step current increase scenario at 140 s, whereas the GP MPC satisfied the constraint well by taking a conservative hydrogen flow rate Q_{H_2} increment. In the period around 65 - 85 s, the NN MPC kept the hydrogen pressure under the 2.5 atm limit with the effort of adjusting the input hydrogen flow rate, while the GP MPC had better handling by applying a lower hydrogen flow rate and higher air flow rate in advance.

6.3.6 Discussion

In this section, a novel GP MPC was proposed for the fuel cell control task. Its performance was validated on the Simulink model. Although the Gaussian

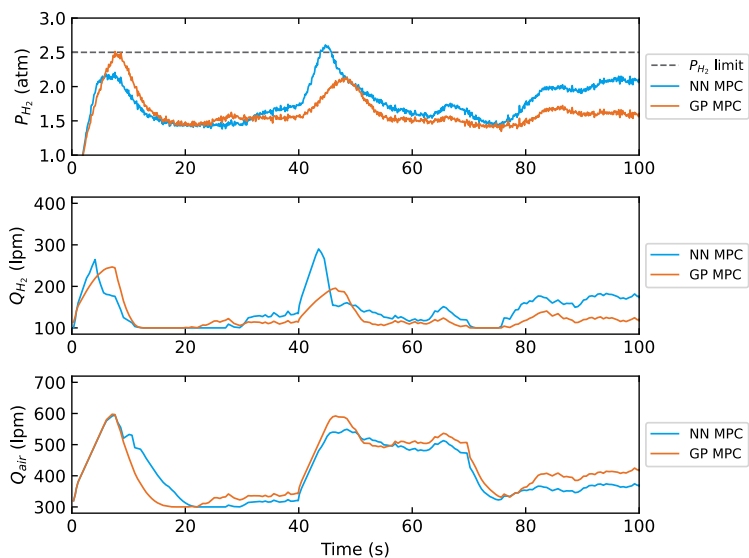


Figure 6.11: Constraint handling and system inputs.

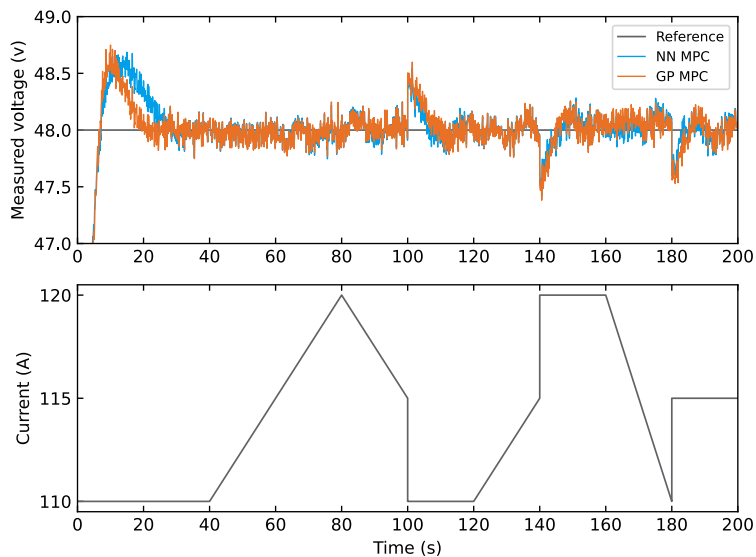


Figure 6.12: Output voltage under the current disturbance.

process had been used to build fuel cell related models [73], [173], it was the first time application of GP MPC on fuel cell control to the author's knowledge. This work extends the knowledge body of the learning control

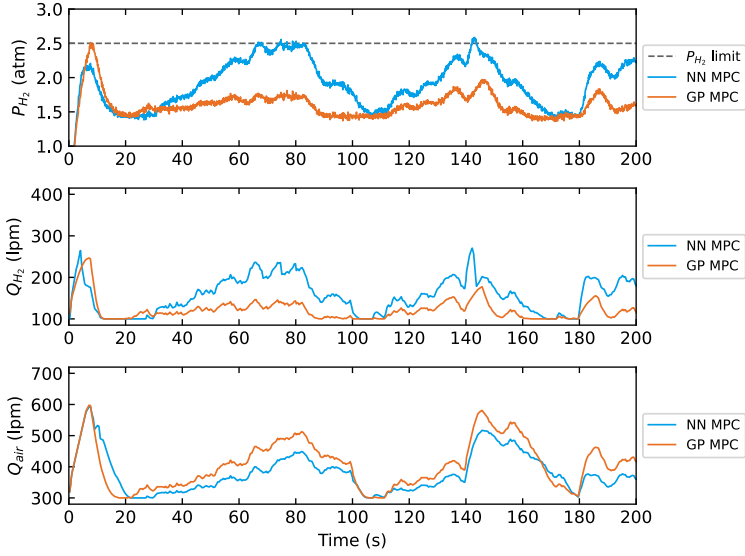


Figure 6.13: Constraint handling and system inputs.

method application on fuel cell control practice.

Even though the MPC based on the physical model had a better performance in terms of the overshoot during system start-up, the GP MPC required less system information, which needed fewer sensors and was more economical. The modeling process of GP MPC relied on collected data, whereas physics-based MPC required a deeper understanding of the system inner principles. The GP MPC considered the safety requirements regarding pressure and actuators as well, which was missed in [62], [133]. Though based on nonlinear GP models, the MPC framework took linearized models and reduced the computational burden, whereas the nonlinear MPC in [190] made it difficult to implement and solve. To compensate for the model imperfection, one constraint taking prediction variance and possible moves into account was added. This gave a satisfactory constraint handling result under model error and linearization error. Other learning-based predictive control approaches shown in [134], [154] used the neural network as the learning model. As compared to the neural network, the Gaussian process had better interpretability and the prediction variance was available, which contributed to the constraints handling in MPC settings. Stochastic MPC was commonly adopted for new energy vehicle energy management [101], [138], [151], and this work referred to the constraint handling method of stochastic MPC.

The Gaussian process is a data-based method that requires sufficient system data. Meanwhile, in this work, each independent GP was built for each variable to be predicted. This was acceptable when the system data was cheap to obtain and limited states were needed. For plants where the data were expensive and more variable predictions were needed, this framework was limited and unsuitable. Another limitation is that the method was only validated in the Simulink model. Validation on real fuel cell stacks is much more desirable.

6.3.7 Conclusion

In this section, a Gaussian process MPC was developed to control the fuel cell voltage. Two Gaussian processes were used to predict the voltage and hydrogen pressure, and the state-space models were formed based on the linearized Gaussian process. A special inequality utilizing GP prediction variance was added to compensate for the model imperfections in satisfying constraints. The experiment results showed that the GP MPC method had a comparative performance of MPC controller with the knowledge of underlying system dynamics. The constraint handling of GP MPC gave a conservative action, but the safety requirements were satisfied well.

Conclusion

The flex-fuel CI engine is a promising concept in terms of alternative fuels, various combustion modes, and fuel choices during the transition from fossil fuel to renewable energy sources. Meanwhile, in the long run, the fuel cell together with hydrogen energy which has low or zero carbon emission and environmental impact shows great potential. The modeling and control methods of flex-fuel CI engine and fuel cell are investigated in this thesis.

The modeling parts included the flex-fuel engine combustion process and intake system, and the system scale fuel cell model. The flex-fuel engine is highly sensitive to inlet conditions. The gas system models were established to describe the relationship between actuators EGR, VGT, hot and cool valves to inlet conditions including intake temperature, pressure, and oxygen concentration. Ignition delay was a key indicator of the combustion process and fuel properties of flex-fuel CI engines. The physical model and data-based modeling approach of ignition delay were studied. The results showed that the physical model had a better extrapolation ability which was desirable in control applications and data-based models had higher prediction accuracy but needed more computational power and careful regulation. A fuel-cell physical model was built to illuminate the electrochemical behavior which focused on the macro performances of the fuel-cell system. Gaussian process models to predict the fuel cell voltage and hydrogen pressure were established

with collected simulated data.

Model predictive control approaches based on physical models were applied to the flex-fuel CI engine and the fuel cell.

An adaptive MPC method was proposed to control the combustion process of the flex-fuel CI engine. The control targets were the combustion phasing and ignition delay, and the actuators were the EGR, VGT valves, and main injection timings. MPC was used for multi-input multi-output control problems and the adaptivity was done by estimating the physical ignition delay model parameters with real-time data online by Kalman filter. The proposed adaptive MPC approach showed the successful application in the fuel transition scenario with diesel, gasoline/n-heptane mixture, and ethanol/n-heptane mixture. The possible ignition delay range calculated from the physical model could work as an indicator of the engine fuel properties.

An MPC with control constraints was developed to keep the fuel cell voltage at a reference value under current disturbance while satisfying the hydrogen pressure safety requirements. The inputs were the hydrogen volumetric flow rate and air volumetric flow rate. The state-space model was built by the simplification and linearization of the detailed system scale model. The proposed MPC controller fulfilled the control task successfully and its performance was compared with that of a PI controller.

Learning-based MPC integrated the learning models trained from system data to the state-space model to improve the controller performance.

One learning-based MPC method that decoupled the robustness and performance in an optimization framework was proposed and applied to the control of combustion phasing when running with diesel. This approach maintained two models of the system, the base model and the learning model. The learning model was a linear model used to capture the influence on combustion duration. The comparison of LBMPC and MPC showed the improvement of performance by LBMPC.

A Gaussian process MPC was developed for the fuel cell voltage control task with current disturbance and hydrogen pressure limit. Two Gaussian processes trained with fuel-cell data collected from the simulation to predict voltage and hydrogen pressure were utilized in the state-space model. The Gaussian process MPC showed comparable performance with MPC based on the detailed system physical model. A benefit of GP MPC over MPC was that the GP MPC required less system information during operation, while MPC demanded more measurements.

Future work

Flex-fuel CI engine

Future work includes implementing the gas system controller based on the gas system models in Sec. 2.3.2 and using the gas system controller as a subsystem of the whole combustion process controller instead of using one stationary point MAP for better decoupling. For the learning-based MPC application on the engine, only diesel was used. This scenario is not as interesting as the fuel transition scenario. Learning-based MPC utilizing data-based models proposed in Sec. 2.3.3 for flex-fuel CI engine control in a broad fuel choice scenario is valuable work. This thesis didn't consider emissions. Further work should investigate the emission characteristics and set constraints on pollution levels regarding the strict emission demands.

Fuel cell

This thesis only investigated one specific control task of PEFC and did not consider other subsystems in the fuel cell. Apart from the desired constant voltage, the fuel cell control should also consider the efficient operation interval, which is a desired aspect in practice. Along with the reaction subsystem explored in this work, the thermal, water management, and power electronics subsystems also arose control tasks like temperature and moisture level maintenance that is important to ensure a stable and efficient fuel-cell operation. Possible future work could include efficiency considerations and focus on the overall system management. The controllers were only validated in simulation. Experiments with fuel-cell equipment are much appreciated.

Model predictive control

The MPC methods used in this work are based on linearized models, both for physical-based models and data-based models. With the fast development of computing power, the direct use of nonlinear models within the MPC framework may be possible in the near future. The complexity of the control system also puts higher demands on the system hardware and software implementation. By the optimization of software architecture, the system could support more time-consuming computations like nonlinear optimization and support a wider operating range with higher engine RPM. In the experiment settings of both the flex-fuel engine and the fuel cell, many sensors

are assumed to be available in the controller design. It is convenient in a laboratory environment but is not common in practice. The design of related observers is an interesting supplementary approach.

BIBLIOGRAPHY

- [1] (), [Online]. Available: <https://www.leinelinde.com/> (cit. on p. 51).
- [2] (), [Online]. Available: https://intertechnology.com/Kistler/pdfs/Pressure_Model_7061B.pdf (cit. on p. 51).
- [3] (), [Online]. Available: <https://keller-druck.com/en/products/pressure-transmitters/analog-pressure-transmitters/series-23> (cit. on p. 52).
- [4] (), [Online]. Available: <https://www.bosch-motorsport.com/content/downloads/Raceparts/en-GB/51865867208058251.html> (cit. on p. 52).
- [5] (), [Online]. Available: <https://www.bronkhorst.com/int/products/liquid-flow/mini-cori-flow/m15/> (cit. on p. 52).
- [6] (), [Online]. Available: <https://www.ni.com/sv-se/support/model.pxie-8135.html> (cit. on p. 53).
- [7] *2020 climate and energy package - climate action - european commission*, Feb. 2017. [Online]. Available: https://ec.europa.eu/clima/policies/strategies/2020_en (cit. on pp. 1, 2).
- [8] N. Abani, S. Kokjohn, S. W. Park, M. Bergin, A. Munnannur, W. Ning, Y. Sun, and R. D. Reitz, “An improved spray model for reducing numerical parameter dependencies in diesel engine CFD simulations”, in *SAE World Congress & Exhibition*, Detroit, MI, USA: SAE International, Apr. 2008, SAE Technical Paper 2008-01-0970. DOI: <https://doi.org/10.4271/2008-01-0970> (cit. on p. 15).

- [9] A. Abd El Monem, A. M. Azmy, and S. Mahmoud, “Effect of process parameters on the dynamic behavior of polymer electrolyte membrane fuel cells for electric vehicle applications”, *Ain Shams Engineering Journal*, vol. 5, no. 1, pp. 75–84, 2014 (cit. on p. 39).
- [10] M. Abramowitz, I. A. Stegun, et al., *Handbook of Mathematical Functions: With Formulas, Graphs, and Mathematical Tables*. National Bureau of Standards Washington, DC, 1972, vol. 55 (cit. on p. 18).
- [11] A. Afram, F. Janabi-Sharifi, A. S. Fung, and K. Raahemifar, “Artificial neural network (ANN) based model predictive control (MPC) and optimization of HVAC systems: A state of the art review and case study of a residential HVAC system”, *Energy and Buildings*, vol. 141, pp. 96–113, 2017, ISSN: 0378-7788. DOI: <https://doi.org/10.1016/j.enbuild.2017.02.012>. [Online]. Available: <https://www.sciencedirect.com/science/article/pii/S0378778816310799> (cit. on p. 89).
- [12] K. H. Ahn, “Estimation of ethanol content and control of air-to-fuel ratio in flex fuel vehicles”, Ph.D. dissertation, Department of Mechanical Engineering, University of Michigan, Michigan, United States, Jun. 2011, ISBN: 9789177538707 (cit. on p. 71).
- [13] K.-h. Ahn, H. Yilmaz, A. Stefanopoulou, and L. Jiang, “Ethanol content estimation in flex fuel direct injection engines using in-cylinder pressure measurements”, in *SAE 2010 World Congress and Exhibition*, Detroit, MI, USA: SAE International, Apr. 2010, SAE Technical Paper 2010-01-0166 (cit. on pp. 5, 10, 11).
- [14] T. Albin, D. Ritter, R. Zweigel, and D. Abel, “Hybrid multi-objective MPC for fuel-efficient PCCI engine control”, in *2015 European Control Conference (ECC)*, Linz, Austria, Oct. 2015, pp. 2583–2588 (cit. on p. 56).
- [15] J. A. Anderson, *An Introduction to Neural Networks*. Cambridge, MA, USA: MIT Press, 1995 (cit. on p. 19).
- [16] Anonymous, *2030 climate and energy framework - climate action - european commission*, Feb. 2017. [Online]. Available: https://ec.europa.eu/clima/policies/strategies/2030_en#tab-0-0 (cit. on pp. 1, 2).
- [17] —, *2050 low-carbon economy - climate action - european commission*, Feb. 2017. [Online]. Available: https://ec.europa.eu/clima/policies/strategies/2050_en (cit. on pp. 1, 2).

- [18] A. Arce, A. J. del Real, C. Bordons, and D. R. Ramirez, “Real-time implementation of a constrained MPC for efficient airflow control in a PEM fuel cell”, *IEEE Transactions on Industrial Electronics*, vol. 57, no. 6, pp. 1892–1905, 2010. DOI: 10.1109/TIE.2009.2029524 (cit. on p. 87).
- [19] K. Åström and B. Wittenmark, “On self-tuning regulators”, *Automatica*, vol. 9, no. 2, pp. 185–199, 1973, ISSN: 0005-1098. DOI: [https://doi.org/10.1016/0005-1098\(73\)90073-3](https://doi.org/10.1016/0005-1098(73)90073-3). [Online]. Available: <https://www.sciencedirect.com/science/article/pii/0005109873900733> (cit. on p. 55).
- [20] K. J. Åström and B. Wittenmark, *Adaptive Control*. New York, United States: Dover Publications, 2013 (cit. on p. 8).
- [21] K. Åström and T. Hägglund, *Advanced PID Control*. Research Triangle, North Carolina, United States: ISA - The Instrumentation, Systems and Automation Society, 2006, ISBN: 978-1-55617-942-6 (cit. on p. 45).
- [22] K. J. Åström and R. M. Murray, *Feedback Systems: An Introduction for Scientists and Engineers*. Princeton, NJ, USA: Princeton University Press, 2010 (cit. on p. 8).
- [23] A. Aswani, H. Gonzalez, S. S. Sastry, and C. Tomlin, “Provably safe and robust learning-based model predictive control”, *Automatica*, vol. 49, no. 5, pp. 1216–1226, 2013, ISSN: 0005-1098. DOI: <https://doi.org/10.1016/j.automatica.2013.02.003> (cit. on pp. 8, 90, 91, 95, 98).
- [24] A. Aswani, N. Master, J. Taneja, D. Culler, and C. Tomlin, “Reducing transient and steady state electricity consumption in HVAC using learning-based model-predictive control”, *Proceedings of the IEEE*, vol. 100, no. 1, pp. 240–253, 2012. DOI: 10.1109/JPROC.2011.2161242 (cit. on p. 91).
- [25] A. K. Babu, V. A. A. Raj, and G. Kumaresan, “Misfire detection in a multi-cylinder diesel engine: A machine learning approach”, *J. Eng. Sci. Technol*, vol. 11, no. 2, pp. 278–295, 2016 (cit. on p. 16).
- [26] J. A. Badra, F. Khaled, M. Tang, Y. Pei, J. Kodavasal, P. Pal, O. Owoyele, C. Fuetterer, B. Mattia, and F. Aamir, “Engine Combustion System Optimization Using Computational Fluid Dynamics and Machine Learning: A Methodological Approach”, *Journal of Energy Resources Technology*, vol. 143, no. 2, Aug. 2020, 022306, ISSN: 0195-0738. DOI: 10.1115/1.4047978. eprint: <https://>

- asmedigitalcollection.asme.org/energyresources/article-pdf/143/2/022306/6605351/jert\143\2\022306.pdf. [Online]. Available: <https://doi.org/10.1115/1.4047978> (cit. on pp. 90, 91).
- [27] S. Batiyah, R. Sharma, S. Abdelwahed, and N. Zohrabi, “An MPC-based power management of standalone DC microgrid with energy storage”, *International Journal of Electrical Power & Energy Systems*, vol. 120, p. 105 949, 2020 (cit. on p. 73).
- [28] A. G. Baydin, B. A. Pearlmutter, A. A. Radul, and J. M. Siskind, “Automatic differentiation in machine learning: A survey”, *Journal of Machine Learning Research*, vol. 18, no. 153, pp. 1–43, 2018. [Online]. Available: <http://jmlr.org/papers/v18/17-468.html> (cit. on p. 101).
- [29] J. Bayer and D. E. Foster, “Zero-dimensional soot modeling”, *SAE Transactions*, vol. 112, pp. 1446–1458, 2003, ISSN: 0096736X, 25771531. [Online]. Available: <http://www.jstor.org/stable/44741366> (cit. on p. 16).
- [30] J. Bengtsson, P. Strandh, R. Johansson, P. Tunestål, and B. Johansson, “Model predictive control of homogeneous charge compression ignition (HCCI) engine dynamics”, in *2006 IEEE Conference on Computer Aided Control System Design, 2006 IEEE International Conference on Control Applications, 2006 IEEE International Symposium on Intelligent Control*, Munich, Germany, Oct. 2006, pp. 1675–1680 (cit. on p. 56).
- [31] B. Berger, F. Rauscher, and B. Lohmann, “Analysing Gaussian processes for stationary black-box combustion engine modelling”, *IFAC Proceedings Volumes*, vol. 44, no. 1, pp. 10 633–10 640, 2011, ISSN: 1474-6670. DOI: <https://doi.org/10.3182/20110828-6-IT-1002.01160> (cit. on p. 32).
- [32] D. Bergmann, K. Harder, J. Niemeyer, and K. Graichen, “Nonlinear MPC of a heavy-duty diesel engine with learning Gaussian process regression”, *IEEE Transactions on Control Systems Technology*, pp. 1–17, 2021, ISSN: 1558-0865. DOI: 10.1109/TCST.2021.3054650 (cit. on pp. 91, 98).
- [33] J. Bezanson, S. Karpinski, V. B. Shah, and A. Edelman, “Julia: A fast dynamic language for technical computing”, *arXiv preprint arXiv:1209.5145*, 2012 (cit. on p. 53).

- [34] Y. Bicer, I. Dincer, and M. Aydin, “Maximizing performance of fuel cell using artificial neural network approach for smart grid applications”, *Energy*, vol. 116, pp. 1205–1217, 2016, ISSN: 0360-5442. DOI: <https://doi.org/10.1016/j.energy.2016.10.050>. [Online]. Available: <https://www.sciencedirect.com/science/article/pii/S0360544216314840> (cit. on p. 100).
- [35] D. Blom, M. Henningsson, K. Ekholm, P. Tunestål, and R. Johansson, “HCCI engine modeling and control using conservation principles”, in *SAE World Congress and Exhibition*, Detroit, MI, USA: SAE International, 2008, SAE Technical Paper 2008-01-0789 (cit. on p. 56).
- [36] R. Bosch, *Bosch Automotive Handbook, 8th Edition*. Chichester, West Sussex, England: Wiley, 2011 (cit. on p. 10).
- [37] P. Bouffard, A. Aswani, and C. Tomlin, “Learning-based model predictive control on a quadrotor: Onboard implementation and experimental results”, in *IEEE International Conference on Robotics and Automation*, Saint Paul, MN, USA, May 2012, pp. 279–284 (cit. on p. 90).
- [38] S. Boyd, S. P. Boyd, and L. Vandenberghe, *Convex Optimization*. Cambridge, United Kingdom: Cambridge University Press, 2004 (cit. on p. 47).
- [39] *Carro flex chega aos 15 anos com 30,5 milhões de unidades*, Mar. 2018. [Online]. Available: <http://www.automotivebusiness.com.br/inovacao/56/carro-flex-chega-aos-15-anos-com-305-milhoes-de-unidades> (cit. on pp. 5, 71).
- [40] N. Chatrattanawet, T. Hakhen, S. Kheawhom, and A. Arpornwichanop, “Control structure design and robust model predictive control for controlling a proton exchange membrane fuel cell”, *Journal of Cleaner Production*, vol. 148, pp. 934–947, 2017 (cit. on p. 73).
- [41] K. Chen, J. Yi, and D. Song, “Gaussian processes model-based control of underactuated balance robots”, in *2019 International Conference on Robotics and Automation (ICRA)*, Montreal, Quebec, Canada, 2019, pp. 4458–4464. DOI: 10.1109/ICRA.2019.8794097 (cit. on p. 90).
- [42] P.-C. Chen, “The dynamics analysis and controller design for the PEM fuel cell under gas flowrate constraints”, *International Journal of Hydrogen Energy*, vol. 36, no. 4, pp. 3110–3122, 2011 (cit. on p. 72).

- [43] Y. Choi and J.-Y. Chen, “Fast prediction of start-of-combustion in HCCI with combined artificial neural networks and ignition delay model”, *Proceedings of the Combustion Institute*, vol. 30, no. 2, pp. 2711–2718, 2005, ISSN: 1540-7489. DOI: <https://doi.org/10.1016/j.proci.2004.08.143> (cit. on p. 32).
- [44] J. M. Corrêa, F. A. Farret, L. N. Canha, and M. G. Simoes, “An electrochemical-based fuel-cell model suitable for electrical engineering automation approach”, *IEEE Transactions on Industrial Electronics*, vol. 51, no. 5, pp. 1103–1112, 2004 (cit. on pp. 36, 37).
- [45] C. R. Cutler and B. L. Ramaker, “Dynamic matrix control - A computer control algorithm”, *Joint Automatic Control Conference*, vol. 17, p. 72, 1980. DOI: 10.1109/JACC.1980.4232009 (cit. on p. 55).
- [46] A. Dalvi and M. Guay, “Control and real-time optimization of an automotive hybrid fuel cell power system”, *Control Engineering Practice*, vol. 17, no. 8, pp. 924–938, 2009, ISSN: 0967-0661. DOI: <https://doi.org/10.1016/j.conengprac.2009.02.009>. [Online]. Available: <https://www.sciencedirect.com/science/article/pii/S0967066109000380> (cit. on p. 87).
- [47] W. R. W. Daud, R. E. Rosli, E. H. Majlan, S. A. A. Hamid, R. Mohamed, and T. Husaini, “PEM fuel cell system control: A review”, *Renewable Energy*, vol. 113, pp. 620–638, Dec. 2017, ISSN: 0960-1481. DOI: 10.1016/j.renene.2017.06.027. [Online]. Available: <https://www.sciencedirect.com/science/article/pii/S0960148117305281> (visited on 03/04/2021) (cit. on pp. 6, 7).
- [48] V. Desaraju, A. Spitzer, and N. Michael, “Experience-driven predictive control with robust constraint satisfaction under time-varying state uncertainty”, in *Proceedings of Robotics: Science and Systems*, Cambridge, Massachusetts, United States, Jul. 2017, ISBN: 978-0-9923747-3-0. DOI: 10.15607/RSS.2017.XIII.067 (cit. on p. 89).
- [49] D. Egan, R. Koli, Q. Zhu, and R. Prucka, “Use of machine learning for real-time non-linear model predictive engine control”, in *WCX SAE World Congress Experience*, Detroit, MI, USA: SAE International, Apr. 2019. DOI: <https://doi.org/10.4271/2019-01-1289>. [Online]. Available: <https://doi.org/10.4271/2019-01-1289> (cit. on p. 91).
- [50] L. Eriksson, “Mean value models for exhaust system temperatures”, in *SAE 2002 World Congress & Exhibition*, Detroit, MI, USA: SAE International, Mar. 2002, SAE Technical Paper 2002-01-0374. DOI: <https://doi.org/10.4271/2002-01-0374> (cit. on p. 16).

- [51] ———, “Modeling and control of turbocharged SI and DI engines”, *Oil & Gas Science and Technology-Revue de l’IFP*, vol. 62, no. 4, pp. 523–538, 2007 (cit. on p. 16).
- [52] L. Eriksson and L. Nielsen, *Modeling and Control of Engines and Drivelines*. Chichester, West Sussex, United Kingdom: John Wiley & Sons, 2014 (cit. on p. 16).
- [53] K. Ettihir, L. Boulon, M. Becherif, K. Agbossou, and H. Ramadan, “Online identification of semi-empirical model parameters for PEMFCs”, *International Journal of Hydrogen Energy*, vol. 39, no. 36, pp. 21 165–21 176, 2014 (cit. on p. 36).
- [54] A. A. El-Fergany, “Extracting optimal parameters of PEM fuel cells using salp swarm optimizer”, *Renewable Energy*, vol. 119, pp. 641–648, 2018 (cit. on p. 40).
- [55] R. Finesso and E. Spessa, “Ignition delay prediction of multiple injections in diesel engines”, *Fuel*, vol. 119, pp. 170–190, 2014, ISSN: 0016-2361. DOI: <https://doi.org/10.1016/j.fuel.2013.11.040> (cit. on p. 32).
- [56] P. Fragiaco and F. Piraino, “Numerical modelling of a PEFC powertrain system controlled by a hybrid strategy for rail urban transport”, *Journal of Energy Storage*, vol. 17, pp. 474–484, 2018 (cit. on p. 72).
- [57] J. A. Gatowski, E. N. Balles, K. M. Chun, F. E. Nelson, J. A. Ekchian, and J. B. Heywood, “Heat release analysis of engine pressure data”, *SAE Transactions*, vol. 93, pp. 961–977, 1984, ISSN: 0096736X, 25771531. [Online]. Available: <http://www.jstor.org/stable/44721530> (cit. on p. 21).
- [58] R. Geirhos, C. R. M. Temme, J. Rauber, H. H. Schütt, M. Bethge, and F. A. Wichmann, “Generalisation in humans and deep neural networks”, in *Advances in Neural Information Processing Systems 31*, 2018, pp. 7538–7550. [Online]. Available: <http://papers.nips.cc/paper/7982-generalisation-in-humans-and-deep-neural-networks.pdf> (cit. on p. 16).
- [59] M. G. Genton, “Classes of kernels for machine learning: A statistics perspective”, *J. Mach. Learn. Res.*, vol. 2, pp. 299–312, Mar. 2002, ISSN: 1532-4435 (cit. on p. 18).

- [60] M. Gheisarnejad, J. Boudjadar, and M.-H. Khooban, “A new adaptive type-II fuzzy-based deep reinforcement learning control: Fuel cell air-feed sensors control”, *IEEE Sensors Journal*, vol. 19, no. 20, pp. 9081–9089, 2019. DOI: 10.1109/JSEN.2019.2924726 (cit. on pp. 11, 100).
- [61] A. Goshtasbi and T. Ersal, “Degradation-conscious control for enhanced lifetime of automotive polymer electrolyte membrane fuel cells”, *Journal of Power Sources*, vol. 457, p. 227996, 2020 (cit. on p. 73).
- [62] J. Gruber, C. Bordons, and A. Oliva, “Nonlinear MPC for the airflow in a PEM fuel cell using a Volterra series model”, *Control Engineering Practice*, vol. 20, no. 2, pp. 205–217, 2012, ISSN: 0967-0661. DOI: <https://doi.org/10.1016/j.conengprac.2011.10.014>. [Online]. Available: <https://www.sciencedirect.com/science/article/pii/S0967066111002322> (cit. on pp. 87, 112).
- [63] J. Gruber, M. Doll, and C. Bordons, “Design and experimental validation of a constrained MPC for the air feed of a fuel cell”, *Control Engineering Practice*, vol. 17, no. 8, pp. 874–885, 2009, ISSN: 0967-0661. DOI: <https://doi.org/10.1016/j.conengprac.2009.02.006>. [Online]. Available: <https://www.sciencedirect.com/science/article/pii/S096706610900029X> (cit. on p. 87).
- [64] F. Guéniat, L. Mathelin, and M. Y. Hussaini, “A statistical learning strategy for closed-loop control of fluid flows”, *Theoretical and Computational Fluid Dynamics*, vol. 30, no. 6, pp. 497–510, 2016 (cit. on p. 8).
- [65] X. Guo, H. Zhang, Z. Hu, S. Hou, M. Ni, and T. Liao, “Energetic, exergetic and ecological evaluations of a hybrid system based on a phosphoric acid fuel cell and an organic rankine cycle”, *Energy*, vol. 217, p. 119365, 2021 (cit. on p. 7).
- [66] L. Guzzella and C. Onder, *Introduction to Modeling and Control of Internal Combustion Engine Systems*. Berlin/Heidelberg, Germany: Springer Science & Business Media, 2009 (cit. on p. 9).
- [67] S. Hahn, J. Braun, H. Kemmer, and H.-C. Reuss, “Adaptive operation strategy of a polymer electrolyte membrane fuel cell air system based on model predictive control”, *International Journal of Hydrogen Energy*, vol. 46, no. 33, pp. 17306–17321, 2021 (cit. on p. 73).

- [68] I.-S. Han and C.-B. Chung, “Performance prediction and analysis of a PEM fuel cell operating on pure oxygen using data-driven models: A comparison of artificial neural network and support vector machine”, *International Journal of Hydrogen Energy*, vol. 41, no. 24, pp. 10 202–10 211, 2016, ISSN: 0360-3199. DOI: <https://doi.org/10.1016/j.ijhydene.2016.04.247>. [Online]. Available: <https://www.sciencedirect.com/science/article/pii/S036031991530389X> (cit. on pp. 11, 100).
- [69] R. Hannah and R. Max. (2018). “CO2 and other greenhouse gas emissions”, [Online]. Available: <https://ourworldindata.org/co2-and-other-greenhouse-gas-emissions> (cit. on p. 1).
- [70] A. Hanuschkin, S. Schober, J. Bode, J. Schorr, B. Böhm, C. Krüger, and S. Peters, “Machine learning–based analysis of in-cylinder flow fields to predict combustion engine performance”, *International Journal of Engine Research*, vol. 22, no. 1, pp. 257–272, 2021. DOI: 10.1177/1468087419833269. [Online]. Available: <https://doi.org/10.1177/1468087419833269> (cit. on p. 91).
- [71] F. Hashemi, S. Rowshanzamir, and M. Rezakazemi, “CFD simulation of PEM fuel cell performance: Effect of straight and serpentine flow fields”, *Mathematical and Computer Modelling*, vol. 55, no. 3, pp. 1540–1557, 2012, ISSN: 0895-7177. DOI: <https://doi.org/10.1016/j.mcm.2011.10.047>. [Online]. Available: <https://www.sciencedirect.com/science/article/pii/S0895717711006522> (cit. on p. 15).
- [72] H. He, S. Quan, and Y.-X. Wang, “Hydrogen circulation system model predictive control for polymer electrolyte membrane fuel cell-based electric vehicle application”, *International Journal of Hydrogen Energy*, 2020 (cit. on p. 73).
- [73] Y.-J. He and Z.-F. Ma, “A data-driven Gaussian process regression model for two-chamber microbial fuel cells”, *Fuel Cells*, vol. 16, no. 3, pp. 365–376, 2016. DOI: <https://doi.org/10.1002/face.201500109>. eprint: <https://onlinelibrary.wiley.com/doi/pdf/10.1002/face.201500109> (cit. on pp. 100, 111).
- [74] M. Henningsson, “Data-rich multivariable control of heavy-duty engines”, PhD Thesis TFRT-1092, Dept. of Automatic Control, Lund University, Lund, Sweden, 2012. [Online]. Available: <https://lup.lub.lu.se/search/ws/files/3068636/2439874.pdf> (cit. on p. 16).

- [75] M. Henningsson, B. Bernhardsson, P. Tunestål, and R. Johansson, “A machine learning approach to information extraction from cylinder pressure sensors”, in *SAE 2012 World Congress & Exhibition*, Detroit, MI, USA: SAE International, Apr. 2012. DOI: <https://doi.org/10.4271/2012-01-0440> (cit. on p. 16).
- [76] J. J. Hernández, J. Sanz-Argent, J. M. Carot, and J. M. Jabaloyes, “Ignition delay time correlations for a diesel fuel with application to engine combustion modelling”, *International Journal of Engine Research*, vol. 11, no. 3, pp. 199–206, 2010. DOI: 10.1243/14680874JER06209 (cit. on p. 32).
- [77] L. Hewing, K. P. Wabersich, M. Menner, and M. N. Zeilinger, “Learning-based model predictive control: Toward safe learning in control”, *Annual Review of Control, Robotics, and Autonomous Systems*, vol. 3, no. 1, pp. 269–296, 2020. DOI: 10.1146/annurev-control-090419-075625. eprint: <https://doi.org/10.1146/annurev-control-090419-075625> (cit. on pp. 16, 89, 90).
- [78] J. B. Heywood, *Internal Combustion Engine Fundamentals*. New York, United States: McGraw-Hill Education, 2018 (cit. on pp. 3, 4, 23, 57, 92).
- [79] D. Hrovat, S. Di Cairano, H. E. Tseng, and I. V. Kolmanovsky, “The development of model predictive control in automotive industry: A survey”, in *2012 IEEE International Conference on Control Applications*, Dubrovnik, Croatia, Oct. 2012, pp. 295–302. DOI: 10.1109/CCA.2012.6402735 (cit. on p. 55).
- [80] Y. Hu, H. Chen, P. Wang, H. Chen, and L. Ren, “Nonlinear model predictive controller design based on learning model for turbocharged gasoline engine of passenger vehicle”, *Mechanical Systems and Signal Processing*, vol. 109, pp. 74–88, 2018, ISSN: 0888-3270. DOI: <https://doi.org/10.1016/j.ymsp.2018.02.012>. [Online]. Available: <https://www.sciencedirect.com/science/article/pii/S0888327018300682> (cit. on pp. 91, 98).
- [81] G. Ingesson, L. Yin, R. Johansson, and P. Tunestål, “Simultaneous control of combustion timing and ignition delay in multi-cylinder partially premixed combustion”, *SAE International Journal of Engines*, vol. 8, no. 5, pp. 2089–2098, 2015 (cit. on pp. 11, 56, 69, 99).
- [82] —, “An investigation on ignition-delay modelling for control”, *International Journal of Powertrains*, vol. 6, no. 3, pp. 282–306, 2017 (cit. on pp. 31, 32, 69).

- [83] V. M. Janakiraman, X. Nguyen, and D. Assanis, “Stochastic gradient based extreme learning machines for stable online learning of advanced combustion engines”, *Neurocomputing*, vol. 177, pp. 304–316, 2016, ISSN: 0925-2312. DOI: <https://doi.org/10.1016/j.neucom.2015.11.024>. [Online]. Available: <https://www.sciencedirect.com/science/article/pii/S0925231215017439> (cit. on p. 90).
- [84] H. Javaherian, Derong Liu, Yi Zhang, and O. Kovalenko, “Adaptive critic learning techniques for automotive engine control”, in *Proceedings of the 2004 American Control Conference*, vol. 5, Boston, MA, USA, Jun. 2004, 4066–4071 vol.5. DOI: 10.23919/ACC.2004.1383945 (cit. on p. 91).
- [85] J. Jia, Q. Li, Y. Wang, Y. T. Cham, and M. Han, “Modeling and dynamic characteristic simulation of a proton exchange membrane fuel cell”, *IEEE Transactions on Energy Conversion*, vol. 24, no. 1, pp. 283–291, 2009. DOI: 10.1109/TEC.2008.2011837 (cit. on p. 38).
- [86] R. Johansson, *System Modeling and Identification*. New Jersey, United States: Prentice-Hall, 1993, ISBN: 0-13-482308-7 (cit. on pp. 17, 60).
- [87] S. Julier and J. Uhlmann, “Unscented filtering and nonlinear estimation”, *Proceedings of the IEEE*, vol. 92, no. 3, pp. 401–422, 2004. DOI: 10.1109/JPROC.2003.823141 (cit. on p. 47).
- [88] J. Kabzan, L. Hewing, A. Liniger, and M. N. Zeilinger, “Learning-based model predictive control for autonomous racing”, *IEEE Robotics and Automation Letters*, vol. 4, no. 4, pp. 3363–3370, 2019. DOI: 10.1109/LRA.2019.2926677 (cit. on p. 89).
- [89] R. E. Kalman, “A new approach to linear filtering and prediction problems”, *Journal of Basic Engineering*, vol. 82, no. 1, pp. 35–45, Mar. 1960, ISSN: 0021-9223. eprint: https://asmedigitalcollection.asme.org/fluidsengineering/article-pdf/82/1/35/5518977/35_1.pdf (cit. on pp. 47, 60).
- [90] M. Kandidayeni, A. Macias, A. Khalatbarisoltani, L. Boulon, and S. Kelouwani, “Benchmark of proton exchange membrane fuel cell parameters extraction with metaheuristic optimization algorithms”, *Energy*, vol. 183, pp. 912–925, 2019 (cit. on pp. 36, 37, 39).
- [91] H. Kazemi, H. N. Mahjoub, A. Tahmasbi-Sarvestani, and Y. P. Fallah, “A learning-based stochastic MPC design for cooperative adaptive cruise control to handle interfering vehicles”, *IEEE Transactions on Intelligent Vehicles*, vol. 3, no. 3, pp. 266–275, Sep. 2018, ISSN: 2379-8904 (cit. on p. 89).

- [92] A. Keawtubtimthong, D. Koolpiruck, S. Wongs, Y. Laoonual, and A. Kaewpunya, “Development of engine control technique for flex-fuel motorcycle”, in *ECTI-CON2010: The 2010 ECTI International Conference on Electrical Engineering/Electronics, Computer, Telecommunications and Information Technology*, Chiang Mai, Thailand, 2010, pp. 159–162 (cit. on p. 71).
- [93] N. J. Killingsworth, S. M. Aceves, D. L. Flowers, and M. Krstic, “A simple HCCI engine model for control”, in *2006 IEEE Conference on Computer Aided Control System Design, 2006 IEEE International Conference on Control Applications, 2006 IEEE International Symposium on Intelligent Control*, Munich, Germany, Oct. 2006, pp. 2424–2429 (cit. on p. 16).
- [94] M. Klein and L. Eriksson, “A specific heat ratio model for single-zone heat release models”, in *SAE 2004 World Congress and Exhibition*, Detroit, MI, USA: SAE International, Mar. 2004, SAE Technical Paper 2004-01-1464. DOI: <https://doi.org/10.4271/2004-01-1464> (cit. on p. 23).
- [95] T. Kobayashi, M. Fukushima, H. Kanematsu, Y. Utsumi, and Y. Shimamoto, “Design and prototyping of a fuel cell controlling equipment for small hybrid driving airship system”, in *Advanced Materials Research*, vol. 933, 2014, pp. 444–449 (cit. on pp. 11, 72).
- [96] S.-C. Kong, C. D. Marriott, R. D. Reitz, and M. Christensen, “Modeling and experiments of HCCI engine combustion using detailed chemical kinetics with multidimensional CFD”, *SAE Transactions*, vol. 110, pp. 1007–1018, 2001, ISSN: 0096736X, 25771531. [Online]. Available: <http://www.jstor.org/stable/44724373> (cit. on p. 15).
- [97] K. Kurniawan, A. H. Budiman, F. Hermawan, and A. Rahmawan, “Design of control and human machine interface (HMI) for proton exchange membrane fuel cell”, *Indonesian Journal of Energy*, vol. 3, no. 1, pp. 12–18, 2020 (cit. on pp. 11, 72).
- [98] J. H. Lee, “Model predictive control: Review of the three decades of development”, *International Journal of Control, Automation and Systems*, vol. 9, no. 3, p. 415, Jun. 2011, ISSN: 2005-4092. DOI: 10.1007/s12555-011-0300-6. [Online]. Available: <https://doi.org/10.1007/s12555-011-0300-6> (visited on 04/07/2021) (cit. on p. 55).
- [99] U. Lenz and D. Schroeder, “Artificial intelligence for combustion engine control”, in *International Congress & Exposition*, Detroit, MI, USA: SAE International, Feb. 1996. DOI: <https://doi.org/10.4271/>

960328. [Online]. Available: <https://doi.org/10.4271/960328> (cit. on p. 91).
- [100] C. Li, L. Yin, S. Shamun, M. Tuner, B. Johansson, R. Solsjö, and X.-S. Bai, “Transition from HCCI to PPC: The sensitivity of combustion phasing to the intake temperature and the injection timing with and without EGR”, in *SAE 2016 World Congress and Exhibition*, Detroit, MI, United States, Apr. 2016, SAE Technical Paper 2016-01-0767 (cit. on pp. 64, 71).
- [101] L. Li, S. You, C. Yang, B. Yan, J. Song, and Z. Chen, “Driving-behavior-aware stochastic model predictive control for plug-in hybrid electric buses”, *Applied Energy*, vol. 162, pp. 868–879, 2016, ISSN: 0306-2619. DOI: <https://doi.org/10.1016/j.apenergy.2015.10.152>. [Online]. Available: <https://www.sciencedirect.com/science/article/pii/S030626191501394X> (cit. on p. 112).
- [102] S. Li, R. Wei, G. Zhang, Y. Qi, G. Yang, and Q. Shen, “Numerical investigation on the impact of membrane thickness on transport phenomena in PEM fuel cells”, *Int. J. Electrochem. Sci.*, vol. 15, pp. 4138–4147, 2020 (cit. on p. 7).
- [103] Z. Li, R. Outbib, S. Giurgea, and D. Hissel, “Diagnosis for PEMFC systems: A data-driven approach with the capabilities of online adaptation and novel fault detection”, *IEEE Transactions on Industrial Electronics*, vol. 62, no. 8, pp. 5164–5174, 2015. DOI: 10.1109/TIE.2015.2418324 (cit. on p. 17).
- [104] B. Likar and J. Kocijan, “Predictive control of a gas–liquid separation plant based on a Gaussian process model”, *Computers & Chemical Engineering*, vol. 31, no. 3, pp. 142–152, 2007, ISSN: 0098-1354. DOI: <https://doi.org/10.1016/j.compchemeng.2006.05.011>. [Online]. Available: <https://www.sciencedirect.com/science/article/pii/S009813540600127X> (cit. on p. 90).
- [105] D. C. Liu and J. Nocedal, “On the limited memory BFGS method for large scale optimization”, *Mathematical Programming*, vol. 45, no. 1, pp. 503–528, 1989 (cit. on p. 42).
- [106] J. Liu, C. Ulishney, and C. E. Dumitrescu, “Random forest machine learning model for predicting combustion feedback information of a natural gas spark ignition engine”, *Journal of Energy Resources Technology*, vol. 143, no. 1, Jul. 2020, 012301, ISSN: 0195-0738. DOI: 10.1115/1.4047761. eprint: <https://asmedigitalcollection.asme.org/energyresources/article-pdf/143/1/012301/6657943/>

- jert_143_1_012301.pdf. [Online]. Available: <https://doi.org/10.1115/1.4047761> (cit. on p. 90).
- [107] J. S. Liu and R. Chen, “Sequential Monte Carlo methods for dynamic systems”, *Journal of the American Statistical Association*, vol. 93, no. 443, pp. 1032–1044, 1998. DOI: 10.1080/01621459.1998.10473765. eprint: <https://doi.org/10.1080/01621459.1998.10473765> (cit. on p. 47).
- [108] M. Liu, Y. Shi, and X. Liu, “Distributed MPC of aggregated heterogeneous thermostatically controlled loads in smart grid”, *IEEE Transactions on Industrial Electronics*, vol. 63, no. 2, pp. 1120–1129, Feb. 2016, ISSN: 1557-9948. DOI: 10.1109/TIE.2015.2492946 (cit. on p. 55).
- [109] L. Ljung, *System Identification*. London, United Kingdom: Pearson Education, 1998, ISBN: 9780136566953 (cit. on p. 16).
- [110] J. Luna, S. Jemei, N. Yousfi-Steiner, A. Husar, M. Serra, and D. Hissel, “Nonlinear predictive control for durability enhancement and efficiency improvement in a fuel cell power system”, *Journal of Power Sources*, vol. 328, pp. 250–261, 2016, ISSN: 0378-7753. DOI: <https://doi.org/10.1016/j.jpowsour.2016.08.019>. [Online]. Available: <https://www.sciencedirect.com/science/article/pii/S0378775316310187> (cit. on p. 87).
- [111] R. Ma, T. Yang, E. Breaz, Z. Li, P. Briois, and F. Gao, “Data-driven proton exchange membrane fuel cell degradation predication through deep learning method”, *Applied Energy*, vol. 231, pp. 102–115, 2018, ISSN: 0306-2619. DOI: <https://doi.org/10.1016/j.apenergy.2018.09.111>. [Online]. Available: <https://www.sciencedirect.com/science/article/pii/S0306261918314181> (cit. on p. 17).
- [112] J. Macedo-Valencia, J. Sierra, S. Figueroa-Ramírez, S. Díaz, and M. Meza, “3D CFD modeling of a PEM fuel cell stack”, *International Journal of Hydrogen Energy*, vol. 41, no. 48, pp. 23 425–23 433, 2016, ISSN: 0360-3199. DOI: <https://doi.org/10.1016/j.ijhydene.2016.10.065>. [Online]. Available: <https://www.sciencedirect.com/science/article/pii/S0360319916318687> (cit. on p. 15).
- [113] J. M. Maciejowski, *Predictive Control: with Constraints*. Essex, England: Pearson Education, 2002 (cit. on pp. 46, 57, 77).
- [114] J. H. Mack, S. M. Aceves, and R. W. Dibble, “Demonstrating direct use of wet ethanol in a homogeneous charge compression ignition (HCCI) engine”, *Energy*, vol. 34, no. 6, pp. 782–787, 2009 (cit. on p. 6).

- [115] A. A. Malikopoulos, P. Y. Papalambros, and D. N. Assanis, “A learning algorithm for optimal internal combustion engine calibration in real time”, ser. International Design Engineering Technical Conferences and Computers and Information in Engineering Conference, vol. Volume 6: 33rd Design Automation Conference, Parts A and B, Sep. 2007, pp. 91–100. DOI: 10.1115/DETC2007-34718. eprint: https://asmedigitalcollection.asme.org/IDETC-CIE/proceedings-pdf/IDETC-CIE2007/48078/91/2680414/91_1.pdf. [Online]. Available: <https://doi.org/10.1115/DETC2007-34718> (cit. on p. 90).
- [116] V. Manente, B. Johansson, and P. Tunestål, “Partially premixed combustion at high load using gasoline and ethanol, a comparison with diesel”, in *SAE World Congress and Exhibition*, Detroit, MI, USA: SAE International, Apr. 2009, SAE Technical Paper 2009-01-0944 (cit. on p. 5).
- [117] R. F. Mann, J. C. Amphlett, M. A. Hooper, H. M. Jensen, B. A. Peppley, and P. R. Roberge, “Development and application of a generalised steady-state electrochemical model for a PEM fuel cell”, *Journal of Power Sources*, vol. 86, no. 1-2, pp. 173–180, 2000 (cit. on p. 36).
- [118] D. Mayne, J. Rawlings, C. Rao, and P. Scokaert, “Constrained model predictive control: Stability and optimality”, *Automatica*, vol. 36, no. 6, pp. 789–814, 2000, ISSN: 0005-1098. DOI: [https://doi.org/10.1016/S0005-1098\(99\)00214-9](https://doi.org/10.1016/S0005-1098(99)00214-9). [Online]. Available: <https://www.sciencedirect.com/science/article/pii/S0005109899002149> (cit. on p. 55).
- [119] T. L. McKinley and A. G. Alleyne, “Adaptive model predictive control of an SCR catalytic converter system for automotive applications”, *IEEE Transactions on Control Systems Technology*, vol. 20, no. 6, pp. 1533–1547, 2012 (cit. on p. 56).
- [120] M. Mehrpooya, B. Ghorbani, B. Jafari, M. Aghbashlo, and M. Pouriman, “Modeling of a single cell micro proton exchange membrane fuel cell by a new hybrid neural network method”, *Thermal Science and Engineering Progress*, vol. 7, pp. 8–19, 2018, ISSN: 2451-9049. DOI: <https://doi.org/10.1016/j.tsep.2018.04.012>. [Online]. Available: <https://www.sciencedirect.com/science/article/pii/S2451904917303888> (cit. on pp. 11, 100).

- [121] O. Ö. Mengi, “Comparison of MPC based advanced hybrid controllers for STATCOM in medium scale PEM fuel cell systems”, *International Journal of Hydrogen Energy*, vol. 45, no. 43, pp. 23 327–23 342, 2020 (cit. on p. 73).
- [122] K. Min, S. Kang, F. Mueller, J. Auckland, and J. Brouwer, “Dynamic simulation of a stationary proton exchange membrane fuel cell system”, *Journal of Fuel Cell Science and Technology*, vol. 6, no. 4, 2009 (cit. on p. 35).
- [123] M. Mohri, A. Rostamizadeh, and A. Talwalkar, *Foundations of Machine Learning*. Cambridge, MA, USA: MIT Press, 2018 (cit. on p. 16).
- [124] R. Moriyasu, M. Ueda, T. Ikeda, M. Nagaoka, T. Jimbo, A. Matsunaga, and T. Nakamura, “Real-time MPC design based on machine learning for a diesel engine air path system”, *IFAC-PapersOnLine*, vol. 51, no. 31, pp. 542–548, 2018, 5th IFAC Conference on Engine and Powertrain Control, Simulation and Modeling E-COSM 2018, ISSN: 2405-8963. DOI: <https://doi.org/10.1016/j.ifacol.2018.10.119>. [Online]. Available: <https://www.sciencedirect.com/science/article/pii/S2405896318325837> (cit. on p. 91).
- [125] E. Mosca, G. Zappa, and J. Lemos, “Robustness of multipredictor adaptive regulators: MUSMAR”, *Automatica*, vol. 25, no. 4, pp. 521–529, 1989, ISSN: 0005-1098. DOI: [https://doi.org/10.1016/0005-1098\(89\)90095-2](https://doi.org/10.1016/0005-1098(89)90095-2). [Online]. Available: <https://www.sciencedirect.com/science/article/pii/0005109889900952> (cit. on p. 55).
- [126] R. Müller and B. Schneider, “Approximation and control of the engine torque using neural networks”, in *SAE 2000 World Congress*, Detroit, MI, USA: SAE International, Mar. 2000. DOI: <https://doi.org/10.4271/2000-01-0929> (cit. on p. 91).
- [127] V. Naoumov, A. Demin, I. Andersson, and A. Sokolov, “Modeling of combustion and non-equilibrium ionization in spark ignition engines”, *SAE Transactions*, vol. 111, pp. 300–307, 2002, ISSN: 0096736X, 25771531. [Online]. Available: <http://www.jstor.org/stable/44743061> (cit. on p. 16).
- [128] G. Napoli, M. Ferraro, G. Brunaccini, G. Dispenza, and V. Antonucci, “Data driven model for a fuel cell stack development in a complex multi-source hybrid renewable energy system”, *Renewable Energy & Power Quality Journal*, vol. 1, pp. 983–988, 2010 (cit. on p. 17).

- [129] A. Narjiss, D. Depernet, F. Gustin, and D. Hissel, “High frequency power converter for fuel cell stacks parallel association”, in *2008 IEEE Vehicle Power and Propulsion Conference*, IEEE, Harbin, Hei Longjiang, China, 2008, pp. 1–4 (cit. on p. 72).
- [130] V. Nenchev and C. A. Hans, “Optimal adaptive predictive control of a combustion engine”, in *2015 European Control Conference (ECC)*, Linz, Austria, Oct. 2015, pp. 1409–1413 (cit. on pp. 56, 69).
- [131] C. J. Ostafew, A. P. Schoellig, and T. D. Barfoot, “Learning-based nonlinear model predictive control to improve vision-based mobile robot path-tracking in challenging outdoor environments”, in *IEEE International Conference on Robotics and Automation (ICRA)*, Hong Kong, China, Jun. 2014, pp. 4029–4036 (cit. on p. 91).
- [132] *Outlook for energy: A perspective to 2040*, Aug. 2019. [Online]. Available: <https://www.exxonmobil.co.uk/Energy-and-environment/Looking-forward/Outlook-for-Energy/Outlook-for-Energy-A-perspective-to-2040#Buildingaperspective> (cit. on pp. 1–3).
- [133] Q. Ouyang, J. Chen, F. Wang, and H. Su, “Nonlinear MPC controller design for AIR supply of PEM fuel cell based power systems”, *Asian Journal of Control*, vol. 19, no. 3, pp. 929–940, 2017 (cit. on pp. 87, 112).
- [134] D. F. Pereira, F. da Costa Lopes, and E. H. Watanabe, “Neural generalized predictive control for tracking maximum efficiency and maximum power points of PEM fuel cell stacks”, in *IECON 2018 - 44th Annual Conference of the IEEE Industrial Electronics Society*, Washington, DC, USA, 2018, pp. 1878–1883. DOI: 10.1109/IECON.2018.8591290 (cit. on p. 112).
- [135] G. Pillonetto, F. Dinuzzo, T. Chen, G. De Nicolao, and L. Ljung, “Kernel methods in system identification, machine learning and function estimation: A survey”, *Automatica*, vol. 50, no. 3, pp. 657–682, 2014, ISSN: 0005-1098. DOI: <https://doi.org/10.1016/j.automatica.2014.01.001>. [Online]. Available: <https://www.sciencedirect.com/science/article/pii/S000510981400020X> (cit. on p. 17).
- [136] A. Propoi, “Use of linear programming methods for synthesizing sampled-data automatic systems”, *Automation and Remote Control*, vol. 24, no. 7, pp. 837–844, 1963 (cit. on p. 55).

- [137] J. T. Pukrushpan, “Modeling and control of fuel cell systems and fuel processors”, Ph.D. dissertation, Department of Mechanical Engineering, University of Michigan Ann Arbor, Michigan, USA, May 2003. [Online]. Available: <http://deepblue.lib.umich.edu/bitstream/2027.42/123461/2/3079516.pdf> (cit. on pp. 6, 7).
- [138] S. Quan, Y.-X. Wang, X. Xiao, H. He, and F. Sun, “Disturbance prediction-based enhanced stochastic model predictive control for hydrogen supply and circulating of vehicular fuel cells”, *Energy Conversion and Management*, vol. 238, p. 114167, 2021, ISSN: 0196-8904. DOI: <https://doi.org/10.1016/j.enconman.2021.114167>. [Online]. Available: <https://www.sciencedirect.com/science/article/pii/S0196890421003435> (cit. on p. 112).
- [139] C. Rasmussen and C. Williams, *Gaussian Processes for Machine Learning*. Cambridge, MA, USA: MIT Press, Jan. 2006, p. 248 (cit. on pp. 17, 19).
- [140] A. Raut, M. Bidarvatan, H. Borhan, and M. Shahbakhti, “Model predictive control of an RCCI engine”, in *2018 Annual American Control Conference (ACC)*, Milwaukee, WI, USA, Jun. 2018, pp. 1604–1609 (cit. on p. 56).
- [141] R. Reitz and C. Rutland, “Development and testing of diesel engine CFD models”, *Progress in Energy and Combustion Science*, vol. 21, no. 2, pp. 173–196, 1995, ISSN: 0360-1285. DOI: [https://doi.org/10.1016/0360-1285\(95\)00003-Z](https://doi.org/10.1016/0360-1285(95)00003-Z) (cit. on p. 15).
- [142] R. D. Reitz and G. Duraisamy, “Review of high efficiency and clean reactivity controlled compression ignition (RCCI) combustion in internal combustion engines”, *Progress in Energy and Combustion Science*, vol. 46, pp. 12–71, 2015, ISSN: 0360-1285 (cit. on p. 5).
- [143] U. Rosolia, A. Carvalho, and F. Borrelli, “Autonomous racing using learning model predictive control”, in *2017 American Control Conference (ACC)*, Seattle, WA, USA, May 2017, pp. 5115–5120 (cit. on p. 91).
- [144] M. A. Sadiq Al-Baghdadi, “A CFD study of hygro-thermal stresses distribution in PEM fuel cell during regular cell operation”, *Renewable Energy*, vol. 34, no. 3, pp. 674–682, 2009, ISSN: 0960-1481. DOI: <https://doi.org/10.1016/j.renene.2008.05.023>. [Online]. Available: <https://www.sciencedirect.com/science/article/pii/S0960148108002206> (cit. on p. 15).

- [145] Y. Al-Sagheer and R. Steinberger-Wilckens, “Energy management controller for fuel cell hybrid electric vehicle based on sat-nav data”, *Fuel Cells*, vol. 20, no. 4, pp. 420–430, 2020. DOI: <https://doi.org/10.1002/face.201900196>. eprint: <https://onlinelibrary.wiley.com/doi/pdf/10.1002/face.201900196> (cit. on p. 73).
- [146] K. Sankar, K. Aguan, and A. K. Jana, “A proton exchange membrane fuel cell with an airflow cooling system: Dynamics, validation and nonlinear control”, *Energy Conversion and Management*, vol. 183, pp. 230–240, 2019 (cit. on pp. 38, 39).
- [147] P. J. Sarma, C. L. Gardner, S. Chugh, A. Sharma, and E. Kjeang, “Strategic implementation of pulsed oxidation for mitigation of co poisoning in polymer electrolyte fuel cells”, *Journal of Power Sources*, vol. 468, p. 228 352, 2020 (cit. on p. 72).
- [148] Y. Shao, L. Xu, X. Zhao, J. Li, Z. Hu, C. Fang, J. Hu, D. Guo, and M. Ouyang, “Comparison of self-humidification effect on polymer electrolyte membrane fuel cell with anodic and cathodic exhaust gas recirculation”, *International Journal of Hydrogen Energy*, vol. 45, no. 4, pp. 3108–3122, 2020 (cit. on p. 7).
- [149] M. El-Sharkh, A. Rahman, and M. Alam, “Neural networks-based control of active and reactive power of a stand-alone PEM fuel cell power plant”, *Journal of Power Sources*, vol. 135, no. 1, pp. 88–94, 2004, ISSN: 0378-7753. DOI: <https://doi.org/10.1016/j.jpowsour.2004.03.071>. [Online]. Available: <https://www.sciencedirect.com/science/article/pii/S0378775304004902> (cit. on pp. 11, 100).
- [150] A. Sharma, V. Sugumaran, and S. B. Devasenapati, “Misfire detection in an IC engine using vibration signal and decision tree algorithms”, *Measurement*, vol. 50, pp. 370–380, 2014, ISSN: 0263-2241. DOI: <https://doi.org/10.1016/j.measurement.2014.01.018> (cit. on p. 32).
- [151] D. Shen, C.-C. Lim, and P. Shi, “Robust fuzzy model predictive control for energy management systems in fuel cell vehicles”, *Control Engineering Practice*, vol. 98, p. 104 364, 2020, ISSN: 0967-0661. DOI: <https://doi.org/10.1016/j.conengprac.2020.104364>. [Online]. Available: <https://www.sciencedirect.com/science/article/pii/S0967066120300381> (cit. on p. 112).
- [152] X. Shen, Y. Wu, and T. Shen, “Logical control scheme with real-time statistical learning for residual gas fraction in IC engines”, *Science China Information Sciences*, vol. 61, no. 1, p. 010 203, 2018 (cit. on p. 8).

- [153] P. Shih, B. C. Kaul, S. Jagannathan, and J. A. Drallmeier, “Reinforcement-learning-based output-feedback control of nonstrict nonlinear discrete-time systems with application to engine emission control”, *IEEE Transactions on Systems, Man, and Cybernetics, Part B (Cybernetics)*, vol. 39, no. 5, pp. 1162–1179, Oct. 2009, ISSN: 1941-0492. DOI: 10.1109/TSMCB.2009.2013272 (cit. on p. 91).
- [154] A. Shokuhi-Rad, A. Jamali, M. Naghashzadegan, N. Nariman-zadeh, and A. Hajiloo, “Optimum pareto design of non-linear predictive control with multi-design variables for PEM fuel cell”, *International Journal of Hydrogen Energy*, vol. 37, no. 15, pp. 11 244–11 254, 2012, ISSN: 0360-3199. DOI: <https://doi.org/10.1016/j.ijhydene.2012.03.092>. [Online]. Available: <https://www.sciencedirect.com/science/article/pii/S0360319912007409> (cit. on p. 112).
- [155] (2019). “The fuel cell industry review 2019”, [Online]. Available: <https://www.e4tech.com/news/2018-fuel-cell-industry-review-2019-the-year-of-the-gigawatt.php> (cit. on p. 7).
- [156] G. J. Thompson, C. M. Atkinson, N. N. Clark, T. W. Long, and E. Hanzevack, “Technical note: Neural network modelling of the emissions and performance of a heavy-duty diesel engine”, *Proceedings of the Institution of Mechanical Engineers, Part D: Journal of Automobile Engineering*, vol. 214, no. 2, pp. 111–126, 2000. DOI: 10.1177/095440700021400201 (cit. on p. 16).
- [157] R. H. Thring, “Homogeneous-charge compression-ignition (HCCI) engines”, in *1989 SAE International Fall Fuels and Lubricants Meeting and Exhibition*, Baltimore, Maryland, USA: SAE International, Sep. 1989, SAE Technical Paper 892068 (cit. on p. 5).
- [158] N. Tietze, “Model-based calibration of engine control units using Gaussian process regression”, Ph.D. dissertation, Department of Electrical Engineering and Information Technology, Technische Universität, Darmstadt, Germany, 2015. [Online]. Available: <http://tuprints.ulb.tu-darmstadt.de/4572/> (cit. on p. 32).
- [159] A. Vahidi, A. Stefanopoulou, and H. Peng, “Model predictive control for starvation prevention in a hybrid fuel cell system”, in *Proceedings of the 2004 American Control Conference*, IEEE, vol. 1, Boston, MA, USA, 2004, pp. 834–839 (cit. on p. 73).
- [160] C. Vong and P. Wong, “Engine ignition signal diagnosis with wavelet packet transform and multi-class least squares support vector machines”, *Expert Systems with Applications*, vol. 38, no. 7,

- pp. 8563–8570, 2011, ISSN: 0957-4174. DOI: <https://doi.org/10.1016/j.eswa.2011.01.058> (cit. on p. 32).
- [161] C.-M. Vong, P.-K. Wong, and Y.-P. Li, “Prediction of automotive engine power and torque using least squares support vector machines and bayesian inference”, *Engineering Applications of Artificial Intelligence*, vol. 19, no. 3, pp. 277–287, 2006, ISSN: 0952-1976. DOI: <https://doi.org/10.1016/j.engappai.2005.09.001> (cit. on p. 32).
- [162] A. Wächter and L. T. Biegler, “On the implementation of an interior-point filter line-search algorithm for large-scale nonlinear programming”, *Mathematical Programming*, vol. 106, no. 1, pp. 25–57, 2006 (cit. on p. 47).
- [163] J. Wahlström and L. Eriksson, “Modelling diesel engines with a variable-geometry turbocharger and exhaust gas recirculation by optimization of model parameters for capturing non-linear system dynamics”, *Proceedings of the Institution of Mechanical Engineers, Part D: Journal of Automobile Engineering*, vol. 225, no. 7, pp. 960–986, 2011. DOI: [10.1177/0954407011398177](https://doi.org/10.1177/0954407011398177) (cit. on pp. 26, 30).
- [164] F.-C. Wang, H.-T. Chen, Y.-P. Yang, and J.-Y. Yen, “Multivariable robust control of a proton exchange membrane fuel cell system”, *Journal of Power Sources*, vol. 177, no. 2, pp. 393–403, 2008 (cit. on p. 72).
- [165] F.-C. Wang, Y.-P. Yang, C.-W. Huang, H.-P. Chang, and H.-T. Chen, “System identification and robust control of a portable proton exchange membrane full-cell system”, *Journal of Power Sources*, vol. 164, no. 2, pp. 704–712, 2007 (cit. on pp. 11, 72).
- [166] S. Wang, D. Yu, J. Gomm, G. Page, and S. Douglas, “Adaptive neural network model based predictive control for air–fuel ratio of SI engines”, *Engineering Applications of Artificial Intelligence*, vol. 19, no. 2, pp. 189–200, 2006, ISSN: 0952-1976. DOI: <https://doi.org/10.1016/j.engappai.2005.08.005> (cit. on pp. 32, 69).
- [167] Y.-X. Wang and Y.-B. Kim, “Real-time control for air excess ratio of a PEM fuel cell system”, *IEEE/ASME Transactions on Mechatronics*, vol. 19, no. 3, pp. 852–861, 2014. DOI: [10.1109/TMECH.2013.2262054](https://doi.org/10.1109/TMECH.2013.2262054) (cit. on pp. 73, 87).

- [168] Y. Wang, C. Ocampo-Martinez, and V. Puig, “Stochastic model predictive control based on Gaussian processes applied to drinking water networks”, *IET Control Theory Applications*, vol. 10, no. 8, pp. 947–955, 2016, ISSN: 1751-8652. DOI: [10.1049/iet-cta.2015.0657](https://doi.org/10.1049/iet-cta.2015.0657) (cit. on p. 90).
- [169] K. I. Wong, P. K. Wong, C. S. Cheung, and C. M. Vong, “Modeling and optimization of biodiesel engine performance using advanced machine learning methods”, *Energy*, vol. 55, pp. 519–528, 2013, ISSN: 0360-5442. DOI: <https://doi.org/10.1016/j.energy.2013.03.057> (cit. on p. 16).
- [170] P. K. Wong, H. C. Wong, C. M. Vong, Z. Xie, and S. Huang, “Model predictive engine air-ratio control using online sequential extreme learning machine”, *Neural Computing and Applications*, vol. 27, no. 1, pp. 79–92, 2016 (cit. on p. 98).
- [171] C. H. Woo and J. B. Benziger, “PEM fuel cell current regulation by fuel feed control”, *Chemical Engineering Science*, vol. 62, no. 4, pp. 957–968, 2007 (cit. on p. 72).
- [172] H.-W. Wu, “A review of recent development: Transport and performance modeling of PEM fuel cells”, *Applied Energy*, vol. 165, pp. 81–106, 2016 (cit. on p. 35).
- [173] Y. Xie, J. Zou, C. Peng, Y. Zhu, and F. Gao, “A novel PEM fuel cell remaining useful life prediction method based on singular spectrum analysis and deep Gaussian processes”, *International Journal of Hydrogen Energy*, vol. 45, no. 55, pp. 30 942–30 956, 2020, ISSN: 0360-3199. DOI: <https://doi.org/10.1016/j.ijhydene.2020.08.052>. [Online]. Available: <https://www.sciencedirect.com/science/article/pii/S0360319920330524> (cit. on p. 111).
- [174] J. Xue, Q. Gao, and W. Ju, “Reinforcement learning for engine idle speed control”, in *2010 International Conference on Measuring Technology and Mechatronics Automation*, vol. 2, Changsha, Hunan, China, Mar. 2010, pp. 1008–1011. DOI: [10.1109/ICMTMA.2010.249](https://doi.org/10.1109/ICMTMA.2010.249) (cit. on p. 91).
- [175] T. Yamada, N. Hayakawa, Y. Kami, and T. Kawai, “Universal air-fuel ratio heated exhaust gas oxygen sensor and further applications”, in *International Congress & Exposition*, Detroit, MI, USA: SAE International, Feb. 1992, SAE Technical Paper 920234. DOI: <https://doi.org/10.4271/920234> (cit. on p. 25).

- [176] Y.-P. Yang, F.-C. Wang, H.-P. Chang, Y.-W. Ma, and B.-J. Weng, “Low power proton exchange membrane fuel cell system identification and adaptive control”, *Journal of Power Sources*, vol. 164, no. 2, pp. 761–771, 2007 (cit. on p. 72).
- [177] Y. Yildiz, A. M. Annaswamy, D. Yanakiev, and I. Kolmanovsky, “Spark-ignition-engine idle speed control: An adaptive control approach”, *IEEE Transactions on Control Systems Technology*, vol. 19, no. 5, pp. 990–1002, 2011 (cit. on p. 56).
- [178] L. Yin, “Model predictive control (MPC) of an advanced multi-cylinder engine for transient operations”, Ph.D. dissertation, Dept. of Energy Sciences, Lund University, Lund, Sweden, 2018, ISBN: 978-91-7753-694-9 (cit. on pp. 30, 57, 69, 70).
- [179] L. Yin, G. Turesson, P. Tunestål, and R. Johansson, “Evaluation and transient control of an advanced multi-cylinder engine based on partially premixed combustion”, *Applied Energy*, vol. 233, pp. 1015–1026, 2019 (cit. on pp. 11, 56, 99).
- [180] S. Yu, R. Sadanandan, and X.-S. Bai, “Numerical studies of flame extinction and re-ignition behaviors in a novel, ultra-lean, non-premixed model GT burner using LES-ESF method”, *Fuel*, vol. 262, p. 116617, 2020, ISSN: 0016-2361. DOI: <https://doi.org/10.1016/j.fuel.2019.116617> (cit. on p. 15).
- [181] X. Zeng and J. Wang, “A physics-based time-varying transport delay oxygen concentration model for dual-loop exhaust gas recirculation (EGR) engine air-paths”, *Applied Energy*, vol. 125, pp. 300–307, 2014, ISSN: 0306-2619 (cit. on p. 31).
- [182] Y.-J. Zhai, D.-W. Yu, H.-Y. Guo, and D. Yu, “Robust air/fuel ratio control with adaptive DRNN model and AD tuning”, *Engineering Applications of Artificial Intelligence*, vol. 23, no. 2, pp. 283–289, 2010, ISSN: 0952-1976. DOI: <https://doi.org/10.1016/j.engappai.2009.12.006> (cit. on p. 32).
- [183] B. Zhang, F. Lin, C. Zhang, R. Liao, and Y.-X. Wang, “Design and implementation of model predictive control for an open-cathode fuel cell thermal management system”, *Renewable Energy*, vol. 154, pp. 1014–1024, 2020, ISSN: 0960-1481. DOI: <https://doi.org/10.1016/j.renene.2020.03.073>. [Online]. Available: <https://www.sciencedirect.com/science/article/pii/S0960148120303980> (cit. on p. 73).

- [184] H. Zhang, J. Jiang, H. Qin, W. Zhao, X. Li, and J. Li, “Fuel adaptive analysis and methane conversion rate prediction based on Gaussian process regression for an SR-SOFC system”, in *39th Chinese Control Conference (CCC)*, Shenyang, Liaoning, China, Jul. 2020, pp. 5407–5412. DOI: [10.23919/CCC50068.2020.9188404](https://doi.org/10.23919/CCC50068.2020.9188404) (cit. on pp. 11, 100).
- [185] S. Zhang, U. Reimer, Y. Rahim, S. Beale, and W. Lehnert, “Numerical modeling of polymer electrolyte fuel cells with analytical and experimental validation”, *Journal of Electrochemical Energy Conversion and Storage*, vol. 16, no. 3, 2019 (cit. on p. 36).
- [186] X. Zhang, M. Ni, J. Wang, L. Yang, X. Mao, S. Su, Z. Yang, and J. Chen, “Configuration design and parametric optimum selection of a self-supporting PEMFC”, *Energy Conversion and Management*, vol. 225, p. 113 391, 2020 (cit. on p. 7).
- [187] Y. Zhou, A. Ravey, and M.-C. Péra, “Multi-objective energy management for fuel cell electric vehicles using online-learning enhanced Markov speed predictor”, *Energy Conversion and Management*, vol. 213, p. 112 821, 2020, ISSN: 0196-8904. DOI: <https://doi.org/10.1016/j.enconman.2020.112821>. [Online]. Available: <https://www.sciencedirect.com/science/article/pii/S0196890420303599> (cit. on pp. 11, 100).
- [188] L. Zhu and J. Chen, “Prognostics of PEM fuel cells based on Gaussian process state space models”, *Energy*, vol. 149, pp. 63–73, 2018, ISSN: 0360-5442. DOI: <https://doi.org/10.1016/j.energy.2018.02.016>. [Online]. Available: <https://www.sciencedirect.com/science/article/pii/S0360544218302421> (cit. on pp. 11, 100).
- [189] C. Ziogou, S. Papadopoulou, M. C. Georgiadis, and S. Voutetakis, “On-line nonlinear model predictive control of a PEM fuel cell system”, *Journal of Process Control*, vol. 23, no. 4, pp. 483–492, 2013, ISSN: 0959-1524. DOI: <https://doi.org/10.1016/j.jprocont.2013.01.011>. [Online]. Available: <https://www.sciencedirect.com/science/article/pii/S0959152413000218> (cit. on p. 87).
- [190] C. Ziogou, S. Voutetakis, M. C. Georgiadis, and S. Papadopoulou, “Model predictive control (MPC) strategies for PEM fuel cell systems – A comparative experimental demonstration”, *Chemical Engineering Research and Design*, vol. 131, pp. 656–670, 2018, Energy Systems Engineering, ISSN: 0263-8762. DOI: <https://doi.org/10.1016/j.cherd.2018.01.024>. [Online]. Available: <https://www.sciencedirect.com/science/article/pii/S0263876218300024>.

sciencedirect.com/science/article/pii/S0263876218300261
(cit. on pp. 55, 112).

Paper I

Learning Based Model Predictive Control of Combustion Timing in Multi-Cylinder Partially Premixed Combustion Engine

Xiufei Li, Lianhao Yin, Per Tunestål, Rolf Johansson

SAE Technical Paper 2019-24-0016, 2019

This paper applied learning-based model predictive control (LBMPC) to combustion phasing control. Learning-based model predictive control decouples the robustness and performance in an optimization framework by maintaining two models of the system, the base model and the learning model. The learning model is a linear model used to capture the influence on combustion duration. The comparison of LBMPC and MPC shows the improvement of performance by LBMPC.

I designed the controller, performed the experiments, processed the data, and wrote the paper with the support from my supervisors. Lianhao Yin assisted with the idea and experiment design.

Paper II

Adaptive Model Predictive Control of Combustion in Flex-Fuel Heavy Duty Compression-Ignition Engine

Xiufei Li, Per Tunestål, Rolf Johansson

21st IFAC World Congress (virtual), July, 2020

This paper proposed an adaptive model predictive control approach to control the combustion process of the flex-fuel CI engine. The control targets are the combustion phasing and ignition delay, and the actuators are the EGR, VGT valves, and main injection timings. MPC is used for the multi-input multi-output control problem with constraints and adaptivity is done by estimating the physical ignition delay model parameters with real-time data online by Kalman filter. The adaptive MPC approach shows the successful application in the fuel transition scenario with diesel, gasoline/n-heptane mixture, and ethanol/n-heptane mixture. The possible ignition delay range calculated from the physical model can work as an indicator of the engine fuel properties.

I designed the controller, performed the experiments, processed the data, and wrote the paper with the support from my supervisors.

Paper III

A Multi-Input and Single-Output Voltage Control for a Polymer Electrolyte Fuel Cell System using Model Predictive Control Method

Xiufei Li, Yuanxin Qi, Shian Li, Per Tunestål, Martin Andersson

International Journal of Energy Research, 2021

This paper developed a polymer electrolyte fuel cell (PEFC) system model and studied its performances under different operating conditions. Then two different controllers, a proportional-integral (PI) controller, and a model predictive control (MPC) controller are proposed and applied in the PEFC system to control its output voltage at the desired value by regulating the hydrogen and air flow rates at the same time. Simulation results demonstrate that the developed PEFC system model is qualified to capture the system's behavior. And both the developed PI and MPC controllers are effective at controlling the PEFC system's output voltage, while the MPC controller

presents superior performance with faster response and smaller overshoot.

I designed the controller and performed the experiments with the support from my supervisors. Yuanxin Qi built the fuel cell system model and wrote the introduction, model, discussion, and conclusion parts under the supervision of Martin Andersson.

Paper IV

Voltage Control for a Polymer Electrolyte Fuel Cell System by Gaussian Process Model Predictive Control

Xiufei Li, Yuanxin Qi, Martin Andersson, Rolf Johansson, Per Tunestål

Submitted to International Journal of Hydrogen Energy, 2022

This paper proposed a Gaussian process model predictive control approach to stabilize the polymer electrolyte fuel cell system's output voltage by controlling its hydrogen and air flow rates at the same time. Two Gaussian process models are built to describe the system dynamics. The hydrogen pressure and input change rate limits are considered. The Gaussian process prediction variance is incorporated in the constraint handling to compensate model errors. Simulation results show that the Gaussian process MPC can control the voltage at the desired 48 V while satisfying the safety constraints all the time under a workload disturbance ranging from 110-120 A. The Gaussian process MPC eliminates the requirement of the underlying true system model and needs less system information as compared to the MPC based on system physical model.

I designed the controller, performed the simulations, processed the data, and wrote the paper with the support from my supervisors.

Paper V

Neural Network Based Model Predictive Control of Voltage for a Polymer Electrolyte Fuel Cell System with Constraints

Xiufei Li, Yuanxin Qi, Martin Andersson, Rolf Johansson, Per Tunestål

Submitted to eTransportation, 2022

This paper developed a neural network (NN) based model predictive control algorithm to control the fuel cell output voltage with safety constraints. The developed NN MPC controller regulates the polymer electrolyte fuel cell system's output voltage by controlling the hydrogen and air flow rates at the same time. The safety constraints regarding the hydrogen pressure limit and input change rate limit are considered. The neural network model is built to describe the system voltage and hydrogen pressure behavior. Simulation results show that the NN MPC can control the voltage at the desired value while satisfying the safety constraints under workload disturbance. The NN MPC shows a comparable performance of the MPC based on the detailed underlying system physical model.

I designed the controller, performed the simulations, processed the data, and wrote the paper with the support from my supervisors.



Faculty of Engineering
Department of Energy Sciences

ISBN 978-91-8039-181-8
ISRN LUTMDN/TMHP-22/1167-SE
ISSN 0282-1990

